2009:043

MASTER'S THESIS

Computing, Visualizing and Analyzing Ion Trajectories

S. Shahab Fatemi Moghareh

Luleå University of Technology

Master Thesis, Continuation Courses
Space Science and Technology
Department of Space Science, Kiruna

2009:043 - ISSN: 1653-0187 - ISRN: LTU-PB-EX--09/043--SE

Computing, Visualizing and Analyzing Ion Trajectories

Shahab Fatemi

Master's thesis
Luleå University of Technology
Department of Space Science
Kiruna Space Campus
Spring semester 2009

Swedish Institute for Space Physics

Computing, Visualizing and Analyzing Ion Trajectories

Sayed Shahab Fatemi Moghareh
Luleå University of Technology
Department of Space Science
Kiruna Space Campus
Spring semester 2009

Acknowledgments

My endless thanks to God who has built this magnificent world of mystery. He is always with me, never forgets me and makes the best for me.

I have to thank my supervisor Associate Prof. Mats Holmström who has given me the best of support and guidance and shared with me his knowledge and experiences on the subject of this study and gave me the chance of doing this work. It has been wonderful experience for me to have the honor of working with him. Thanks so much.

I would like to thank all my teachers and assistants in Luleå University of Technology, department of space physics in Kiruna (IRV) and Julius-Maximilians University Würzburg. Special thanks to Dr. Victoria Barabash, Dr. Johnny Ejemalm, Dr. Martin Bohm, Dr. Hans Weber, Prof. Klaus Schilling, Prof. Wolfgang Dröge, Mrs. Anette Snällfot-Brändström, Mrs. Maria Winnebäck, Mrs. Heidi Schaber and Mrs. Ursula Shahmary. Special thanks to Mr. Sven Molin, the space master coordinator, who never left me and the other space master students alone and many thanks to all Erasmus Mundus staffs for their best of support.

I would like to thank all Swedish Institute of Space Physics (IRF) staffs and students, especially Solar System Physics and Space Technology (SSPT) group members for their support and help and also many thanks to all IRF and IRV PhD students.

Many thanks to all my friends in the space master program because of making wonderful memories. I have learnt many things from them and I am proud on myself having friends like them. I should also have special thanks to my Persian friends, Kia Tavakoli, Atousa Shaikholislam, Parisa Jouzdani, Mohsen Atef, Rashin Abtahi, Navid Khosravi, Nazila Kaveh and Mehrdad Seifi who have never left me alone since I have been living abroad.

Last but not least, I have to thank my family, especially my parents, Alireza Fatemi and Mahin Haj-Mahmoudzadeh, my sister, Shahrzad Fatemi and my brother, Kamal Fatemi, who have always supported and encouraged me during my life.

Abstract

The motion, velocities and trajectories of ions, and the effect of different electromagnetic field conditions on their motion are analyzed in detail. A numerical method is chosen to be used in a model to simulate ion trajectories in uniform and non-uniform electromagnetic fields. The outputs are stored in a file format which can be visualized using different software packages. Ion trajectories and their response to solar wind magnetic field and induced electric field are studied using the simulation model. Since this model can be applied to any solar wind condition, the Earth's moon environment is chosen as a real example for ion trajectories.

After an analysis of the interaction of solar wind with the moon, a computational model for simulating its interaction with any other body is introduced. The outputs of this model are used to study ion trajectories at the moon wake. Finally, trajectories and velocities of ions coming from the moon's surface towards an observer orbiting the moon (in conditions of uniform electromagnetic field) are studied, and results for different observer positions are compared and discussed. This has applications for ion observations from a Lunar orbit.

Contents

Chapter 1

Introduction

Ion is an atom that bears electric charges and the number of electrons are different from the number of protons. This charge difference can be either positive or negative. The positively charged ions are called *cations* and the negatively charged ions are called *anions*. In the literatures the ions which are electrically charged are called *charged particles* .
Plasma which is the fourth state of the matter (see chapter 4) contains charged particles. In our solar system the main source for producing plasmas is the Sun. Million tons of charged particles are erupted every day from the Sun, move with high velocities between 300 [km/s] and 1000 [km/s], propagates into space and affect all celestial bodies in our solar system. The motion of these particles are affected by different forces, mainly electric and magnetic fields. *Pressure gradient* and *gravity force* can also affect charged particle motions. All descriptions of plasma behavior are based on the motions of charged particles, therefore understanding this motion will help us to have better understanding about plasma.
In this report, the motion of charged particles, their velocity and kinetic energy as a function of time are calculated and visualized. A numerical method is introduced to compute ion trajectories and velocities in different electromagnetic conditions and a simulation code was written to simulate ion motions. It should be noted that the means of ion here is ion trajectories only and we will not discuss about the chemistry of ions.
Our simulation model can be applied for any electric and magnetic field conditions and can be used for example to study ion trajectories near Mars, Venus, Titan and etc. We applied it to the Earth's Moon as an example of studying ion trajectory behaviors near the Moon.

1.1 Application for the Moon

The Earth has only one *Moon* which is the fifth largest Moon in our solar system. It is the second brightest object for us in the sky after the Sun. As the Moon orbits around the Earth once per month, the angle between the Earth, the Moon and the Sun changes; we see this as the cycle of the Moon's phases.
The Moon subtle atmosphere mainly contains helium and radon, but some other constituents such as argon, potassium, sodium, oxygen and methane have been observed either by in-situ instruments onboard satellites orbiting around the Moon or by Earth based spectrometers. The lack of strong magnetic field and no evidence of detached bow shock cause that the ionized particles coming with the solar wind impact the lunar surface, ionize neutrals, accelerate them to escape the Moon and to be one of the main reasons for an insignificant lunar atmosphere. This makes

Earth's Moon as an ideal place to study plasma flow and the effects of solar wind interaction with a surface of a solar system body.
Charged particles coming with the solar wind can impact the Moon surface with the same velocity as the solar wind and:
1- leave the surface and move to different places,
2- ionize the other particles at the Moon surface and lose their energy,
3- accelerate other particles, might leave the lunar surface with the same energy as the solar wind.
The first series of bursts ions were observed by *Apollo 14* ion detector in the lunar wake in December 1969 [22]. It was reported at that time that most likely those ion bursts are a result of the direct interaction between the solar wind and the Moon. The same event was observed in early January 2009 by *SARA* ; the IRF ion analyzer onboard Chandrayaan 1; (see Chapter 5) at the Moon wakeside. Ions that are not part of the direct solar wind has been observed by Apollo and *Chandrayaan-1* . Both these mysterious ions and their origin are interesting examples and a reason to choose Moon for studying plasma motion. We will study the possibility to find incoming ions with kinetic energy almost the same as the solar wind or higher at the Moon wakeside.

A software was written in C++ to simulate particle motion in different solar wind conditions by the usage of numerical methods. This software can save particle trajectories and velocities in different file formats. Therefore we need to know about particles motion, Moon environment and solar wind conditions near the Moon. Then the dynamics of the charged particles is studied and their equation of motion in different solar wind conditions are explained in chapter 2. Different numerical methods which can be used to solve the charged particles equation of motion are studied in chapter 3 and one of them is chosen as the method of our simulation code. To well understand the Moon and the solar wind effects and properties near the Moon, a model is introduced to simulate solar wind interaction with solar system bodies in chapter 4 and a software called *VisIt* is used to visualized electric and magnetic field variations near the Moon. In the beginning of this project, visualizations of ion trajectories were supposed to be done by *StreamLine* function in VisIt software but because this software is still not bug-free and it takes time to modify its codes and make changes to get StreamLine function to work, ion trajectories outputs are stored in a special file format which can be opened and visualized by VisIt. This file format will be introduced briefly in chapter 4. The solar wind interaction with the Moon and formation of its wakeside are also discussed there. In chapter 5, charged particle trajectories, velocities and energies around the Moon are studied and the possibility of incoming ions from the Moon dayside and nightside are compared.

Notation

All vectors are shown in bold type.

B:	*Magnetic field*	**E**:	*Electric field*	**V**:	*Velocity*	**R**:	*Position*	**F**:	*Force*
J:	*Current density*	ρ:	*Density*	T:	*Temperature*	p:	*Pressure*	m:	*Mass*
n:	*Charge number density*	q:	*Electric charge*						

Chapter 2

Single Particle Dynamics

Studying and understanding the dynamics of particles is crucial to get knowledge of space plasma processes. In this chapter we study charged particle motion in a presence of electric and magnetic fields as a function of time and position. We start with uniform electromagnetic fields[1] and then will discuss about non-uniform fields[2].

2.1 Charged particle motion in uniform magnetic fields

The equation of motion for a particle with mass m, charge q and velocity $\mathbf{V}$ in electric field $\mathbf{E}$ and magnetic field $\mathbf{B}$ is shown by the *Lorentz force* $\mathbf{F}$ and is given as:

$$\textit{Lorentz force}: \quad \mathbf{F} = m\frac{d\mathbf{V}}{dt} = q(\mathbf{E} + \mathbf{V} \times \mathbf{B})$$

$$\begin{cases} \dfrac{d\mathbf{V}}{dt} = \dfrac{q}{m}(\mathbf{E} + \mathbf{V} \times \mathbf{B}) \\ \mathbf{V} = \dfrac{d\mathbf{R}}{dt} \end{cases} \qquad \textit{(equation of motion)} \tag{2.1}$$

where $\mathbf{R}$ is particle trajectory (see [1] and [20]). If we assume that $\mathbf{E}$=$\mathbf{0}$, the Lorentz force equation is reduced to:

$$m\frac{d\mathbf{V}}{dt} = q(\mathbf{V} \times \mathbf{B}) \tag{2.2}$$

If we multiply equation 2.2 with $\mathbf{V}/2$, we have q($\mathbf{V}\times\mathbf{B}$).$\mathbf{V}/2$ at the right side of the equation which is equal to zero because $\mathbf{V}\times\mathbf{B}$ is perpendicular to both $\mathbf{V}$ and $\mathbf{B}$. Therefore its scaler product with $\mathbf{V}$ is zero and we obtain:

$$\frac{1}{2}m\frac{d\mathbf{V}}{dt}.\mathbf{V} = \frac{1}{2}q(\mathbf{V} \times \mathbf{B}).\mathbf{V} = 0 \Rightarrow \frac{d}{dt}(\frac{1}{2}mv^2) = 0 \Rightarrow \frac{d}{dt}(W_{kin}) = 0$$

which means that the kinetic energy of charged particles in the absence of electric field is constant [2].

[1] When the field is constant and does not vary by time and has a homogeneous distribution.
[2] When the field is inhomogeneous or vary by time.

Assume a uniform magnetic field along the $\widehat{\mathbf{z}}$ axis in the Cartesian coordinate system $\mathbf{B}$=B $\widehat{\mathbf{z}}$ and $\mathbf{E}$=$\mathbf{0}$. Denoting the direction perpendicular to magnetic field with $\perp$ and parallel to it with $\|$, the components of equation 2.2 are given by:

$$\frac{d\mathbf{V}_\perp}{dt} = \Omega_c \mathbf{V}_\perp \times \widehat{\mathbf{z}} \qquad , \qquad \frac{dv_z}{dt} = \frac{dv_\|}{dt} = 0 \tag{2.3}$$

and we would have:

$$\frac{d^2 v_x}{dt^2} = -{\Omega_c}^2 \, v_x \quad , \quad \frac{d^2 v_y}{dt^2} = -{\Omega_c}^2 \, v_y \quad , \quad v_z = const \tag{2.4}$$

where Ω_c is *cyclotron* or *gyrofrequency* and defined as:

$$\Omega_c = \frac{qB}{m} \qquad [rad/s] \tag{2.5}$$

The solution of equation 2.3 and 2.4 are:

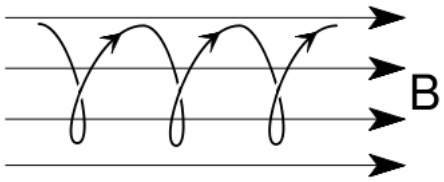

Figure 2.1: Charged particle trajectory in a uniform magnetic field

$$v_x(t) = v_\perp \cos(\Omega_c t + \varphi) \quad , \quad v_y(t) = v_\perp \sin(\Omega_c t + \varphi) \quad , \quad v_z(t) = v_\| \tag{2.6}$$

with ${v_\perp}^2 = {v_x}^2 + {v_y}^2$ where $\mathbf{V}_\perp + \mathbf{V}_\| = \mathbf{V}$

and particle trajectory is given by:

$$x - x_0 = r_L \sin(\Omega_c t + \varphi) \quad , \quad y - y_0 = -r_L \cos(\Omega_c t + \varphi) \quad , \quad z - z_0 = v_\| t \tag{2.7}$$

This shows that a particle in a uniform magnetic field and in the absence of electric field with initial velocity ($v_\perp$, $v_\|$) would have a constant motion along the magnetic field and circular motion about its guiding center (x_0 , y_0, z) with radius of r_L which r_L is defined as *Larmor* or *gyroradius*:

$$r_L = \frac{v_\perp}{\Omega_c} = \frac{m v_\perp}{|q|B} \tag{2.8}$$

for more details see [1], [2] and [3].

2.2 Charged particle motion in uniform electromagnetic fields

We now assume the presence of both electric and magnetic fields which are homogeneous and constant in time (uniform). From the equation of motion (equation 2.1) we have:

$$\frac{d\mathbf{V}_\perp}{dt} = \frac{q}{m}(\mathbf{E}_\perp + \mathbf{V}_\perp \times \mathbf{B}) \quad , \quad \frac{d\mathbf{V}_\|}{dt} = \frac{q}{m}\mathbf{E}_\| \tag{2.9}$$

where $\mathbf{B} = B_x\,\widehat{\mathbf{x}} + B_y\,\widehat{\mathbf{y}} + B_z\,\widehat{\mathbf{z}}$ and $\mathbf{E} = E_x\,\widehat{\mathbf{x}} + E_y\,\widehat{\mathbf{y}} + E_z\,\widehat{\mathbf{z}} = \mathbf{E}_\perp + \mathbf{E}_\parallel$.
Applying the conditions above to equation 2.1 and getting the second derivative gives us:

$$\begin{bmatrix} \frac{d^2v_x}{dt^2} \\ \frac{d^2v_y}{dt^2} \\ \frac{d^2v_z}{dt^2} \end{bmatrix} = (\frac{q}{m})^2 . \begin{bmatrix} -({B_y}^2 + {B_z}^2) & B_xB_y & B_xB_z \\ B_xB_y & -({B_x}^2 + {B_z}^2) & B_yB_z \\ B_xB_z & B_yB_z & -({B_x}^2 + {B_y}^2) \end{bmatrix} . \begin{bmatrix} v_x \\ v_y \\ v_z \end{bmatrix}$$

$$+(\frac{q}{m})^2 . \begin{bmatrix} 0 & B_z & -B_y \\ -B_z & 0 & B_x \\ B_y & -B_x & 0 \end{bmatrix} . \begin{bmatrix} E_x \\ E_y \\ E_z \end{bmatrix} \tag{2.10}$$

It is difficult to solve this equation analytically, then we simplify our assumptions by $\mathbf{B} = B_z\widehat{\mathbf{z}}$ and for the same electric field as before we would have:

$$\begin{cases} \frac{d^2v_x}{dt^2} = {\Omega_c}^2(-v_x + \frac{E_y}{B_z}) \\ \frac{d^2v_y}{dt^2} = -{\Omega_c}^2(v_y + \frac{E_x}{B_z}) \\ \frac{d^2v_z}{dt^2} = 0 \ , \ (\frac{dv_z}{dt} = {\Omega_c}^2\frac{E_z}{B_z} \textit{is obtained from equation of motion}) \end{cases} \tag{2.11}$$

with the solution:

$$\begin{cases} v_x(t) = A\sin(\Omega_c t + \varphi) + \frac{E_y}{B_z} \\ v_y(t) = A\cos(\Omega_c t + \varphi) - \frac{E_x}{B_z} \\ v_z(t) = (\frac{qE_z}{m})t + v_z(0) \end{cases} \tag{2.12}$$

where A and φ are constants. The *particle trajectory* is given by:

$$\begin{cases} x(t) = -\frac{A}{\Omega_c}\cos(\Omega_c t + \varphi) + \frac{E_y}{B_z}t + x(0) \\ y(t) = \frac{A}{\Omega_c}\sin(\Omega_c t + \varphi) - \frac{E_x}{B_z}t + y(0) \end{cases} \tag{2.13}$$

Charged particles in the existence of uniform electric field give an acceleration along the magnetic field lines with the magnitude of

$$acceleration:\ |a| = qE_{\parallel}/m$$

Equations 2.12 and 2.13 are applied for three different assumptions to study the particle velocity and trajectory. A positive charged particle (ion) with the mass of one proton m= 1.6726×10^{-27} [kg] is launched with initial velocity $\mathbf{V}_{init} = 400\,\widehat{\mathbf{x}}$ [km/s] from initial position $\mathbf{R}_{init} = \mathbf{0}$ [km]. First a uniform magnetostatic filed with $\mathbf{B} = +5\,\widehat{\mathbf{z}}$ [nT] in the absence of electric field is assumed. The particle velocity and trajectory as a function of time and position are shown in Figures 2.2 and 2.3[3]. The results are shown for a special time interval from 0 to 40 seconds. Figure 2.2 shows

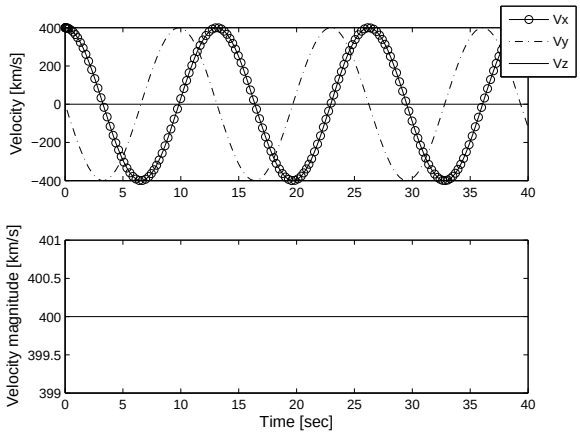

Figure 2.2: Ion velocity components [top] and velocity magnitude [bottom panel]
$\mathbf{B} = +5\,\widehat{\mathbf{z}}$ [nT], $\mathbf{E} = \mathbf{0}$ and $\mathbf{V}_{init} = +400\,\widehat{\mathbf{x}}$ [km/s]

that the x and y components of velocity oscillate between -400 [km/s] and +400 [km/s] while the z component is constant and equal to the initial velocity of $v_{z_{init}}$. The magnitude of the velocity remains constant shown in the bottom panel of Figure 2.2 and it reveals that the kinetic energy is constant and is equal to: $W_{kin} = mv^2/2 \simeq 835eV$ [4] in the example above. Figure 2.3 shows that in the absence of electric field, which is considered as a perturbation, the ion gyrates around its *guiding center* with the gyro frequency of Ω_c=0.479 [Hz] with the gyroradius r_L = 835 km. Since $v_z(0)$ was assumed to be zero and the ion was launched from z=0, there is no motion along the magnetic field line and the ion follows its helical path in the XY plane only.
Second example is a uniform magnetostatic filed $\mathbf{B} = +5\,\widehat{\mathbf{z}}$ [nT] and uniform electrostatic field $\mathbf{E} = 0.1\,\widehat{\mathbf{x}} + 0.1\,\widehat{\mathbf{y}}$ [mV/m]. The ion velocity and trajectory are shown in Figures 2.4 and 2.5 respectively. Three components of the ion velocity as a function of time are shown in the top panel of Figure 2.4 for the assumptions mentioned above. The x component of the ion velocity varies between -360 [km/s] and +400 [km/s] whereas the y component oscillates between -400 [km/s] and +360 [km/s] and the z component remains zero. The velocity magnitude as a function of time is shown in the bottom panel of Figure 2.4 and fluctuates between 352 [km/s] and 408

[3]All plots in this chapter are produced numerically in Cartesian coordinate system by using the methods and software described in chapter 3.
[4]Electron Volt: a unit of energy, 1eV=$1.60217\times10^{-19}\,[J]$

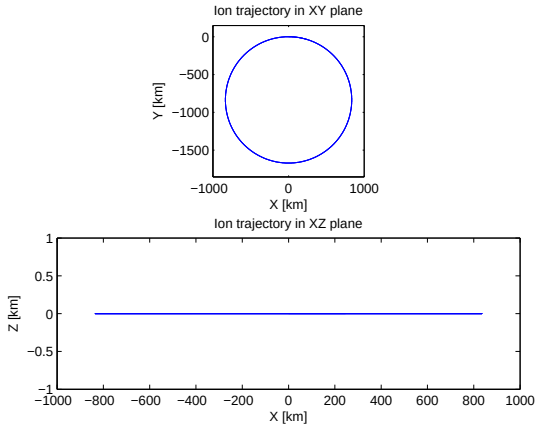

Figure 2.3: Ion trajectory at XY [top] and XZ plane [bottom panel] in uniform magnetic field $\mathbf{B} = +5\ \widehat{\mathbf{z}}$ [nT], $\mathbf{E} = \mathbf{0}$, $\mathbf{V}_{init} = +400\ \widehat{\mathbf{x}}$ [km/s] and $\mathbf{R} = \mathbf{0}$

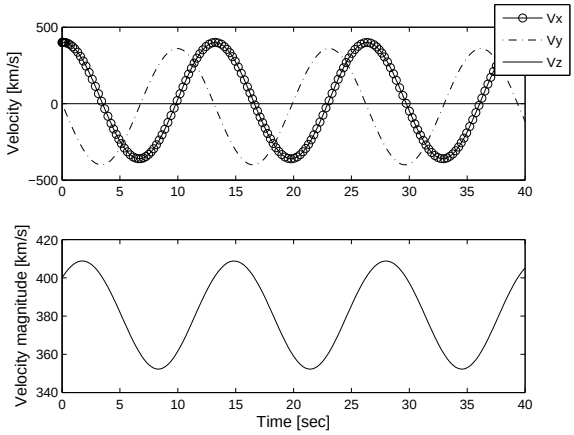

Figure 2.4: Ion velocity components [top] and velocity magnitude [bottom panel] in uniform electromagnetic field.
$\mathbf{B} = +5\ \widehat{\mathbf{z}}$ [nT], $\mathbf{E} = 0.1\ \widehat{\mathbf{x}} + 0.1\ \widehat{\mathbf{y}}$ [mV/m] and $\mathbf{V}_{init} = +400\ \widehat{\mathbf{x}}$ [km/s]

[km/s] with the average velocity of 380 [km/s]. In this case, the kinetic energy varies between 646 eV and 870 eV. The ion trajectory in the XY and XZ planes are shown in the Figure 2.5 at the top and bottom panels respectively. As we see in the top panel, the ion has right and downwards motion in the XY plane due to the electric field disturbance. This motion is called *electric drift motion* and the *drift velocity* is calculated as:

$$\textit{electric drift velocity:} \quad \mathbf{V}_{D_E} = \frac{\mathbf{E} \times \mathbf{B}}{B^2} \tag{2.14}$$

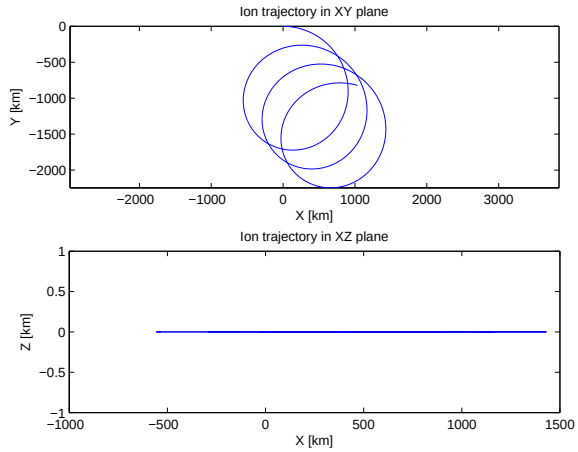

Figure 2.5: Ion trajectory in XY [top] and XZ plane [bottom panel] in uniform electromagnetic field.

$\mathbf{B} = +5\ \widehat{\mathbf{z}}$ [nT], $\mathbf{E} = 0.1\ \widehat{\mathbf{x}} + 0.1\ \widehat{\mathbf{y}}$ [mV/m], $\mathbf{V}_{init} = +400\ \widehat{\mathbf{x}}$ [km/s] and $\mathbf{R}_{init} = \mathbf{0}$ [km]

for more details see [6].
In our example, the ion electric drift velocity is:

$$\mathbf{V}_{D_E} = \frac{\begin{vmatrix} \widehat{\mathbf{x}} & \widehat{\mathbf{y}} & \widehat{\mathbf{z}} \\ E_x & E_y & E_z \\ B_x & B_y & B_z \end{vmatrix}}{({B_x}^2 + {B_y}^2 + {B_z}^2)} = \frac{\begin{vmatrix} \widehat{\mathbf{x}} & \widehat{\mathbf{y}} & \widehat{\mathbf{z}} \\ 10^{-4} & 10^{-4} & 0 \\ 0 & 0 & 5.10^{-9} \end{vmatrix}}{2.5 \times 10^{-17}} = +20\widehat{\mathbf{x}} - 20\widehat{\mathbf{y}} \quad [km/s]$$

Ion drift direction in Figure 2.5 is fulfilled by the calculated drift velocity direction.
Various perturbations such as electric field, a slow change in time of B or non-uniform magnetic field can disturb the ion motion around its guiding center and drift the ion to different directions ([3]). Generally speaking, any external force like $\mathbf{F}_{ext}$ gives a drift in the ion motion. In the existence of electric field, the external force appears as $\mathbf{F}_{ext} = q\mathbf{E}$. Therefore the general formula of the drift velocity can be obtained from:

$$\mathbf{V}_D = \frac{\mathbf{F}_{ext} \times \mathbf{B}}{qB^2} \tag{2.15}$$

(see [2])
Drift motion and its effects are discussed in the next section.
In the third example, the $\widehat{\mathbf{z}}$ component of the electrostatic field is assumed to be non zero but the rest of the speculations are presumed to be the same as the second example. The ion velocity and trajectory are shown in Figures 2.6 and 2.7.
According to the simplified equation of motion in a uniform electromagnetic field (equation 2.11) and its solutions (2.12 and 2.13), we can see when the parallel component of electric field with magnetic field are existed, $\mathbf{V}_{\|}$ velocity would be a linear function of time with the gradient of $qE_{\|}/m$ which makes an unstable perturbation in the particle motion along the magnetic field lines. This is shown in the top panel of Figure 2.6. The bottom panel of Figure 2.6 shows that the ion velocity magnitude is not stable and is increased by time, therefore the ion is accelerated

along the magnetic field.
The electric drift velocity is:

$$\mathbf{V}_{D_E} = \frac{E_y\widehat{\mathbf{x}} - E_x\widehat{\mathbf{y}}}{B_z} = +20\widehat{\mathbf{x}} - 20\widehat{\mathbf{y}} \;\; [km/s]$$

which is the same as the last example and it means that ion's trajectory should be drifted downwards and to the right side shown in the top panel of Figure 2.7, but it also has an upward motion along the magnetic field lines which can be seen in the bottom panel of Figure 2.7.

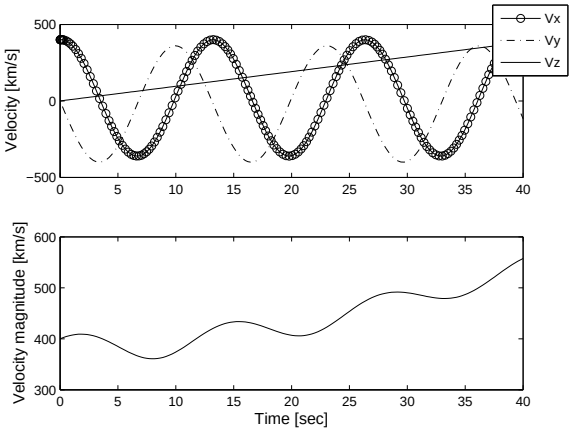

Figure 2.6: Ion velocity components [top] and velocity magnitude [bottom panel] in uniform electromagnetic field.
$\mathbf{B} = +5\ \widehat{\mathbf{z}}$ [nT], $\mathbf{E} = 0.1\ \widehat{\mathbf{x}} + 0.1\ \widehat{\mathbf{y}} + 0.1\ \widehat{\mathbf{z}}$ [mV/m] and $\mathbf{V}_{init} = 400\ \widehat{\mathbf{x}}$ [km/s]

2.3 Electric drift motion

In the existence of any external force to the magnetic field, the charged particles are accelerated, their gyroradius is increased and the particles are drifted in the direction of $\mathbf{F}_{ext} \times \mathbf{B}$ which is perpendicular to the direction of both external force and magnetic field. This drift, as described in the previous section, can be calculated by equation 2.15 and is called *drift velocity*. There are many forces which can make a drift in the particle's motion perpendicular to the magnetic field line but only electric drift is discussed here (for more details see [5] and [6]).
It was shown in the previous section that in a magnetic field $\mathbf{B}$ with presence of an electric field $\mathbf{E}$, the particle's motion is perturbed and drifted perpendicular to the direction of both electric and magnetic field lines and the drift velocity is calculated by equation 2.14. This equation shows that $\mathbf{V}_D$, which in case of electric drift is presented by $\mathbf{V}_{D_E}$, is independent of both particle's mass (m) and charge (q). It means that the electric drift velocity and its direction are the same for all particles (either ions or electrons). The electron and ion trajectory in a simple uniform electric and magnetic field are shown in the Figure 2.8. This figure shows that ions and electrons move at the same direction which means that no electric current is produced.
As a real example of electric drift we can name the *co-rotational electric field* of the Earth. If we assume that the Earth rotates with the angular velocity of ω, the electric field at position $\mathbf{r}$ from

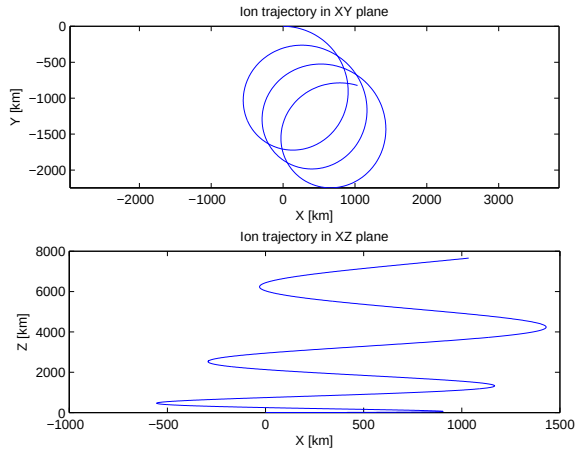

Figure 2.7: Ion trajectory XY [top] and XZ plane [bottom panel] in uniform electromagnetic field. $\mathbf{B} = +5\ \widehat{\mathbf{z}}$ [nT], $\mathbf{E} = 0.1\ \widehat{\mathbf{x}} + 0.1\ \widehat{\mathbf{y}} + 0.1\ \widehat{\mathbf{z}}$ [mV/m], $\mathbf{V}_{init} = 400\ \widehat{\mathbf{x}}$ [km/s] and $\mathbf{R}_{init} = \mathbf{0}$ [km]

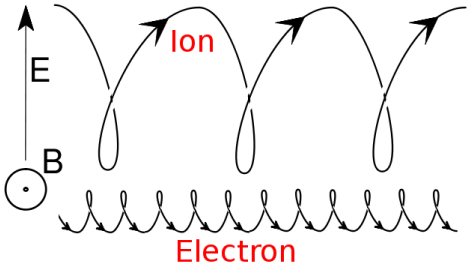

Figure 2.8: Ion and electron trajectories in a uniform electromagnetic field.

the Earth center and inside the Earth's magnetosphere is calculated by:

$$\mathbf{E} = (\omega \times \mathbf{r}) \times \mathbf{B} \tag{2.16}$$

Inside the Earth magnetosphere and within $4R_{Earth}$ at the dayside of the Earth (R_{Earth} is the Earth radius and almost equal to 6378 [km]) the charged particles are forced to co-rotate with the Earth by the co-rotational electric field. This region is called *plasmasphere* [19].

2.4 Charged particle motion in time dependent electromagnetic fields

From Faraday's law we know that an electric field would be induced by a changing magnetic field in time and yields:

$$\textit{Faraday's law:} \quad \nabla \times \mathbf{E} = -\frac{\partial \mathbf{B}}{\partial t} \tag{2.17}$$

Considering $\mathbf{B} = B\widehat{\mathbf{z}}$ and $\mathbf{E} = E_\theta(r)\widehat{\theta}$ in a cylindrical coordinate (see Appendix 1) and applying Faraday's equation gives:

$$\frac{1}{r}\frac{\partial}{\partial r}(rE_\theta) = -\frac{\partial \mathbf{B}}{\partial t}$$

$$\Rightarrow \quad \int_0^r \frac{\partial}{\partial r'}(r' E_\theta)dr' = -\frac{\partial B}{\partial t}\int_0^r r' dr' \quad \Rightarrow \quad rE_\theta = -\frac{1}{2}r^2\frac{\partial B}{\partial t}$$

$$E_\theta = -\frac{1}{2}r\frac{\partial B}{\partial t} \tag{2.18}$$

where all directions are along $\widehat{\theta}$ and we know that in the cylindrical coordinate, $\widehat{r}\times\widehat{\mathbf{z}} = -\widehat{\theta}$. Then we can rewrite the equation 2.18 in the vector form.

$$\mathbf{E}_\theta = \frac{1}{2}\mathbf{r}\times\frac{\partial \mathbf{B}}{\partial t} \tag{2.19}$$

and the equation of motion would be:

$$\frac{d\mathbf{V}}{dt} = \frac{q}{m}(\frac{1}{2}\mathbf{r}\times\frac{\partial \mathbf{B}}{\partial t} + \mathbf{V}\times\mathbf{B}) = (\frac{1}{2}\mathbf{r}\times\frac{\partial(\frac{q}{m}\mathbf{B})}{\partial t}) + (\mathbf{V}\times\frac{q}{m}\mathbf{B})$$

$$= (\frac{1}{2}\mathbf{r}\times\frac{\partial(\Omega_c)\widehat{\Omega}}{\partial t}) + (\mathbf{V}\times\Omega_c\widehat{\Omega}) \tag{2.20}$$

The electric drift velocity is defined as:

$$\mathbf{V}_{D_E} = \frac{\mathbf{E}_\theta\times\mathbf{B}}{B^2} = \frac{1}{2}(\mathbf{r}\times\frac{\partial \mathbf{B}}{\partial t})\times\frac{\mathbf{B}}{B^2} \tag{2.21}$$

for more details see [5].

As the last example in this chapter, we would like to find the solution for the equation of motion of a particle which moves in a uniform magnetic field of $\mathbf{B} = B_z\widehat{\mathbf{z}}$ and non uniform electric field of $\mathbf{E}(t) = E_0(\cos(\Omega_c t)\widehat{\mathbf{x}} + \sin(\Omega_c t)\widehat{\mathbf{y}})$. Applying the mentioned assumptions to the equation of motion and solving them analytically gives the solutions as:

$$\begin{cases} v_x(t) = -\dfrac{qE_0}{m}t\cos(\Omega_c t) \\ \\ v_y(t) = -\dfrac{qE_0}{m}t\sin(\Omega_c t) \\ \\ v_z(t) = v_\parallel \end{cases} \tag{2.22}$$

and the particle trajectory is:

$$\begin{cases} x(t) = -\dfrac{qE_0}{m}\left(\dfrac{t}{\Omega_c}\sin(\Omega_c t) + \dfrac{1}{{\Omega_c}^2}\cos(\Omega_c t) - \dfrac{1}{{\Omega_c}^2}\right) \\ y(t) = -\dfrac{qE_0}{m}\left(-\dfrac{t}{\Omega_c}\cos(\Omega_c t) + \dfrac{1}{{\Omega_c}^2}\sin(\Omega_c t)\right) \\ z(t) = v_{\|}t + z_0 \end{cases} \tag{2.23}$$

Figure 2.9 shows how an ion's velocity and trajectory look like in the electromagnetic condition of our example. It should be noted that in this report all electric and magnetic fields are spatially

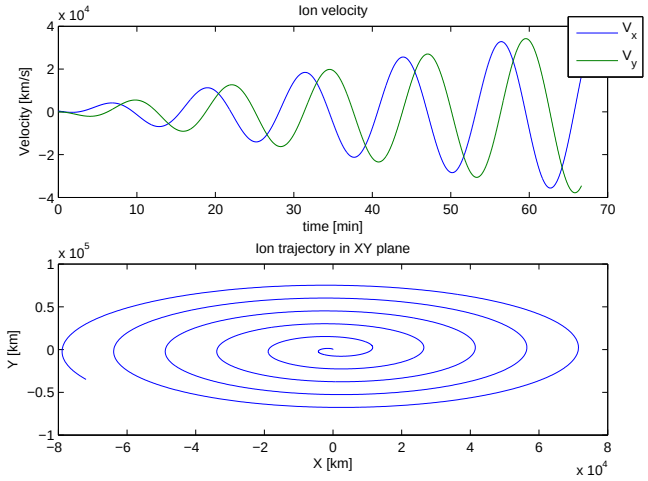

Figure 2.9: Ion velocity [top panel] and trajectory in the XY plane [bottom panel] in a non-uniform electric field with $\mathbf{B} = B_z\widehat{\mathbf{z}}$ and $\mathbf{E}(t) = E_0(\cos(\Omega_c t)\widehat{\mathbf{x}} + \sin(\Omega_c t)\widehat{\mathbf{y}})$.

varying but not time dependent. The example above is the only time dependent fields to show how do they affect charged particle motion.
The dynamics of charged particles in uniform and non-uniform electromagnetic fields were discussed, their velocity and trajectory equations were obtained and visualized in this chapter. In the next chapter, three different numerical methods are studied to solve the charged particles equation of motion and one of them is chosen as the method to use in our simulation model.

Chapter 3

Algorithms for Trajectory Computations

The study of different numerical methods which can solve the mathematical equations is called Numerical Analysis. The dynamics of single particle was studied in chapter 2 and explained that the motion of charged particles are defined by the equation of motion (equation 2.1). Particle motion in the existence of electromagnetic field was defined and its motion, acceleration and drift velocity were discussed. Studying the dynamics of the charged particles in different electric and magnetic fields need to define and solve the equation of motion relative to the electromagnetic conditions or existence of other forces which might affect the particle motion, such as gravity force and pressure gradient. In chapter 2 it was shown that some of the equations are easy to be solved analytically but having complicated conditions or existence of several external forces make the equations either extremely difficult or even impossible to be analyzed by hand. Therefore, numerical methods should be used to solve the equations and of course the numerical methods have some errors and the results are not exactly the same as the real solutions. In addition, it takes time for different computational algorithms to be solved which means that not only the method we choose to solve our problem should be fast enough, but also should have the highest accuracy and the lowest calculation errors. We conclude that finding a method to solve our problem is not the only issue, but choosing the best method which is more suitable for our problem and gives us the more accurate results are essential.
Generally speaking, finding a suitable numerical method to solve a problem always depends on the problem conditions and our expectations by the solutions we get at the end. Hence, before start studying different numerical methods, we should have understod the problem we want to solve and also know the whole expectations we have by solving that problem.

3.1 Single particle motion

The motion of a single particle in uniform and non-uniform electromagnetic field is studied and visualized in this report. The other forces such as gravity force is negligible and since the collisionless plasma (see chapter 4) is studied, the pressure gradient does not exist.
To make the problem more clear, let's assume a hydrogen ion (H^+) with the mass of one proton (1.6726×10^{-27} kg) coming from the solar wind with the same velocity as the solar wind velocity, gyrating along the Interplanetary Magnetic Field (IMF[1]) and drifting to the direction perpendic-

[1]IMF is the Sun magnetic field in interplanetary space. [2].

ular to the IMF and the induction electric field. In this report we would like to visualize the ion motion, at the moon wakeside and to track the ions which hit the surface of the moon and move to the lunar wake. Ions motion should be visualized and their velocity, energy, gyrofrequency, gyroradius and drift velocity should be calculated and studied.
In order to solve this problem, the equation of motion should be applied to a certain condition and to be solved to find out the velocity and trajectory of the ions. The conditions above are somehow similar to the simplified conditions for the other solar system planets. Therefore the equation is applicable to be used almost for all planets and their satellites in our solar system or even in the other solar systems by having a well understanding of the existing forces. Hence, a general condition should be taken into account which we can study and increase the understanding of particle motion in different planetary conditions.
The conditions we assume are absolutely simplified and the rather complicated or specific conditions such as the effect of the magnetic field of the other planets are not considered. For example, for the moon and ion trajectory in the moon wakeside, it is assumed that the moon is outside the earth magnetosphere and the earth magnetic field does not affect the ion motion. It can be assumed when Titan is studied for instance. During solar minimum, Titan is usually inside the Saturn magnetosphere and can be affected even by Jupiter magnetotail.
If a time constant solar wind velocity with a homogeneous electromagnetic field is taken and the other external forces are neglected, a simple equation of motion is obtained which is still difficult to be solved by hand and it is easier to be computed numerically. In chapter 5, the ion motion in a uniform electromagnetic field is discussed and then the ion motion in a non uniform electromagnetic field is studied. The advantage of solving the simplified equation of motion is we do not need to be worry about non uniform electromagnetic field conditions since the ion's velocity and trajectory are calculated as a function of time in a special time period for a specific time step. This will be explained more in chapter 5.
Now we have clear understanding of our problem. We want to launch an ion with an initial velocity in an electromagnetic field, compute its trajectory, velocity and energy for finite time interval, store the whole results for any time steps in one or several files and finally, read the results from the files, visualize and study them and compare the results for different initial conditions. We should also be able to run the simulation backward in time because we want to compute the ions initial conditions for a certain final condition (we will discuss about it later).

3.2 Numerical Methods

The equation of motion (equation 2.1) is an Ordinary Differential Equation (ODE). The equation of motion for a charged particle with the initial condition is re-written again here:

$$\frac{d\mathbf{V}(t)}{dt} = \frac{q}{m}(\mathbf{E}(t) + \mathbf{V}(t) \times \mathbf{B}(t)) \quad ; \quad \frac{d\mathbf{R}(t)}{dt} = \mathbf{V}(t) \tag{3.1}$$

$$\textit{Initial conditions:} \quad \mathbf{R}(t=0) = \mathbf{R}_{init} \quad , \quad \mathbf{V}(t=0) = \mathbf{V}_{init}$$

To solve this equation numerically, a numerical method is needed which solves the first derivative equations. The derivative is defined by:

$$\frac{df(t)}{dt} = lim_{\Delta t \to 0} \frac{f(t+\Delta t) - f(t)}{\Delta t} \tag{3.2}$$

The Taylor series is used to expand f(t+Δt) and if the first derivative function is taken and the higher derivation terms are neglected, the resulting approximation error which is called truncation

error comes up and is specified as the order of Δt shown with $\mathcal{O}(\Delta t^a)$, where 'a' is the error term (for more details see chapter 1 and 2 in [8] and chapter 1 in [9]). Therefore equation 3.2 is written as:

$$\frac{df(t)}{dt} = \frac{f(t+\Delta t) - f(t)}{\Delta t} + \mathcal{O}(\Delta t^a) \tag{3.3}$$

Several numerical methods exist to solve equation 3.3. Here, three of them are introduced and compared briefly, and finally the one which is more suitable for our applications is chosen.

3.2.1 Euler Method

In the Euler method, equation 3.3 is applied to equation 3.1 and it gives us:

$$\begin{cases} \mathbf{V}(t+\Delta t) = \mathbf{V}(t) + \{\frac{q}{m}(\mathbf{E}(t) + \mathbf{V}(t) \times \mathbf{B}(t))\}.\Delta t \\ \\ \mathbf{R}(t+\Delta t) = \mathbf{R}(t) + \mathbf{V}(t).\Delta t \end{cases} \tag{3.4}$$

and if the solution is calculated for n time steps, the Euler method would be:

$$\begin{cases} \mathbf{V}_{n+1} = \mathbf{V}_n + \{\frac{q}{m}(\mathbf{E}_n + \mathbf{V}_n \times \mathbf{B}_n)\}.\Delta t \\ \\ \mathbf{R}_{n+1} = \mathbf{R}_n + \mathbf{V}_n.\Delta t \end{cases} \tag{3.5}$$

when the time steps are defined as t_{n+1}=t_n + Δt and Δt is the time step length.
The Euler method has the truncation error as the order of 2 (a=2) which is numerically unstable except for the extremely small step lengths. Taking very small step lengths can make another error which occurs due to the computational limitations and is called round-off error (see [9] and [8]). Therefore, this method is not used very often.

3.2.2 Leap-Frog Method

The Leap-Frog method is used when only modest accuracy is needed. In this method, the time steps for positions ($\mathbf{R}$) are defined for t_k, t_{k+1}, t_{k+2}, ..., t_n where k is an arbitrary integer number between 0 and n, while the velocities are calculated for the time steps halfaway in between like $t_{k+\frac{1}{2}}$, $t_{k+\frac{3}{2}}$, ...,$t_{n+\frac{1}{2}}$ and that is why the method is called Leap-Frog. If this method is used to solve equation 3.1, the solution will be:

$$\begin{cases} \mathbf{R}_n = \mathbf{R}_{n-1} + \mathbf{V}_{n-\frac{1}{2}}.\Delta t \\ \\ \mathbf{V}_{n+\frac{1}{2}} = \mathbf{V}_{n-\frac{1}{2}} + \{\frac{q}{m}(\mathbf{E}_{n-\frac{1}{2}} + \mathbf{V}_{n-\frac{1}{2}} \times \mathbf{B}_{n-\frac{1}{2}})\}.\Delta t \end{cases} \tag{3.6}$$

The error in Leap-Frog method is $\mathcal{O}(\Delta t^3)$ which is lower than Euler but its problem is difficult to get started. When only the initial conditions are defined for t=0, the conditions for the first half-steps are unknown (see [8]). This is the main problem of Leap-Frog method. The advantages of this method are having good energy conservation and being time reversible (it can be run both forward and backward in time). It means that a negative or positive value can be chosen for Δt (see [20] and [8]).
This method is applied to the Lorentz force and the velocity is calculated ([20]). The final simplified velocity formula is:

$$\mathbf{V}_{n+\frac{1}{2}} = \mathbf{V}_{n-\frac{1}{2}}(1 - \frac{1}{2}{\Omega_c}^2.\Delta t^2) + \frac{q\Delta t}{m}(\mathbf{E} + \mathbf{V}_{n-\frac{1}{2}} \times \mathbf{B})$$

$$+\frac{q^2\Delta t^2}{2m^2}(\mathbf{E} \times \mathbf{B}) + \frac{q^2\Delta t^2}{2m^2}(\mathbf{V}_{n-\frac{1}{2}}.\mathbf{B})\mathbf{B} \tag{3.7}$$

3.2.3 Runge-Kutta Method

Runge-Kutta method is another numerical method to solve ODEs. It is accurate enough with the error term of $\mathcal{O}(\Delta t^4)$ but expensive in running time to compare with the last two methods. It also needs more computer memory and can not be run backward in time.
Solving our equation with this method is as follows:

$$\begin{cases} \mathbf{V}_{n+1} = \mathbf{V}_n + \dfrac{\Delta t}{6}(K_1 + 2K_2 + 2K_3 + K_4) \\ K_1 = f(\mathbf{V}, t) \\ K_2 = f(\mathbf{V} + \dfrac{\Delta t}{2}K_1, t + \dfrac{\Delta t}{2}) \\ K_3 = f(\mathbf{V} + \dfrac{\Delta t}{2}K_2, t + \dfrac{\Delta t}{2}) \\ K_4 = f(\mathbf{V} + \Delta t.K_3, t + \Delta t) \end{cases} \tag{3.8}$$

where f($\mathbf{V}$, t) = $\dfrac{d\mathbf{V}}{dt}$ and the same method should be used to calculate $\mathbf{R}(t)$. Clearly it takes time to calculate all K-coefficients and needs more memory to compare with last two methods (for more details see [13], [14]).

3.3 Test-Particle Methods

There are several modeling methods used to study solar system plasma interactions. The most common ones are magnetohydrodyamic (MHD), hybrid and test-particle/Monte-Carlo simulations. MHD method is not the subject of this report and hybrid model is introduced in chapter 4. The test-particle method is used to examine some of the kinetic aspects of ions and electrons without the additional expense of hybrid or fully electromagnetic simulations (for more details see [20]).

A class called *Numeric* was written in C++ to handle different numerical methods with several functions which can calculate ions velocity and trajectory for any time steps and return the new velocity and position, depends on the chosen method. The class definition and a part of the source code can be found in Appendix 4.
A pickup ion with electric charge of q= 1.6022×10^{-19} [C], mass of one proton m= 1.6726×10^{-27} [kg] and initial velocity of $\mathbf{V}_{init}$= $\mathbf{0}$ [km/s] is launched from $\mathbf{R}_{init} = \mathbf{0}$ [km] when $\mathbf{V}_{sw}$= $+400\,\widehat{\mathbf{x}}$ [km/s], magnetic field $\mathbf{B} = -5\,\widehat{\mathbf{z}}$ [nT] and induced electric field $\mathbf{E} = -2\,\widehat{\mathbf{y}}$ [mV/m].

The general equation of motion for all velocity components (equation 2.10) and their solutions were shown and discussed in chapter 2. Equations 2.12 and 2.13 are the analytical solutions for the equation of motion when $\mathbf{B} = B_z\,\widehat{\mathbf{z}}$. The ion's velocity and trajectory with the conditions above were calculated analytically and also with two different numerical methods; Leap-Frog and Runge-Kutta, forward in time, for time step Δt=0.01 [sec] and 5000 iterations which means for 50 seconds in time. This numerical calculation was done in our simulation model written in C++. Figure 3.1 shows the ion trajectory for the conditions above, calculated theoretically and numerically. In this figure no difference can be distinguished between different methods and the results for all of them seem to be the same, but when it is magnified, the difference between the values of different methods are appeared clearly.

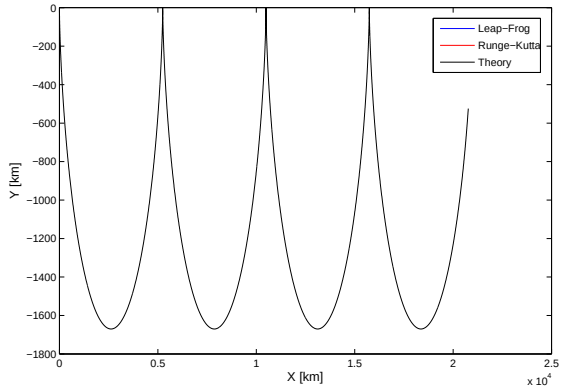

Figure 3.1: Ion trajectory in a uniform electromagnetic field, calculated analytically and numerically.

$\mathbf{V}_{sw}$= +400 $\widehat{\mathbf{x}}$ [km/s], $\mathbf{B} = -5\,\widehat{\mathbf{z}}$ [nT] and $\mathbf{E} = -2\,\widehat{\mathbf{y}}$ [mV/m]

A small part of the Figure 3.1 is zoomed-in and shown in Figure 3.2. We can see, there is a difference between the two numerical method values and the theory. It is clear that Runge-Kutta is more accurate than Leap-Frog and its values are closer to the theory. The difference between the values obtained by numerical methods and theory shows the error for each method. It should be noted that the error depends on the step length and would be changed for different time steps. Figure 3.2 indicates the error for Leap-Frog and Runge-Kutta methods for Δt=0.01 [sec].

3.4 Error Analysis

Different numerical methods make different calculation errors which can be categorized into three groups [2]:

(1) Truncation (approximation) errors,
(2) Round-off errors,
(3) Errors in the input data.

[2]For more details, see chapter 1 in [9]

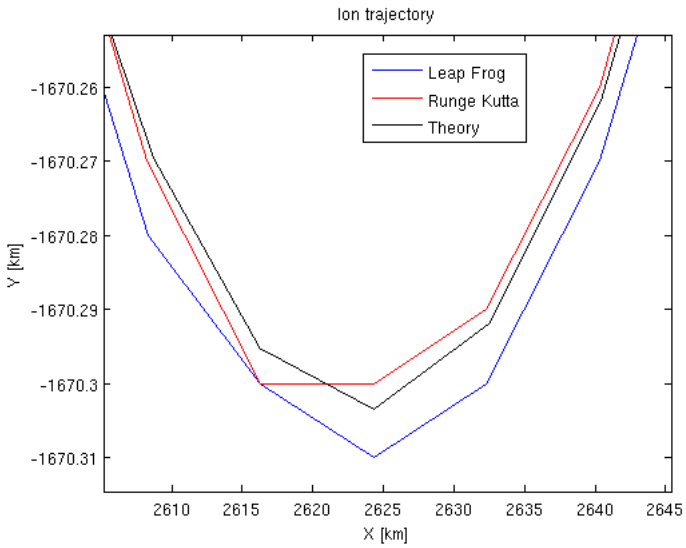

Figure 3.2: A magnified part of the ion trajectories calculated in theory and two numerical methods (Leap-Frog and Runge-Kutta).

The error groups which are discussed in this report are the first and the second ones. They are a function of step length and their error terms vary for different methods. The Leap-Frog and Runge-Kutta error terms were explained briefly in the previous section and it was shown that the error term in Leap-Frog is the order of 3 while in Runge-Kutta is the order of 4 for one time step. These error terms can be used to evaluate our simulation code and their results. The results would be correct if the error terms for our simulation are the same as they are defined theoretically.
If a numerical method has the error of $\mathcal{O}(\Delta t^a)$ where 'a' is the order of error, and this method is used for N=T/Δt step numbers (T can be interpreted as the simulation period), the global error will be:

$$\textit{Global error: } \xi = N\mathcal{O}(\Delta t^a) = \frac{T}{\Delta t}\mathcal{O}(\Delta t^a) = T\mathcal{O}(\Delta t^{a-1}) = T\mathcal{O}(\Delta t^b) \tag{3.9}$$

where 'b' is the global error order which is one degree less than error order 'a'.

To evaluate our simulation and finding global error order, fifteen ions with the same conditions mentioned in the previous section for the pickup ion were launched with different step lengths; once with Leap-Frog and once with Runge-Kutta method. The ions velocities were compared with analytical results and their errors were calculated and plotted in Figure 3.3 as a function of step length.

Figure 3.3 compares two numerical method errors for the step length within the range of [0.001, 0.1]. The global error order for each method is the slope of its error graph in the logarithmic scale which is 3.008 and 1.998 in Figure 3.3 for Runge-Kutta and Leap-Frog methods respectively. This shows that the global error orders are almost the same as they should be and it means that the results we got by using these methods are correct. If we look at Figure 3.3 more carefully, we can see the Leap-Frog error line slope is declined when the step length is decreased. This shows that the error is increased for the smaller step lengths and it is better not to choose the step length

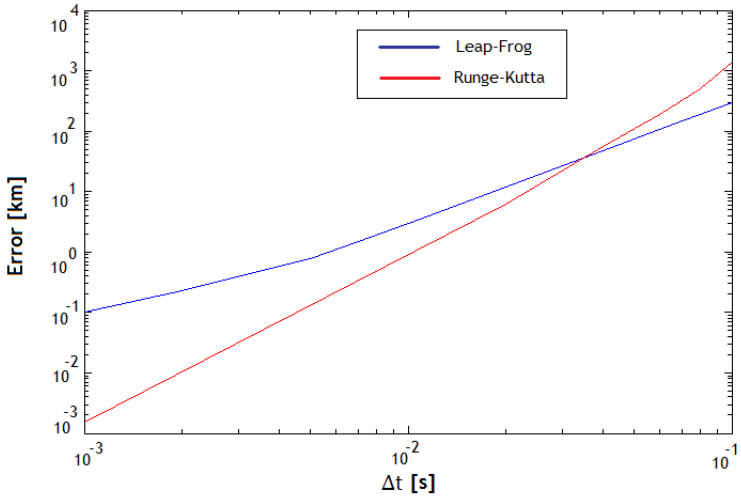

Figure 3.3: Numerical error analysis for Leap-Frog and Runge-Kutta methods for step length $0.001 \leqslant \Delta t \leqslant 0.1$ in the equation of motion.

smaller than 0.007 for the Leap-Frog method in our simulations. For the Runge-Kutta method, the slope is almost constant for whole chosen step lengths.

3.5 Conclusion

Choosing the best numerical method to solve a problem is depend on the problem itself and our expectations from the results. In the order to solve the Lorentz force for computing ion trajectories and finding the ions velocities, among the discussed methods Leap-Frog is chosen and equation 3.7 is used to calculate the velocity because:

1- This method is simple in terms of programming.
2- The method is fast and accurate enough.
3- The error term is reasonable and can be neglected in our application.
4- There is no need for a large memory in the calculation.
5- The method is time reversible. (Simulation can be run forward ($\Delta t \geq 0$) and backward ($\Delta t < 0$) in time).

This method has a problem. It is not a self-starting method ([8]). We have seen before that it was difficult to get the method to be started for the first step because of the halfaway time steps it needs. We solved this problem in this way:

$$\begin{cases} \mathbf{V}_{n+\frac{1}{2}} = \mathbf{V}_n + (\dfrac{\Delta t}{2})\{\dfrac{q}{m}(\mathbf{E}_n + \mathbf{V}_n \times \mathbf{B}_n)\} \\ \\ \mathbf{R}_{n+1} = \mathbf{R}_n + \Delta t\ \mathbf{V}_{n+\frac{1}{2}} \end{cases} \tag{3.10}$$

Choosing a half of the time step, calculating velocity for the half step based on the initial conditions, then computing the position based on the velocity we found and finally, calculating the second half of the velocity. This algorithm as a part of the source code is shown here:

```
.
.
// Calculating velocity for the first half steps.
V = objNum.calcNewVelocity (V, B_Field, E_Field, Mass, 0.5*Delta_t);

for(iStep=0; iStep<NumberOfSteps; i++)
{
        .
        .
        // Computing ion position.
        R = objVect.add(objVect.Mul(Delta_t , V) , R);

        // Calculating velocity for the next step.
        V = objNum.calcNewVelocity (V, B_Field, E_Field, Mass, Delta_t);
        .
        .
}
```

Chapter 4

Hybrid Model and Solar Wind Interaction with the Moon

The dynamics of charged particles were studied in chapter 2 and a numerical method was chosen in chapter 3 to solve the particle's equation of motion. It was explained that in order to find particle's velocity at time t_n, three parameters needed: particle's initial velocity, electric field and magnetic field at time t_{n-1}. It means that particle's initial condition and solar wind electromagnetic field at Δt before the time of our interest should be well-known.
The particle initial conditions velocity and position at $t = 0$ [sec] are assumed to be given, therefore by computing the equation of motion, particle's velocity and position at any time would be taken. The only problem is getting electric and magnetic field at any given time.
Assume that our simulation model, based on Leap-Frog method, is supposed to solve the equation of motion for charge particles. Since the numerical methods are discrete and finding any solution for any given level is related to the one or more steps before that level, the complete data for one or more than one levels of any given level is needed. In the Leap-Frog equation (equation 3.6) the electromagnetic field values for one step before the current step is needed. This means that in our simulation model, we need to have electromagnetic values for the last step only.
Two types of electromagnetic fields (uniform and non-uniform) were explained briefly in chapter 2 and their effects on the particle motion were studied. If we have uniform electromagnetic fields, the values for any numerical step is constant and the same for all steps, but in non-uniform electromagnetic fields, they should be calculated for all steps separately.
In this report, both uniform and non-uniform electromagnetic fields are studied, therefore a method is needed to calculate non-uniform electromagnetic field values for any given step and then to be used in Leap-Frog method to compute particle trajectories. Hybrid model is used to simulate solar wind interaction with the Moon and electric and magnetic fields are calculated as a function of position and stored in a special file format. In consequence, the output file of the hybrid simulation model can be used as a non-uniform field and electromagnetic field can be read at any time for any ion trajectory position.
In this chapter, hybrid model and one of its output file formats are discussed and a method to visualize the hybrid outputs is introduced. The hybrid model outputs are used here to study the electromagnetic field properties at the Moon wakeside and finally is used in chapter 5 as a source of non-uniform electromagnetic fields.

4.1 Plasma and solar wind

The 4^{th} state of matter is called Plasma. Thermonuclear reactions in stars are the sources of plasma in space which makes the energy degradation through radiation at the core of the stars which propagates as highly energetic photons interacting with the matter in their way and ionizes the particles in the space [3]. Some of the plasma properties are:

1. Quasi-neutral: number of electrons and protons are almost the same ($n_e \approx n_p$),

2. Conductor: because it consists of free charges,

3. Kinetic energy of ion is much larger than its potential energy.

(for more details see [2] and [7])

Three fundamental plasma parameters are:

1. Particle density (n_e and n_p measured in $[m^{-3}]$),

2. Temperature (T_e and T_p measured in either [eV][1] or [K]),

3. Steady state magnetic field (**B** measured in [T]).

(for more details see [4] and [2])

The solar wind is the outflow of ionized charged particles (Plasmas), mainly hydrogen (95%) with small fraction of helium, erupted from the Sun, accelerated by the solar corona to form the supersonic solar wind with the velocity of 300 to 1000 [km/s] and the mean velocity value 400 [km/s] at low latitudes in the heliosphere; interacts with all bodies such as planets, satellites, comets, asteroids and etc in its way and affects their magnetospheres, ionospheres and atmospheres if they exist or their surfaces ([7], [6], [2]).

4.2 Kinetic theory and collisionless plasma

In a thermal equilibrium system[2], the single particle velocity distribution function is given by:

$$f(\mathbf{R},\mathbf{V},t) = n\sqrt{(\frac{m}{2\pi k_B T})^3} \quad exp(-\frac{m(\mathbf{V}-\mathbf{u})^2}{2kT}) \tag{4.1}$$

where **R** and **V** are position and velocity vectors, n is number density, T is plasma temperature, m is the particle's mass, k_B is the Boltzmann constant and **u** is plasma flow speed.

The equation of motion in phase space is given by Boltzmann equation:

$$\frac{\partial f}{\partial t} + \mathbf{V}.\nabla f + \frac{\mathbf{F}}{m}.\frac{\partial f}{\partial \mathbf{V}} = 0 \tag{4.2}$$

where **F** is the external force on the particles and is independent on **V** ([2]).
In the collisionless plasma, where the collisions between particles are negligible compared with the

[1] eV: Electron Volt, a unit of energy. 1eV $\simeq$ 11605 [K]

[2] A single temperature can be attributed to the whole system while it is in thermal equilibrium, but it does not mean that the temperature has uniform distribution.

interaction cross-section between particles, the Lorentz force is the only external force which can be applied to equation 4.2. Therefore we get:

$$\frac{\partial f}{\partial t} + \mathbf{V}.\nabla f + \frac{q}{m}(\mathbf{E} + \mathbf{V} \times \mathbf{B}).\frac{\partial f}{\partial \mathbf{V}} = 0 \tag{4.3}$$

Equation 4.3 is called Vlasov equation and is a common equation in kinetic theory.
In collisionless plasma which is the subject of our solar wind assumption, the Coulomb force and drag are neglected and equation 4.3 gives the kinetic description of collisionless plasma. (For more details see chapter 5 in [2], chapter 2 in [1], chapter 10 in [6], chapter 3 in [3] and chapter 2 in [4]).

4.3 MHD equations and hybrid model

A particle trajectory which is moving with finite velocity in a magnetic field is changed because of the exerted force by the magnetic field. The effect of this force is different for electrons and ions, therefore a current is produced. This current can affect the magnetic field, and so the particle motion is modified. Furthermore, electric field is induced by the time-varying magnetic field which changes both the current and magnetic field. Solving the related equations are complicated. The set of these equations are called MagnetoHydroDynamics (MHD) and the Maxwell equations[3], listed in table 4.1.

Table 4.1: Magnetohydrodynamics equations

Gauss's law:	$\nabla.\mathbf{B}=0$	*Poisson's equation:*	$\nabla.\mathbf{E} = \frac{\rho_c}{\epsilon_0}$
Ampère's law:	$\nabla \times \mathbf{B} = \mu_0(\mathbf{J} + \epsilon_0\frac{\partial \mathbf{E}}{\partial t})$	*Faraday's law:*	$\nabla \times \mathbf{E} = -\frac{\partial \mathbf{B}}{\partial t}$
Continuity equation:	$\frac{\partial \rho}{\partial t} + \nabla.\rho\mathbf{V}=0$	*Momentum equation:*	$\frac{\partial \rho\mathbf{V}}{\partial t} + \nabla.(\rho\mathbf{V}\mathbf{V}) = (\mathbf{J} \times \mathbf{B}) - \nabla p$
Induction equation:	$\frac{\partial \mathbf{B}}{\partial t} = \nabla \times (\mathbf{V} \times \mathbf{B}) + \eta\nabla^2\mathbf{B}$	*Energy equation:*	$\frac{\partial e}{\partial t} + \nabla.(e\mathbf{V}) = -p\nabla.\mathbf{u}$
Ohm's law:	$\mathbf{J} = \sigma(\mathbf{E} + \mathbf{V} \times \mathbf{B})$	*Lorentz force:*	$\mathbf{F} = q(\mathbf{E} + \mathbf{V} \times \mathbf{B})$
Ideal gas law:	$p = (n_e+n_p)\mathrm{kT}$		

Hybrid model solves the ion momentum and position equations by using Momentum equation and Lorentz force. N ions are assumed at position $\mathbf{R}_i(t)$ [m] with velocities $\mathbf{V}_i(t)$ [m/s], charge q_i [C] and mass m_i [kg] where i=1,...,N. Charge density of ions $\rho(\mathbf{R}, t)$ $[m^{-3}]$, average velocity $\mathbf{u}(\mathbf{R}, t)$ [m/s] and current density $\mathbf{J}(\mathbf{R}, t) = \rho\mathbf{u}$ $[m^{-2}s^{-1}]$ are defined with spatial averaging[4]. In chapter 2

[3]Hybrid and MHD equations are presented here only but not derived. For derivation refer to any of the space physics or plasma references in bibliography at the end of this report.

[4]Charge and current densities are usually deposited on a grid, using shape function (Hockney and Eastwood, 1989).

was explained that the ion trajectories are computed by the Lorentz force and the equation of motion is:

$$\frac{d\mathbf{R}_i}{dt} = \mathbf{V}_i \quad , \quad \frac{d\mathbf{V}_i}{dt} = \frac{q_i}{m_i}(\mathbf{E} + \mathbf{V}_i \times \mathbf{B}) \quad , \quad i = 1, 2, ..., N.$$

4.3.1 Hybrid assumptions

In hybrid model, several assumptions are taken which are mostly in common for all hybrid solvers:

1. Quasi-neutrality (n_e=n_i): The displacement current is ignored in Ampère's law and $\nabla.\mathbf{J}$=0.

2. Darwin approximation: Ampère's law without displacement current provides the total current. In this assumption the electric field is separated into solenoidal ($\mathbf{E}_s$) and longitudinal ($\mathbf{E}_l$) parts where $\nabla\mathbf{E}_s$=0, $\nabla \times \mathbf{E}_l$=0 and $\partial E_s/\partial t$ are negligible. Then from Ampère's law we get:

$$\mathbf{J} = \frac{\nabla \times \mathbf{B}}{\mu_0} \tag{4.4}$$

3. Massless electron ($m_e/m_p \ll 1$ and $m_e \simeq$0): The electron momentum equation leads to:

$$n_e m_e \frac{d\mathbf{u}_e}{dt} = \mathbf{J}_e \times \mathbf{B} - \nabla p_e + \rho_e \mathbf{E} = \mathbf{0} \tag{4.5}$$

therefore the plasma mass density is only ion mass density $\rho = n_p m_p$ and electron gyro frequency and electron plasma frequency are removed from the calculation due to zero in their denominators.

4. Faraday's law is used to advance the magnetic field in time:

$$\frac{\partial \mathbf{B}}{\partial t} = -\nabla \times \mathbf{E} \tag{4.6}$$

5. $\mathbf{J} \times \mathbf{B}$ and $d\mathbf{J}/dt$ are neglected.

4.3.2 Hybrid equations

Hybrid equation can be written as an Ordinary Differential Equation (ODE) to find $\mathbf{R}_i$, $\mathbf{V}_i$ and $\mathbf{B}_j$, where the magnetic field is stored in a discrete grid $\mathbf{B}_j$.

$$\frac{d}{dt}\begin{bmatrix} \mathbf{R}_i \\ \mathbf{V}_i \\ \mathbf{B}_j \end{bmatrix} = \begin{bmatrix} \mathbf{V}_i \\ \frac{q}{m}(\mathbf{E} + \mathbf{V}_i \times \mathbf{B}) \\ -\nabla_j \times \mathbf{E} \end{bmatrix} \tag{4.7}$$

where $\nabla_j\times$ is a discrete rotation operator and electric field is:

$$\mathbf{E}_j = \frac{1}{\rho}(-\mathbf{J} \times \mathbf{B}_j + \frac{\nabla_j \times \mathbf{B}_j}{\mu_0} \times \mathbf{B}_j) - \nabla p_e \tag{4.8}$$

(for more details about hybrid assumptions and equations refer to [20], [15] and [24])

4.4 Solar wind interactions with objects and visualization

Several methods and softwares exist to simulate plasma flow and solar wind. FLASH code[5] is a programming software which can be used to run hybrid based simulations for modelling the solar wind, its interactions with planets and their satellites and studying the electric and magnetic field variation around celestial bodies. The boundary conditions such as IMF strength and direction, solar wind velocity, plasma density and temperature are applied to the software and the simulation result can be given in HDF5 file format which contains different data such as plasma number density, electric and magnetic fields. The data is stored in different datasets in a file which can be visualized in a software like VisIt.
Hierarchical Data Format version 5 or HDF5 file is organized in a hierarchical structure and is a general purpose library and file format for storing scientific data. Two types of objects can be stored in HDF5 files: datasets and groups. A dataset is essentially a multidimensional array of data elements, and a group is a structure for organizing objects in an HDF5 file. In general HDF5 file is:

1. A completely portable file with no limit on the number or size of data objects.

2. A versatile data model that can represent very complex data objects and a wide variety of metadata.

3. A software library that runs on a range of computational platforms and implements a high-level API with C, C++, Fortran 90, Java and Python interfaces.

Solar wind interaction with Moon was simulated in FLASH code by Mats Holmström and its results are visualized and studied here and in the next chapter.
The output of the hybrid simulation as a HDF5 file is used in our simulation model to compute the ion trajectories and velocities because it provides a virtual reality of non-uniform electric and magnetic field around the Earth's Moon.
One of the new libraries which is used in our simulation code to read HDF5 files is *QuickFlash*[6]. It contains several functions to read HDF5 files. A class named *QFlash* was written in C++ which reads HDF5 files with the usage of QuickFlash library in our simulation code (see Appendix 4). This class and its functions are called to read HDF5 files in our simulation model.
The computed results of ion trajectories are saved in VTK file format which can be visualized in Visit software and ion velocities are saved in a simple text file format.
VisIt is a distributed parallel visualization tool for visualizing data defined on two- and three-dimensional structured and unstructured meshes. It can visualize the data where it is generated and eliminating the need to move the data. VisIt can be controlled by a Graphical User Interface (GUI) or through the Python or Java programming languages.
Visualization Toolkit is a popular toolkit which provides a number of sources and writer objects to read and write data file formats. One of the file formats is VTK which would be used in the next chapters to store the ion trajectories. The advantage of VTK file format is its compatibility with VisIt software. It can be opened, read and shown in VisIt and all of our ion trajectories are saved in this file format. Several templates are defined by the VTK toolkit which are used in different applications ([33]).
A part of our code which stores the ion trajectories in the VTK file format can be found in Appendix 4 .

[5]written by Chicago University. `http://flash.uchicago.edu/website/information/`
[6]Visit quickflash website `http://quickflash.sourceforge.net/home/index.html`

4.5 Solar wind interaction with the Moon

Lack of a global magnetic field and absence of momentous atmosphere make the Earth's Moon as an ideal place for studying solar wind, its properties and effects on solar system objects. Lunar wake signature was found at 85-115 [km] above the Moon with enlarged magnetic fields inside the wake and quite weak fields near the boundary by Lunar Prospector[7] (LP). An ambipolar potential drop of about 300 [V] relative to the solar wind was observed at the wake boundary which decreases electron density and increases electron temperature in the wake [21]. The potential drops about 50 [V] per 1 [km] distance of the surface inside the wake was reported in 1968 [26].
existence of powerless crustal magnetic field which covers up to 20-30 [km] altitude with 50 [nT] strength can not protect the Moon against solar wind hazards. Therefore the solar wind plasma flows onto the Moon and interacts directly with the Moon surface. Thereby, ions are neutralized and leave the interplanetary magnetic field lines and an unstable plasma void is created at the Moon night side, leading to the formation of a plasma cavity and wake structure behind the Moon [23].
In fluid mechanics, when collisional mean free path (λ) is much smaller than the characteristic length of the flow (L), particle-particle interaction dominates over particle-surface interaction, while in the free molecular flow regime ($\lambda \gg L$) it is opposite. In the free molecular regime, no shockwave can be formed in the vicinity of the obstacle and since no bow shock is observed around the Moon, the interaction of the solar wind with the Moon behaves as a free molecular flow [26].
Absence of any intrinsic magnetic field around the Moon, very low electrical conductivity and free molecular flow of solar wind are caused the IMF to convect through the lunar body very quickly. All the charged particles sticking to the Moon are captured by the cold surface of the Moon, neutralized and then re-emitted as cold neutral particles [25]. When the plasma starts moving to the void region, the flow in the surrounding medium is perturbed and finally the magnetic field is perturbed from its interplanetary condition. It has been shown that the magnetic field at the plasma void follows the wave equations and has Laplacian form $\nabla^2\mathbf{B}$=0 [23].
The magnetic field inside the wake is increased while it is decreased outside due to the diamagnetic current system at the wake boundary surface and the pressure gradient across the boundary[21]. Magnetic field structure at the Moon wake as well as IMF orientation and ion thermal speed varies with solar wind β[8] and K_p[9]. It was reported in 1967 [26] that the magnetic field variation and anomalies at the wake are depend on the plasma β factor [25].

Figure 4.1 shows the magnitude of the magnetic field at the equatorial plane of the Moon. The result is obtained from the output of our hybrid model explained in previous section[10] and the result is visualized in VisIt software. It can be seen that the magnetic field has the magnitude of about 7 [nT] at the ramside but is increased at the lunar wake.
Solar wind magnetic field boundary conditions of hybrid simulation is $\mathbf{B}_{sw}$=+4.95 $\hat{\mathbf{x}}$+4.95 $\hat{\mathbf{y}}$ [nT] which magnitude is the same as the values we got in simulation in the ramside. Magnetic field is enhanced inside the wake to B/B_{sw} of 1.1 to 1.3 while it is reduced at the wake boundary to B/B_{sw} of 0.8 to 1 and they can be seen clearly at Figure 4.1. Magnetic field at the boundary between enhanced and reduced region is close to the solar wind. The y-component of solar wind magnetic field is almost the same as the x-component but in our simulation has a little smaller

[7] The Lunar Prospector was a NASA mission, designed for a low polar orbit investigation of the Moon, including mapping of surface composition and possible polar ice deposits, measurements of magnetic and gravity fields, and study of lunar outgassing events. It was launched in January 7, 1998. Visit `http://nssdc.gsfc.nasa.gov/planetary/lunarprosp.html`

[8] Plasma factor $\beta = P_{gas}/P_B$ where P_B is magnetic pressure = $B^2/2\mu_0$ (see [1]).

[9] K_p index estimates the magnetic field disturbances in the horizontal component with an integer number in the range 0-9. For more details see chapter 10 in [1].

[10] done by Mats Holmström in 2009

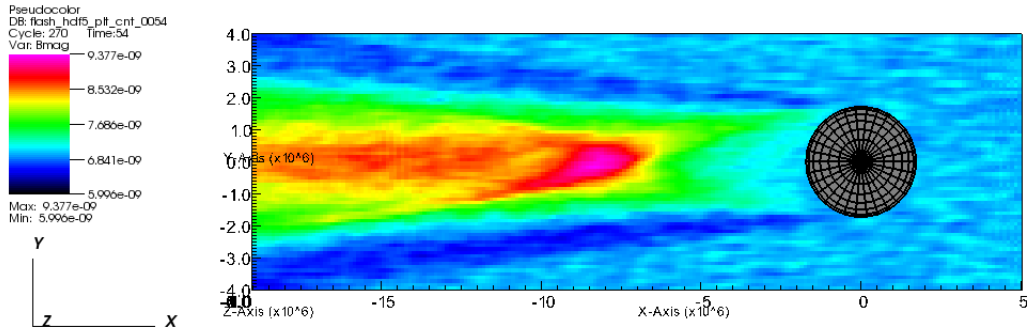

Figure 4.1: Magnitude of the magnetic field variation in tesla at the Moon equatorial plane. The Moon is located at the center of coordinates and is seen from its north pole. x and y axes are in meter.

strength, while the z-component because of the zero initial value is almost close to zero but still can be perturbed at the wake. The same conclusions were obtained from LP and Explorer 35[11] data, reported in several papers which prove our simulation model (see [21], [27], [25]).
Not only the magnetic field but also the electric field, electron density, electron temperature and electrostatic potential are changed at lunar wake. Figure 4.2 shows the magnitude of electric field at the Moon equatorial plane from our hybrid simulation. The x- and y-components of the electric field do not vary too much since the initial magnetic field has only the components along x and y axes and solar wind velocity is along x axis only. Therefore the electric field has mainly variation along z which the variation magnitude is shown in the Figure 4.2. It is increased to E/E_{sw} of 1.1 to 1.5 at the wake.

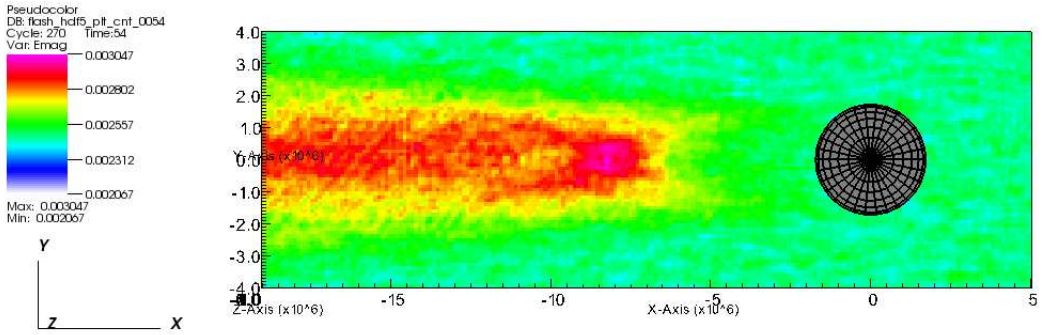

Figure 4.2: Magnitude of the electric field variation in volt per meter at the Moon equatorial plane. The Moon is located at the center of coordinates and is seen from its north pole. x and y axes are in meter.

[11] Explorer 35 was a spin-stabilized spacecraft instrumented for interplanetary studies, at lunar distances, of the interplanetary plasma, magnetic field, energetic particles, and solar X rays. It was launched into an elliptical lunar orbit on July 19, 1967. `http://nssdc.gsfc.nasa.gov/nmc/masterCatalog.do?sc=1967-070A`

LP data analysis shows the electron density drops two orders of magnitude at the wakeside from the solar wind which is correlated with the flow terminator. For the same reason, electrostatic potential is dropped which means that the electrons outrunning the ions faster as they make effort to fill in the wake cavity [21].
It was mentioned before that the lunar wake anomalies in magnetic field magnitude are approximately equal to the solar wind plasma β factor[25]. In this report only the magnetic field deviation is shown and its correlation with solar wind can be studied in future.
A simulation code was written to visualize the magnetic field variation at the Moon wakeside. First a uniform solar wind magnetic field $\mathbf{B}_{sw}$=+4.95 $\widehat{\mathbf{x}}$+4.95 $\widehat{\mathbf{y}}$ [nT] with solar wind velocity $\mathbf{V}_{sw}$= -400 $\widehat{\mathbf{x}}$ [km/s] are assumed. The Moon is located at the center of simulation box (see Appendix 1 about simulation box). A position vector $\mathbf{R}_1$ is taken at -13000 $\widehat{\mathbf{x}}$-4000 $\widehat{\mathbf{y}}$ [km] far from the Moon and out of the simulation box at the Moon wakeside and magnetic field variation as a function of position is calculated according to the function below:

$$\mathbf{R}_{n+1} = \mathbf{R}_n + \frac{\mathbf{B}_{sw}}{|\mathbf{B}_{sw}|} ds$$

'ds' is equaled to 10 [km].
The process is to run at 35 different positions with the step length of 500 [km] along the x-axis toward the Sun. Since the magnetic field is constant, no variation is seen along the field lines and obviously the magnetic field follows its initial condition which is a function of $f(x, y, z)$, $x = y$, $z = 0$ and no deviation is seen in this model, neither at the Moon ramside nor at the wakeside.
The same process was done for the non-uniform electromagnetic conditions by reading the magnetic field data from the output of our hybrid simulation in HDF5 file.
The simulation box in our hybrid model is limited (see Appendix 1), therefore 31 streamlines are taken which are started from $\mathbf{R}_1$ = -9500 $\widehat{\mathbf{x}}$-4000 $\widehat{\mathbf{y}}$ [km] with ds = 10 [km] and $|R_{n+1} - R_n|$ = 500 [km] along the x axis. In the previous example, magnetic field was constant and uniform but here it has different values at different places which should be read from HDF5 file datasets in our simulation code.

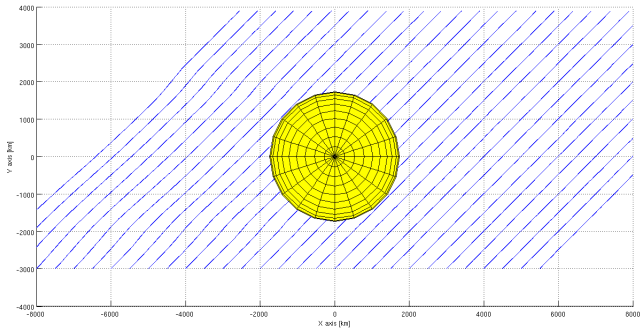

Figure 4.3: Magnetic field deviation at the equatorial plane of the Moon.

Figure 4.3 shows the magnetic field variation at the Moon wakeside in the XY plane. It reveals that the magnetic field streamlines at the lunar wake deviate inward to the Moon which shows that the magnetic strength at the wake is stronger than the other places.

Chapter 5

Ion Trajectories Near the Moon

In previous chapters the dynamics of charged particles was studied and a numerical method was chosen to solve the particles equation of motion. Solar wind interaction with the Moon surface, formation of Moon wakeside and a computational method to simulate solar wind were discussed. In this chapter, the Moon and ion trajectories around it are studied. The backscattered and picked-up ion trajectories and their motions to the nightside of the Moon are discussed. Different solar wind conditions are applied and the ions velocity, kinetic energy and trajectory are calculated numerically and the stored results in the text file format or VTK file format are visualized, studied and explained.
The main part of this chapter is to study the possibility of observing ions with any velocity magnitude and direction at low altitudes above the Moon surface in the Moon wakeside (nightside), coming either from the Moon surface as a backscattered ion or from the Moon tail. It should be noted again that by ion we mean ion trajectory.
This is important to be understood because SARA (Sub-keV Atom Reflecting Analyzer), the IRF[1] instrument onboard Indian satellite Chandrayaan 1[2], is measuring and monitoring solar wind properties at low altitude orbits around the Moon and simulation results can be compared with the real data in future (for more details about SARA see [30], [31] and [32]).
In this chapter, first the ion trajectory in a uniform electromagnetic field, their motion, velocity and energy are studied and then a non-uniform electromagnetic field is applied by reading a hybrid model's outputs (in HDF5 file format, see chapter 4) and the ion properties are analyzed and finally the ion trajectory and velocity at the Moon wakeside and the possibility of observing ions coming from the Moon surface to the wake are investigated.

5.1 Ion trajectory in uniform electromagnetic field

Different numerical methods and their advantages and disadvantages were discussed in chapter 3 and finally, the Leap-Frog method with $0.01 \leq \Delta t \leq 0.1$ [sec] was chosen as the most suitable method to solve the equation of motion (equation 3.1) for our purposes.
In this chapter, the Leap-Frog method with time step length Δt=0.02 [sec] is selected to be used with different initial conditions in the simulation code.
As a first example, a solar wind is assumed with:

[1] Swedish Institute for Space Physics. Official web site: http://www.irf.se
[2] Chandrayaan 1, the first Indian satellite to the Moon was launched in 22 October 2008 from Sriharikota Andhra Pradesh India, orbiting around the Moon in 100 km altitude polar orbit for 2 years.

$$\textit{Solar wind velocity}: \qquad \mathbf{V}_{sw} = -400\,\widehat{\mathbf{x}}\ \ [km/s]$$

$$\textit{IMF}: \quad \mathbf{B}_{sw} = +4.95\,\widehat{\mathbf{x}} + 4.95\,\widehat{\mathbf{y}}\ \ [nT]$$

The conditions above are one of the typical IMF and solar wind velocity states which can be measured at the Moon. In collisionless plasma and from the Ohm's law we get:

$$\textit{Solar wind electric field:} \quad \mathbf{E}_{sw} = -\mathbf{V}_{sw} \times \mathbf{B}_{sw} \tag{5.1}$$

$$\Rightarrow \mathbf{E}_{sw} = +19.8 \times 10^{-4}\,\widehat{\mathbf{z}}\ \ [V/m]$$

Three different pickup hydrogen ions, all with the charge of q= 1.6022×10^{-19} [C], mass of one proton m= 1.6726×10^{-27} [kg] and initial velocity of $\mathbf{V}_{init}$= **0** [km/s] are launched from different positions in our simulation box[3] as follows:

$$\mathbf{R}_{init_1} = +5000\widehat{\mathbf{x}}\ \ [km] \quad , \quad \mathbf{R}_{init_2} = +2000\widehat{\mathbf{x}}\ \ [km]$$

$$\mathbf{R}_{init_3} = -2000\widehat{\mathbf{x}} + 2000\widehat{\mathbf{y}}\ \ [km]$$

The simulation is run for the assumptions above, forward in time with the time step of $\Delta t = 0.02$ [sec] for 20 seconds and the ion's velocity components, velocity magnitude, kinetic energy and trajectories are shown in Figures 5.1 and 5.2.

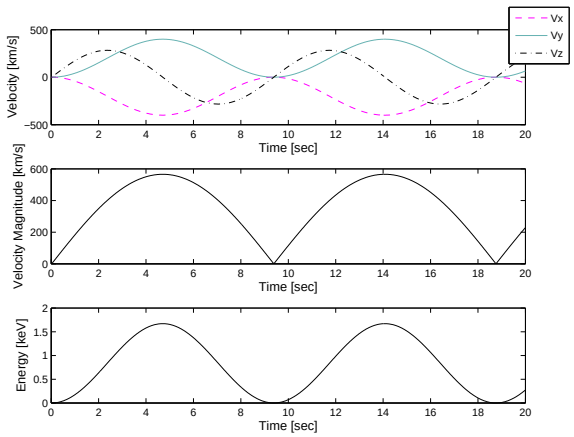

Figure 5.1: From top to bottom: Ion's velocity components ,velocity magnitude and kinetic energy in the uniform magnetic field of $\mathbf{B} = +4.95\,\widehat{\mathbf{x}} + 4.95\,\widehat{\mathbf{y}}\ \ [nT]$ and the solar wind velocity of $\mathbf{V}_{sw} = -400\,\widehat{\mathbf{x}}\ \ [km/s]$

The ions velocity components are illustrated as a function of time in the top panel of Figure 5.1. Since the solar wind conditions and ions initial velocities are the same for all of the pick-up ions,

[3]see Appendix 1 - Simulation box

the velocity functions should be same for all of them too. The velocity component values at time 0 have to be same as the ions initial velocities and it can clearly be seen that the velocity components parallel with magnetic field lines (x and y) oscillate between 0 and the solar wind velocity (±400 [km/s]), whereas the perpendicular velocity component, because of the effect of electric field, fluctuates between -280 and +280 [km/s]. In total, the ion velocity magnitude oscillates between 0 and $400\sqrt{2}$ [km/s] which is shown in Figure 5.1 mid panel. It is easy to calculate the maximum and minimum values of the kinetic energy by having the velocity magnitude. The bottom panel of Figure 5.1 shows the kinetic energy of ions as a function of time in units of keV [4] unit. The maximum ions energy in our example is 1.6703 keV and the minimum is zero.
A particle's gyrofrequency Ω_c was defined in chapter 2 equal to qB/m (equation 2.5). In this example $\Omega_c = 0.6706$ [rad/s] which means the time period is $T_c = 2\pi/\Omega_c = 9.3699$ [s] and it can be seen in Figure 5.1. Ions have their maximum velocity at half a period and reaches again their initial velocity after one gyration.

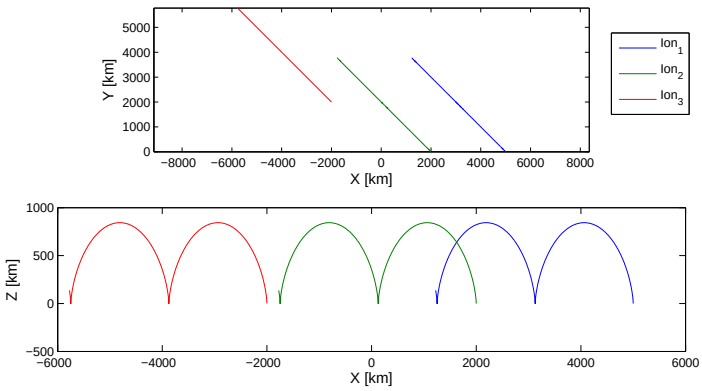

Figure 5.2: Ions trajectories in the XY [top panel] and XZ [bottom panel] plane, launched from $\mathbf{R}_1, \mathbf{R}_2$ and $\mathbf{R}_3$ for 20 seconds.

Figure 5.2 shows three ion trajectories of our example in the XY and XZ plane separately. The top panel shows the ion drift motion which is perpendicular to the both electric and magnetic field lines and the bottom panel illustrates the ions motion along the magnetic field lines. Because of the magnetic field direction which has the both components along the x and y axes and the induced electric field along the z axis, the electric drift velocity which is calculated from equation 2.14 is $\mathbf{V}_{D_E}$ = -0.0014 $\widehat{\mathbf{x}}$ + 0.0014 $\widehat{\mathbf{y}}$ [m/s]. It means that the drift motion is along the -$\widehat{\mathbf{x}}$ and +$\widehat{\mathbf{y}}$ axes, moving to the 2nd quadrant of the coordinate system and it is shown in the Figure 5.2 top panel (for more details about the coordinate system, see Appendix 1). If we assume the Moon as a perfect sphere, located at the center of the coordinate system with a uniform radius of 1737.1 km ([34]), we can easily see from Figure 5.2 that the ion number 2 hits the surface of the Moon. In this example we did not take into account the existence of the Moon, therefore the ion can keep moving freely without any interaction (for the reference frame, see Appendix 1).
The ions gyrations are shown at the bottom panel of Figure 5.2. The ion gyroradius can be calculated from equation 2.8 and is $r_L \approx 843$ [km].

[4] 1keV = 1000 eV , 1 eV = 1.60217×10^{-19} [J]

In the second example, six ions are launched, all from the same initial position $\mathbf{R}_{init} = +5000\widehat{\mathbf{x}}$ [km] in the solar wind conditions the same as the last example, with different initial velocities as follows:

Table 5.1: Ions initial velocities in example 2

	Ion1	Ion2	Ion3	Ion4	Ion5	Ion6
$\mathbf{V}_{init}$	$0.25\mathbf{V}_{sw}^{(*)}$	$0.75\mathbf{V}_{sw}$	$1.0\mathbf{V}_{sw}$	$-0.25\mathbf{V}_{sw}$	$-0.75\mathbf{V}_{sw}$	$-1.0\mathbf{V}_{sw}$

(*): $\mathbf{V}_{sw}$ = -400 $\widehat{\mathbf{x}}$ [km/s]

The simulation is run forward in time with $\Delta t = 0.02$ [sec] for 20 seconds and the ions velocity and kinetic energies are shown in Figure 5.3 and the ions trajectories are illustrated in Figure 5.4. The first column of Figure 5.3 shows the ions velocity components, the second column shows the velocity magnitudes and the last column at the right side of the figure depicts the ions energies. From top to the bottom panels show different ions with the order of ions in table 5.1. We see from the first column that the ions velocity components oscillate with smaller amplitude when their initial velocity become closer to the solar wind velocity and then when it has exactly the same magnitude and direction as the solar wind (ion no.3 in the 3rd row), stops oscillating and keeps moving with the solar wind velocity. When an ion moves in the opposite direction of the solar wind, having higher initial velocity increases the ions velocity amplitude and as it is shown in the second column of the Figure 5.3, the velocity magnitude gets higher which means the kinetic energy is increased. Therefore the highest energy range belongs to the ion with larger initial velocity magnitude and in the opposite direction of the solar wind (ion no.6 in the 6th row) whereas the lowest one is for the ions move with the same velocity magnitude and direction as the solar wind (ion no.3 in the 3rd row).

The ion trajectories of our second example are shown in Figure 5.4. Obviously when an ion has the initial velocity magnitude and direction same as the solar wind, it neither gyrates, nor drifts in a uniform electromagnetic field. This is true otherwise the solar wind direction should be affected by the uniform electric and magnetic field. When the difference between the solar wind velocity and the ion's initial velocity is increased, the ion drifts more.
The more difference between ion's initial velocity and the solar wind velocity, the more gyration and drift for the ions and the first 3 rows of the second column of the figure 5.4 show this event. From the second 3 rows we understand that the cause of having twisted motion for an ion is having an initial velocity in the opposite direction of the solar wind. It provides a force in the adverse direction of motion and pushes the ion back along its motion. In this case, the larger velocity difference with the solar wind velocity provides larger force and gives more twisted motion and finally it follows a complete circular motion when the ion has the same velocity as the solar wind but in the opposite direction.

In summary, an ion in a uniform electromagnetic field and a constant solar wind velocity in time:

(1): starts to gyrate in a plane normal to the magnetic field with the gyrofrequency of Ω_c and gyroradius of r_c.

(2): its velocity magnitude varies between V_{init} which is zero for pickup ion and V_{max}. The V_{max} depends on the difference between ions initial velocity and the solar wind velocity and also the magnetic field strength.

(3): accelerates along the magnetic field with a constant acceleration of $q\mathbf{E}_{\|}/m$. If $\mathbf{E}_{\|} = 0$, the particle moves along the magnetic field with its initial velocity.

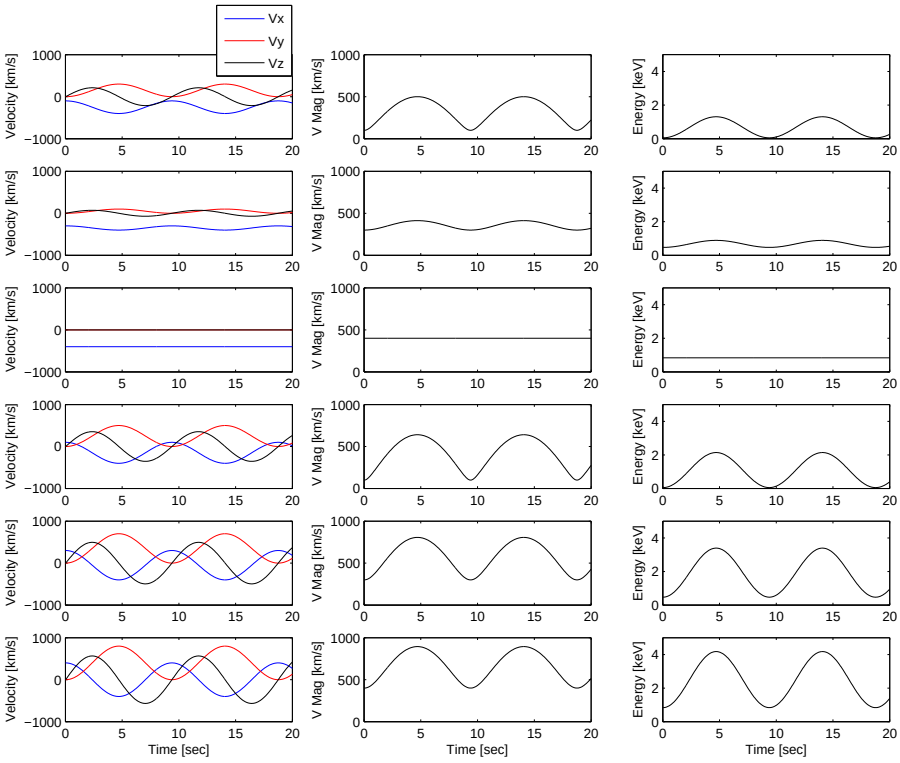

Figure 5.3: Ions velocity components [first column], magnitudes [second column] and kinetic energy [third column] as a function of time for the initial velocity conditions of table 5.1. The 1st row: $\mathbf{V}_{init} = +0.25\mathbf{V}_{sw}$, the 2nd row: $\mathbf{V}_{init} = +0.75\mathbf{V}_{sw}$, the 3rd row: $\mathbf{V}_{init} = +\mathbf{V}_{sw}$, the 4th row: $\mathbf{V}_{init} = -0.25\mathbf{V}_{sw}$, the 5th row: $\mathbf{V}_{init} = -0.75\mathbf{V}_{sw}$ and the 6th row: $\mathbf{V}_{init} = -\mathbf{V}_{sw}$. $\mathbf{V}_{sw}$ = -400 $\widehat{\mathbf{x}}$ [km/s]

(4): drifts perpendicular to both **B** and **E** fields with a drift velocity of $\mathbf{V}_D$.

(5): having initial velocity in the opposite direction of the solar wind makes a force in the opposite direction of the particles motion, starts twisting and changes the drift direction of motion and gets the higher range of kinetic energy.

5.2 Ion trajectory in a non-uniform electromagnetic field

Hybrid model and the way that is used to simulate solar wind interaction with the planets and also the output format of the simulation results were discussed in chapter 4. A hybrid simulation for the solar wind interaction with the Earth's Moon was done by Mats Holmström, and its output in HDF5 file format is used in this section as a real sample of non-uniform electromagnetic fields for studying the ion trajectories near the Moon, especially at the wakeside. Several ions are launched

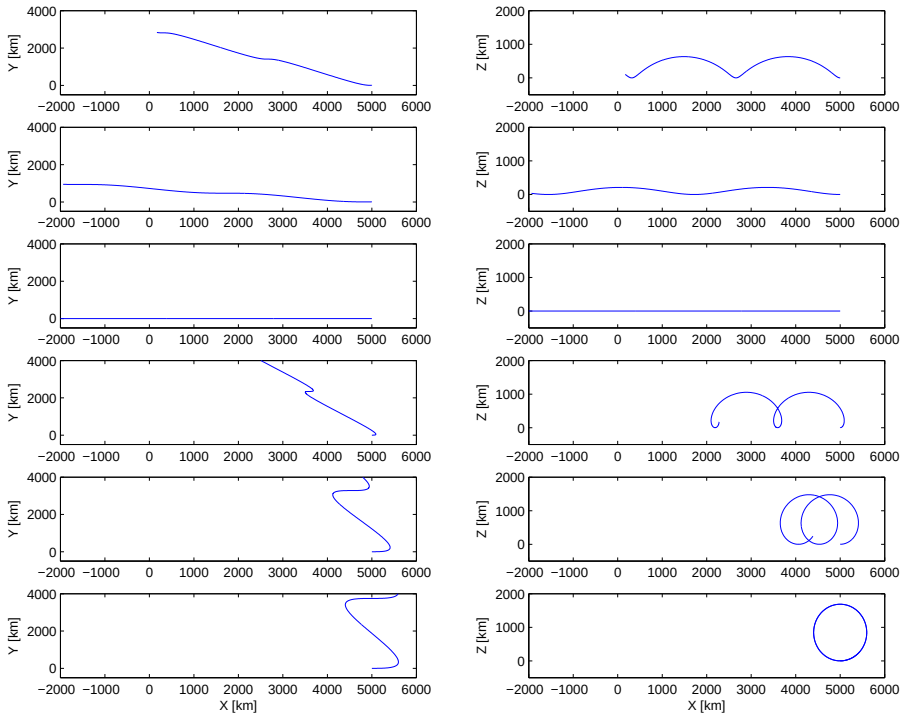

Figure 5.4: Ions trajectory in the XY [first column] and XZ [second column] plane for the initial velocity conditions of table 5.1, launched from the initial position of $\mathbf{R}_{init} = +5000\widehat{\mathbf{x}}$ [km] for 20 seconds.

and their trajectories are saved in VTK file format and visualized in VisIt software (for more details see chapter 4).
Any solar wind hybrid model has its own parameters which are defined before running the simulation code. The size of the simulation box, solar wind velocity and magnetic field strength and direction are the boundary conditions which need to be defined. The hybrid model boundary conditions of the solar wind interaction with the Moon are defined in table 5.2.

Fifteen ions with the same initial velocities of $\mathbf{V}_{init} = -500\,\widehat{\mathbf{x}}$ [km/s] are launched in the solar wind conditions of table 5.2 and in the non-uniform electromagnetic field, from different initial positions as defined in table 5.3. It should be noted that fields in the hybrid result are function of position, not function of time.
The simulation code is run for all of those ions for the time step $\Delta t = 0.02$ [sec] with 2000 time steps and their trajectories, average velocities, gyrofrequencies, average drift velocities and kinetic energies are shown and compared. (For better understanding and easy comparing ions properties, each ion is captioned by a special name). The ion trajectories are shown in figure 5.5.

The Moon with the radius of 1737.1 [km] should be located at the center of this figure but for better visualizing the ions path, it is hidden and the interactions with the Moon surface are

Table 5.2: Inflow boundary conditions in hybrid model

Parameters	**Values**	
Solar wind velocity	-500 $\widehat{\mathbf{x}}$	[km/s]
Electron number density	5.10^6	$[m^{-3}]$
Ion temperature	4.83×10^4	[K]
Electron temperature	10^4	[K]
Magnetic field	4.95 $\widehat{\mathbf{x}}$ + 4.95 $\widehat{\mathbf{y}}$	[nT]

Table 5.3: Ions initial positions

Ion name	$\mathbf{R}_{init}$ [km]	**Ion name**	$\mathbf{R}_{init}$ [km]
AN$^{(*)}$	+9000 $\widehat{\mathbf{x}}$ - 3000 $\widehat{\mathbf{y}}$	AP$^{(**)}$	+9000 $\widehat{\mathbf{x}}$ + 3000 $\widehat{\mathbf{y}}$
BN	+9000 $\widehat{\mathbf{x}}$ - 2500 $\widehat{\mathbf{y}}$	BP	+9000 $\widehat{\mathbf{x}}$ + 2500 $\widehat{\mathbf{y}}$
CN	+9000 $\widehat{\mathbf{x}}$ - 2000 $\widehat{\mathbf{y}}$	CP	+9000 $\widehat{\mathbf{x}}$ + 2000 $\widehat{\mathbf{y}}$
DN	+9000 $\widehat{\mathbf{x}}$ - 1750 $\widehat{\mathbf{y}}$	DP	+9000 $\widehat{\mathbf{x}}$ + 1750 $\widehat{\mathbf{y}}$
EN	+9000 $\widehat{\mathbf{x}}$ - 1500 $\widehat{\mathbf{y}}$	EP	+9000 $\widehat{\mathbf{x}}$ + 1500 $\widehat{\mathbf{y}}$
FN	+9000 $\widehat{\mathbf{x}}$ - 1000 $\widehat{\mathbf{y}}$	FP	+9000 $\widehat{\mathbf{x}}$ + 1000 $\widehat{\mathbf{y}}$
GN	+9000 $\widehat{\mathbf{x}}$ - 500 $\widehat{\mathbf{y}}$	GP	+9000 $\widehat{\mathbf{x}}$ + 500 $\widehat{\mathbf{y}}$
O	+9000 $\widehat{\mathbf{x}}$		

(*): N denotes Negative, used for the ions which their initial positions are at the 4^{th} quadrant of the equatorial plane.

(**): P denotes Positive, used for the ions which their initial positions are at the 1^{st} quadrant of the equatorial plane.

neglected. The Moon wakeside is at the left side of the figure and the Sun is far beyond to the right. We can see that the x-component of the magnetic field is almost constant at the Moon dayside with nearly the same value chosen in the hybrid model as upstream boundary conditions (see table 5.2). At the wakeside, the story is different. Both electric and magnetic fields vary from time to time and place to place. In our model at some places at the wake, the magnetic field has the highest strength and of course these variations affect the ions trajectories, velocities and finally their kinetic energies.

The trajectories of fifteen ions of our example are shown in Figure 5.5 with the black color lines. The name of each ion is written near its initial position at the right side of the figure. The ions are separated into three groups: the ions with the positive initial position at the y axis are named 'P-ions' and denoted by P at the end of their name. The ions with the negative initial position at the y axis are called 'N-ions' and denoted by N at the end of their name and the third group is only 'O-ion' which passes the center of the Moon. The first letter of the ions name is used to determine ions only. There is another definition we use for these ions. The ions which pass either near the Moon surface/terminator like DN and DP or go through the Moon region such as EN, EP, FN, FP, GN, GP and O are named 'in-ions'. The rest are called 'out-ions'.

We can clearly see that the ions deviate to the wakeside and their trajectories are bent to the region with the higher magnetic and electric field strength. The deviation for DN and DP ions are more than the others in our example. These ions pass very close by the Moon terminator and turn aside to the wake. Obviously the ions which are far from the wake perturbation such as AN, BN, AP and BP are not affected as much as the other ions and keep moving almost at the same electromagnetic conditions they have had since start at the dayside.

Here some questions might pop up in our mind. What does make DN and DP to be different with the others? Are the other ions such as FN, GN, O, FP and GP which are passing the wake at different electric and magnetic field conditions compared to their initial positions showing any

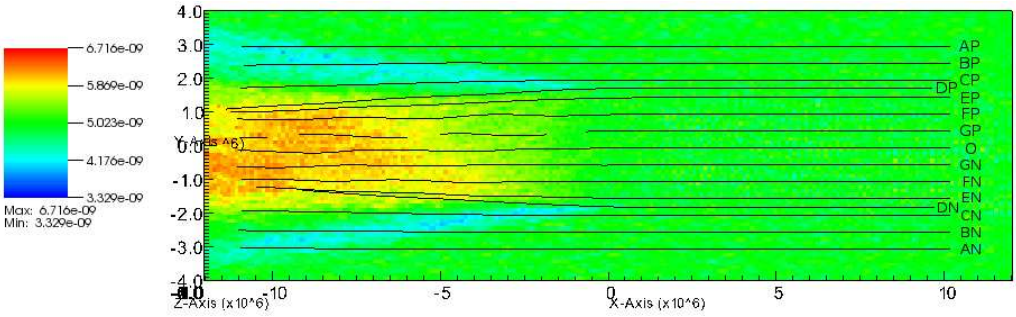

Figure 5.5: Ion trajectories in a non-uniform electromagnetic field shown in VisIt software. The simulation box is in meter, magnetic field is in tesla and ion trajectories are shown at the Moon equatorial plane. The x-component of the magnetic field is shown in color and the colorbar displays the magnetic field variation range. The horizontal axis is the x-axis and the vertical axis is the y-axis. For different ions positions see table 5.3.

deviation or drift motion?
Answering these questions need deep understanding of ion properties. Since Figure 5.5 shows only the ion trajectories, we collected all the ions properties we could have from our simulation, such as velocity components, energy, electric field and magnetic field for any time steps and stored them separately for each ion in a text file format. Next figures show plots of those files done in Matlab.

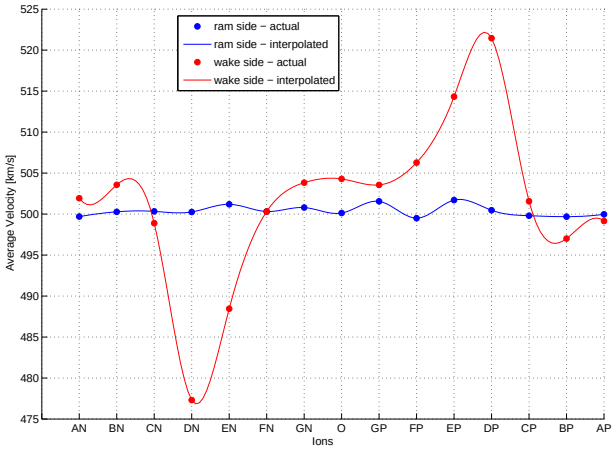

Figure 5.6: Ions actual and interpolated average velocity upstream of the Moon (blue dots and blue curve) and downstream (red dots and red curve).

Figure 5.6 compares the average velocity of fifteen sample ions at the Moon ramside and wakeside. The actual value of each ion is shown by a dot and the interpolated values is plotted by a curve.

The blue curve indicates the average velocity at the Moon ramside. It can be clearly seen that most of the ions have the constant velocity same as the solar wind, except some of the 'in-ions' which pass the region between the Moon center and the Moon terminator at the first quadrant of the equatorial plane. Those have slight fluctuations due to the electric and magnetic field variations. It should be noted that it was assumed there is no interaction between the solar wind and the Moon in this example and particles go through the Moon.

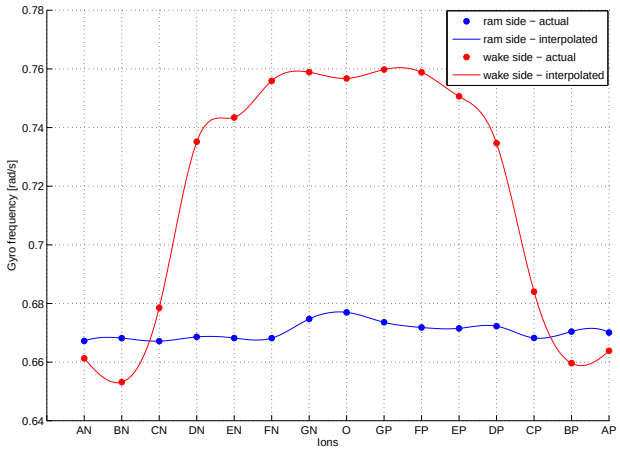

Figure 5.7: Ions actual and interpolated gyrofrequency at the upstream of the Moon (blue dots and blur curve) and downstream (red dots and red curve).

In contrast, the ion average velocities at the wakeside are revealed by the red curve. According to the graph of the wakeside, ions DN and DP have the lowest and highest average velocities respectively. The ions average velocity has a dip of 477 [km/s] for DN ion, while it has a peak of 522 [km/s] for DP ion. It can be interpreted that ions with initial position close to the Moon terminator along the y axis at the fourth quadrant of the equatorial plane have the lowest average velocity but the ions at the opposite position in the first quadrant have the highest average velocity among the other ions at the Moon wakeside. For both DP and DN ions, the difference between the ions average velocity and the solar wind velocity is almost the same and is equal to 22 [km/s] but of course with the opposite direction. The average velocity is changed when the ions initial position moves further from the Moon along the y axis and become almost the same as the solar wind velocity with a trivial difference due to the electromagnetic perturbation.

In conclusion, the ions which come from the fourth quadrant of the Moon equatorial plane (x¿0 and y¡0) and pass the Moon close to the terminator have lower velocity than the solar wind, lose their energy and because the magnetic field is increased at the nightside, the ions are drifted inside the wake. On the contrary, the incoming ions from the first quadrant of the Moon equatorial plane (x¿0 and y¿0) which pass close to the Moon terminator have higher velocity which means they are accelerated more and have higher kinetic energies. In addition, the magnetic field is increased and the ions are forced to bend to the wakeside. This phenomenon was shown in the previous section for a uniform electromagnetic field in Figure 5.4. It was shown that when the ion velocity with the same direction as the solar wind is increased up to the solar wind velocity magnitude,

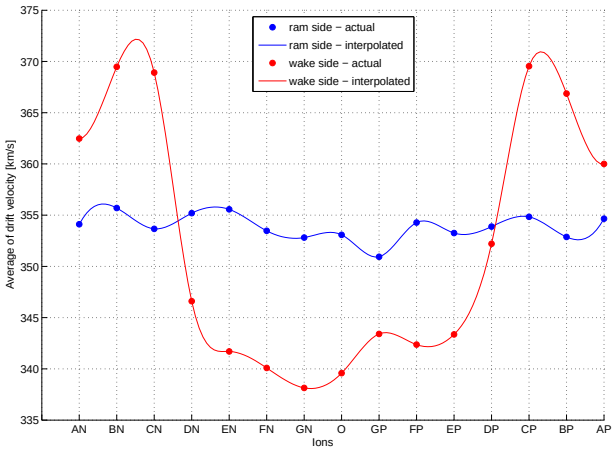

Figure 5.8: Ions actual and interpolated average drift velocity upstream of the Moon (blue dots and blur curve) and downstream (red dots and red curve).

the ion trajectories are drifted less and become more parallel with the solar wind direction; but in contrast, decreasing ion velocity causes the ions to drift more and lets the velocity to become closer to the magnetic field direction. The same event happens in the non-uniform electromagnetic field but because of the stronger magnetic field at the Moon wakeside, the ions with the higher and lower energy than the solar wind are moved to the lunar wake.

The ions gyrofrequency at the Moon ramside and wakeside and their comparison are shown in Figure 5.7. The same as Figure 5.6, the ramside actual values are shown by blue dots and the wakeside actual values are displayed by red dots. The interpolated function for each side is shown by a curve.

The gyrofrequency at the ramside almost remains constant, whereas in the wakeside there is a gradual rise for the 'in-ions'. There is also a dramatic variation in the gyrofrequency for the ions near the Moon terminator compare with the other regions. It implies that the magnetic field at the wakeside is stronger than the other places, but it neither is constant, nor symmetric at the wake. Equation 2.5 in chapter 2 shows that the gyrofrequency is a function of magnetic field and from Figure 5.7, obviously can be seen that the 'P-ions' have the higher gyrofrequency to compare with the contemporary 'N-ions'. It reveals that the magnetic field at 'P-ions' region is stronger than the other places at the wake.

Ions average drift velocity (see chapter 2) at the Moon dayside and nightside are shown and compared in Figure 5.8. There is a small fluctuation in the drift velocity at the ramside but again we see that there is a large difference between the 'in-ions' and 'out-ions' drift velocity at the wake. Among the 'in-ions', the drift velocity is considerably lower for the 'N-ions' to compare with the contemporary 'P-ions' due to the electric and magnetic field differences.

For better understanding of ions properties especially at the wakeside, the ions kinetic energies are plotted in Figure 5.9. The kinetic energy at the ramside is almost constant while it fluctuates at the wake. As we discussed earlier, and we see in this figure, the 'N-ions' energy which pass close to the Moon is decreased 15% and in the contrast there is 15% increase for the 'P-ions' at the same position. It can also be seen that the most energy inconstancy belongs to the 'P-ions' at

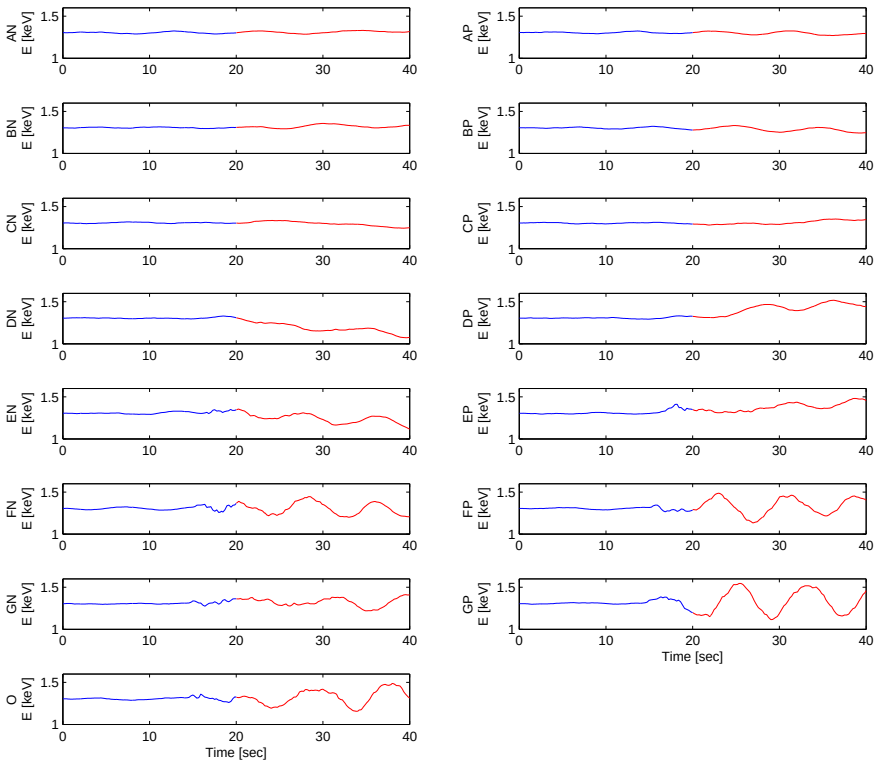

Figure 5.9: Ions kinetic energy variation at the upstream of the Moon (blue dots and blur curve) and downstream (red dots and red curve) as a function of time.

the wakeside.

Figure 5.10 shows the ion trajectories from three different views. Figure 5.10 (a) shows the ion trajectories at the XY (equatorial) plane, the same as Figure 5.5 but more clear. In Figure 5.10 (c) we see that the 'in-ions' vary along the Z axis more than the others, especially those ones which pass the center of the Moon. This can also be seen in Figure 5.10 (b), but it is not that clear for all ions.

The electric and magnetic field variations along the ion trajectories for the DP and DN ions are shown in Figure 5.11 top and bottom panels respectively. As it was explained before, both electric and magnetic fields are increased at the wakeside, especially at the second quadrant of the equatorial plane. We see that the maximum magnetic field strength for DP ion is 8.49 [nT] while for DN is 0.27 [nT] less. Moreover, the maximum electric field for DP ion is 0.16 [mV/m] higher than the maximum electric field for DN for the whole simulation area.

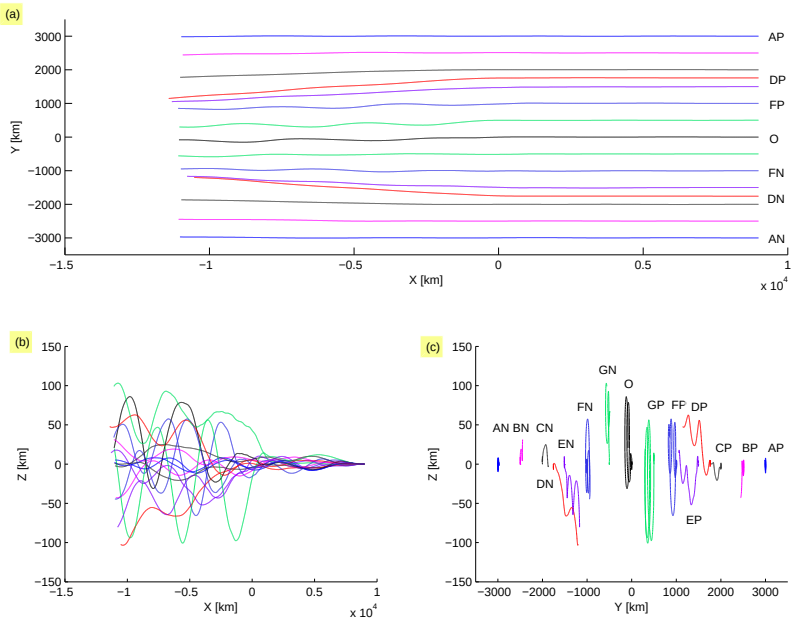

Figure 5.10: Ions trajectories in the (a) XY (b) XZ (c) YZ planes.

5.3 Ion trajectories interaction with the lunar surface

The Moon, its interaction with the solar wind and the formation of its wake were discussed in chapter 4 and the properties of the wake, variation of electric and magnetic field and how the plasma cavity behind the Moon is formed were explained briefly.
In this section, the ion trajectories coming from the Moon surface to the Moon wakeside with the same velocity magnitude as the solar wind but in different velocity angles are described. Their initial velocity magnitude and direction when they leave the Moon and their initial position at the Moon surface are studied and described.
In this order, a fixed observer position at the Moon wakeside is assumed and the ions with the final velocity magnitude of the solar wind but in all possible directions at observer position are launched backward in time. The ions trajectories are continued until they hit the Moon surface or go out of the simulation box. When any of them hits the Moon surface, its velocity and position at the surface are the initial velocity and position for that ion trajectory. It means that if an ion with those initial conditions is launched forward in time, it would have been reached to the observer at the wakeside with the final velocity of our interest.
To make this issue more clear, let's assume that the Chandrayaan-1 satellite is located at the Moon wakeside and its onboard instrument, SARA, is the observer we were discussing about. We want to find out the source of the incoming ions to the observer and first we want to know if it is possible to see any ion coming from the Moon surface to the observer position or not and second if the answer is yes, we would like to know from where that ion comes from and at which initial velocity. Of course in the case of the Earth's Moon, there are several sources for incoming ions

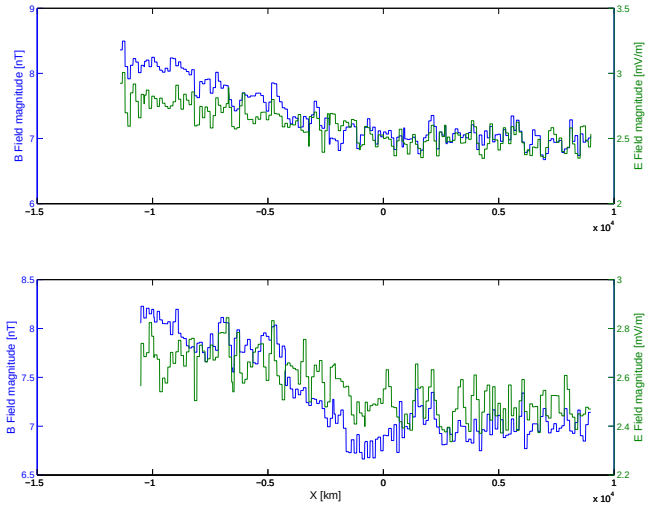

Figure 5.11: Electric and magnetic fields along the ion trajectories: DP [top panel] and DN [bottom panel].

to the observer position such as the solar wind itself, Moon surface, Earth magnetosphere and etc. Studying the ion's trajectory when the Moon passes the Earth's bow shock and goes to the magnetosphere is not the subject of this research, therefore we assume the Moon is somewhere out of the Earth's magnetosphere.
Under the assumptions above, we want to find out:

(1): What is the final velocity direction of the incoming ions from any place at the Moon surface to the observer position, if the final velocity magnitude has to be the same as the solar wind?

(2): From which places on the Moon surface (in longitude and latitude) does the ions reach the observer position?

(3): What are the initial velocity and the kinetic energy of those ions in the latest questions?

(4): Is it possible that several trajectories leave the Moon surface at the same initial position but with different initial velocity and reach the observer? If yes, how many or how much in percentage of the total ions?

(5): Which fraction of total incoming ions from the Moon surface are coming from the dayside?

Assume that the observer is at 100 [km] altitude from the Moon surface in the equatorial plane at the wakeside with the subsatellite point longitude of +180° and latitude of 0° (see Appendix 1). Therefore the observer position from the center of the Moon is $\mathbf{R}_{obs}$ = -1837.1 $\widehat{\mathbf{x}}$ [km]. If the solar wind has the constant velocity of $\mathbf{V}_{sw}$ = -400 $\widehat{\mathbf{x}}$ [km/s] and the uniform IMF to be $\mathbf{B}$ =

4.95 $\widehat{\mathbf{x}}$+4.95 $\widehat{\mathbf{y}}$ [nT], the induced electric field will be $\mathbf{E}$ = 1.98 $\widehat{\mathbf{z}}$ [mV/m] (see equation 5.1).
If the ions final velocity directions are defined in a spherical coordinate system, each velocity vector would have three components: velocity magnitude $|\mathbf{V}_{obs}|$ which is the same as the solar wind velocity, elevation θ and azimuth φ angles which are defined as $|\mathbf{V}_{obs}| = 400$ [km/s], $-90° \leqslant \theta \leqslant +90°$, $0° \leqslant \varphi$¡360° and the angular resolution is one degree (For more details see Appendix 1). Hence, for any observer position, there are 179×360 + 2 = 64442 velocity vectors. (when $\theta = \pm 90°$, the vector would be the same for all azimuth angles and that is why they are counted as 2 vectors only at ±90° elevation angle).
The ion's velocity at the observer position for any azimuth and elevation angle is calculated as follows:

$$\begin{cases} V_{obs_x} = |\mathbf{V}_{sw}|\ \cos(\varphi)\ \cos(\theta) \\ \qquad\qquad\qquad\qquad\qquad -90° \leqslant \theta \leqslant +90° \\ V_{obs_y} = |\mathbf{V}_{sw}|\ \sin(\varphi)\ \cos(\theta) \\ \qquad\qquad\qquad\qquad\qquad 0° \leqslant \varphi < 360° \\ V_{obs_z} = -|\mathbf{V}_{sw}|\ \sin(\theta) \end{cases}$$

64442 ions are launched from $\mathbf{R}_{obs}$ = -1837.1 $\widehat{\mathbf{x}}$ [km] with the $|\mathbf{V}_{obs}|$=400 [km/s] for different velocity angles with one degree resolution, backward in time with Δt=-0.02 [sec], until they either hit the Moon surface with the radius of 1737.1 km, located at the center of coordinate system or they go out of the simulation box with the size of $-5000 \leq x \leq +5000$ [km], $-4000 \leq y \leq +4000$ [km] and $-4000 \leq z \leq +4000$ [km] (see Appendix 1). Achievement to the conditions mentioned above stops the simulation process for each ion separately.

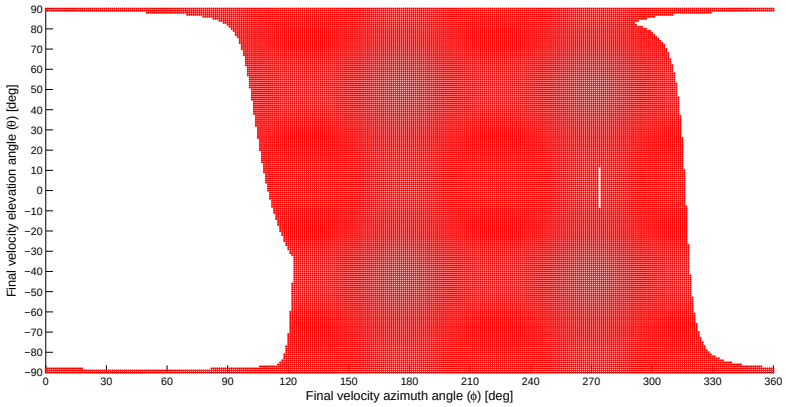

Figure 5.12: Ions final velocity directions which are coming from the Moon surface. The ion velocity magnitude is 400 [km/s] and $\mathbf{R}_{obs}$= -1837.1 $\widehat{\mathbf{x}}$ [km], where the $\widehat{\mathbf{x}}$ axis is pointing to the Sun.

Figure 5.12 shows the ions final velocity directions at the observer position (-1837.1 $\widehat{\mathbf{x}}$ [km]) which are coming from the Moon surface. Statistically around 58% of the ion trajectories of our example are coming from the surface and shown by the red color in the figure.
The fraction of the incoming ion trajectories with the solar wind velocity from the Moon surface and the final azimuth velocity angles of $0° \leqslant \varphi \leqslant 90°$ and $330° \leqslant \varphi$¡360° (almost opposite to

the solar wind direction) and the elevation angles between -85 and +85 is nearly zero and for the other velocity directions is high. There is also a void region for the azimuth angle of 275° and the elevation between -7° and +12° that our observer could not see any incoming ions from the Moon surface. Since this region is very tiny and the angular resolution of our simulation is one degree, we can not say anything definitely to be true about it. It can be factual or it may happen either because of numerical errors or due to the definition of initial conditions. Now the question is from which side of the Moon do the ions come from?

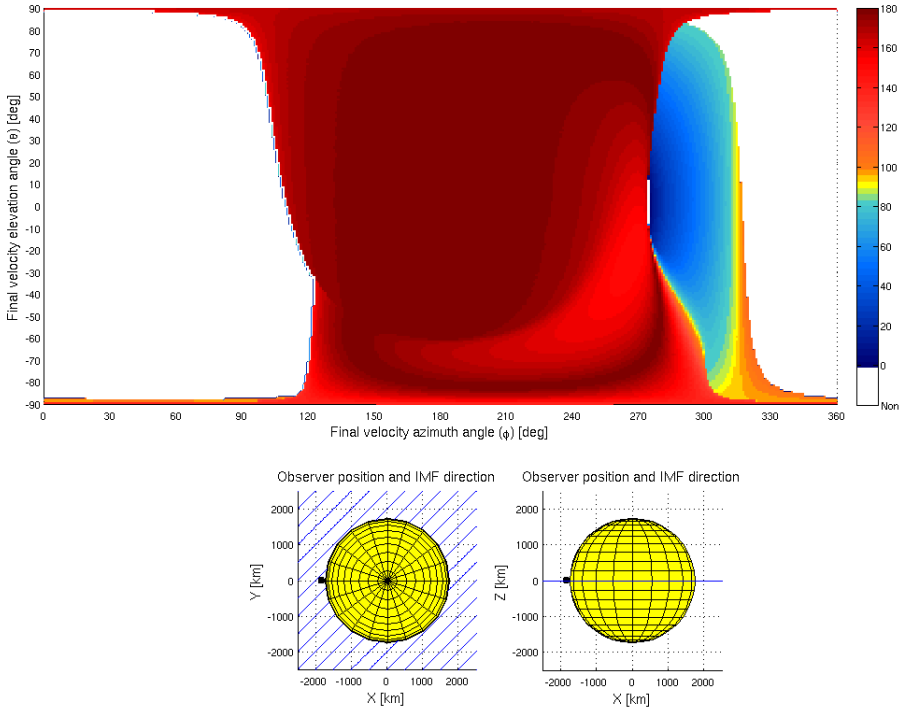

Figure 5.13: [Top panel] The SZA of the trajectory's initial point on the Moon surface as a function of final velocity direction at the observer position. The white color region captioned my NON in the colorbar means there is no interaction with the Moon surface for those final velocity angles. [Bottom panel] IMF direction around the Moon shown by blue lines and the observer position.
$\mathbf{R}_{obs}$ = -1837.1 $\hat{\mathbf{x}}$ [km], $|\mathbf{V}_{obs}|$ = 400 [km/s], $\mathbf{V}_{sw}$ = -400 $\hat{\mathbf{x}}$ [km/s] and $\mathbf{B}$ = 4.95 $\hat{\mathbf{x}}$+4.95 $\hat{\mathbf{y}}$ [nT]

The ion's initial position as a function of Solar Zenith Angle (SZA)[5] at the Moon surface is shown in top panel of Figure 5.13 as a function of final velocity direction at observer position. The horizontal and vertical axes of the plot show the final velocity azimuth and elevation angles respectively and the initial position as a function of SZA is illustrated by the color. The trajectories final velocity angle that do not intersect the Moon are indicated by white color.
As we see from the color bar, the majority of ion trajectories have the SZA larger than 90° as their initial position, which means that they come from the nightside of the Moon. Among the incoming ions from the Moon surface with the same velocity magnitude as the solar wind, only

[5]For more details about SZA and its definition see Appendix 1.

13% of them come from the dayside and around 0.5% from the $85° \leqslant SZA \leqslant 95°$ to the observer position; shown by the blue and yellow colors in Figure 5.13 top panel respectively. We can also claim that if we observe an ion with the final velocity azimuth angle between 275° and 310°, most probably it comes from the dayside, especially when it has elevation angle larger than -20°.
It can be seen when the ions final velocity azimuth angle is between 130° and 270° that their initial SZA would be larger than 140° and almost 3/4 of them have the SZA near 180°.
The Moon, observer position and the IMF direction in the XY and XZ planes are shown in Figure 5.13 bottom panel. Clearly the direction of IMF is the same as it was shown in chapter 4.

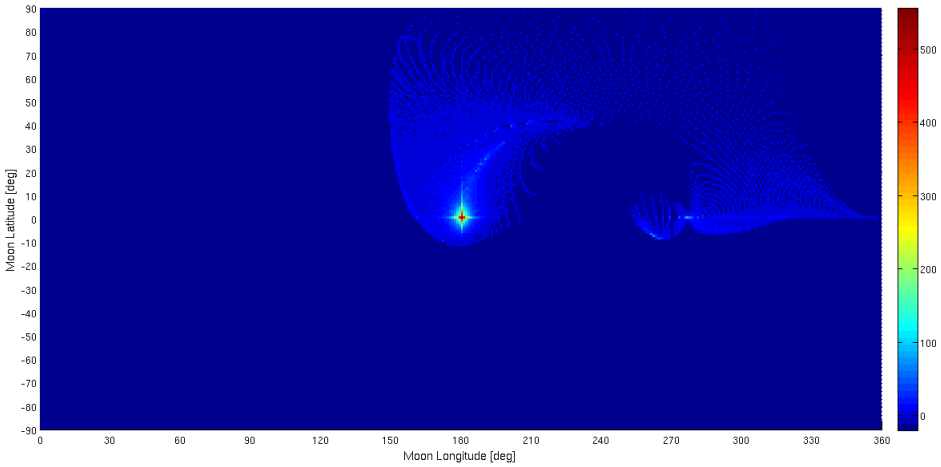

Figure 5.14: Number of ions trajectory starting points at the Moon surface per 1×1 degree bin, moving to the Moon wakeside at uniform electromagnetic field.
$\mathbf{R}_{obs}$ = -1837.1 $\hat{\mathbf{x}}$ [km], $|\mathbf{V}_{obs}|$ = 400 [km/s], $\mathbf{V}_{sw}$ = -400 $\hat{\mathbf{x}}$ [km/s] and $\mathbf{B}$ = 4.95 $\hat{\mathbf{x}}$+4.95 $\hat{\mathbf{y}}$ [nT]

Figure 5.14 shows the number of ion trajectories initial positions at the Moon surface, leaving the Moon and moving to the observer position with the final velocity magnitude of solar wind velocity. The horizontal and vertical axes in this figure show the Moon longitude and latitude respectively (For more details about the Moon longitude and latitude definitions, see Appendix 1). The whole Moon surface is shown with dark blue color and the number of ions trajectories are displayed with the color bar.
It can be seen that the majority of ion trajectories to the observer position come from the Moon northern hemisphere but as it was discussed before, most of them come from the nightside, especially from the the solar point (see Appendix 1). Figure 5.14 reveals that more than 500 ion trajectories among the number of ions in our simulation have the initial position at the solar point. This does not mean that all of them have exactly the same initial position, but it happens due to the one degree resolution of our simulation and since the observer is so close to this region. For better understanding, some of the ions and the places they start their trajectories at the Moon surface are shown in Appendix 2.
Ion's initial velocity magnitude at the Moon surface is shown by the colorbar in Figure 5.15 as a function of final velocity direction at the observer position. Figure 5.15, instead of Figure 5.13 which shows the ions SZA at the Moon surface, displays the magnitude of ions initial velocity at the Moon. As we can see, there is a large difference between the velocity magnitude of different ions at the Moon surface. If we choose a specific place on the Moon to launch an ion and we expect

to be reached to our observer position with the velocity magnitude of 400 [km/s], it should have an especial initial velocity where its velocity magnitude can be specified from Figure 5.15 and the position can be obtained from Figure 5.13. Of course from the mentioned figures, the exact ion initial position and velocity magnitude can not be specified but they show some general views of those ions characteristics as a function of SZA and velocity magnitude.

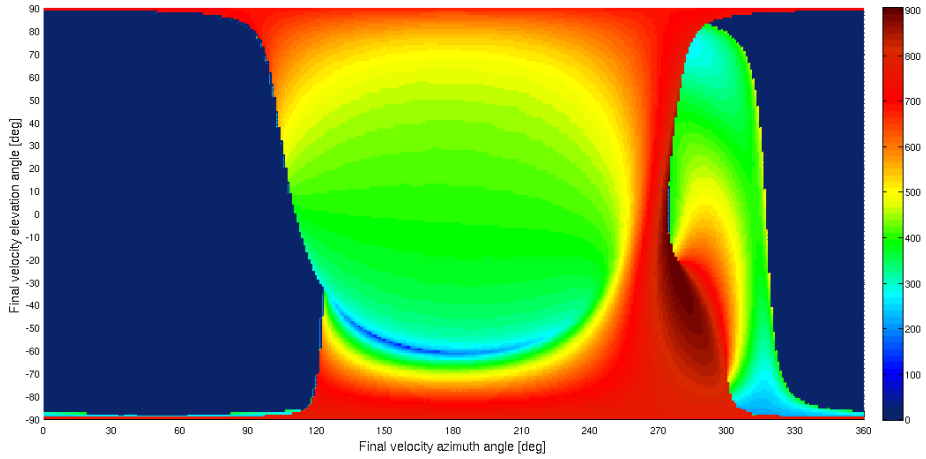

Figure 5.15: Ions initial velocity magnitude at the Moon surface shown by color map as a function of trajectorys velocity direction at the observer position indicated by azimuth and zenith angles. $\mathbf{R}_{obs}$ = -1837.1 $\widehat{\mathbf{x}}$ [km], $|\mathbf{V}_{obs}|$ = 400 [km/s], $\mathbf{V}_{sw}$ = -400 $\widehat{\mathbf{x}}$ [km/s] and $\mathbf{B}$ = 4.95 $\widehat{\mathbf{x}}$+4.95 $\widehat{\mathbf{y}}$ [nT]

The average of ion trajectories initial velocity magnitude and direction at the Moon surface are shown in Figures 5.16 and 5.17. We discussed about Figure 5.14 and showed that majority of ion trajectory initial positions come from the Moon latitude larger than -10° and we can see from Figure 5.16 that by increasing the initial position latitude, the initial velocity magnitude is increased. Since the observer is located at the Moon equatorial plane, all ion trajectories have the same initial velocity magnitude as the solar wind velocity at the Moon equator and around it, either at the Moon dayside or nightside. By moving from the equator and going close to the north pole, the initial velocity magnitude is increased from 400 [km/s] to 900 [km/s] which means that the incoming ions from higher latitudes need larger velocity magnitude to be observed by the observer at the equator. Comparing ion trajectory initial velocities at the Moon dayside and nightside shows that their velocity magnitudes have almost the same values for the same latitudes. For instance, the ions with the initial latitude of 0° have the initial velocity magnitude of around 400 [km/s].

Figure 5.17 indicates that the ion trajectory initial velocity elevation angle at the Moon nightside is almost negative while it has positive angle at the dayside. At the higher latitudes, either for the nightside or dayside, the elevation angle is close to zero. Because of the observer position, it is understandable that the ions with the high initial latitude should have zero or negative velocity elevation angle to reach the observer at the equatorial plane and the colorbar proves our postulation (see Appendix 3).

We discussed earlier that our observer can be assumed to be SARA, the Chandrayaan onboard instrument. In the latest example, the observer was considered to be fixed in its position and all the results explained earlier are for that specific location. Since the satellite moves and the

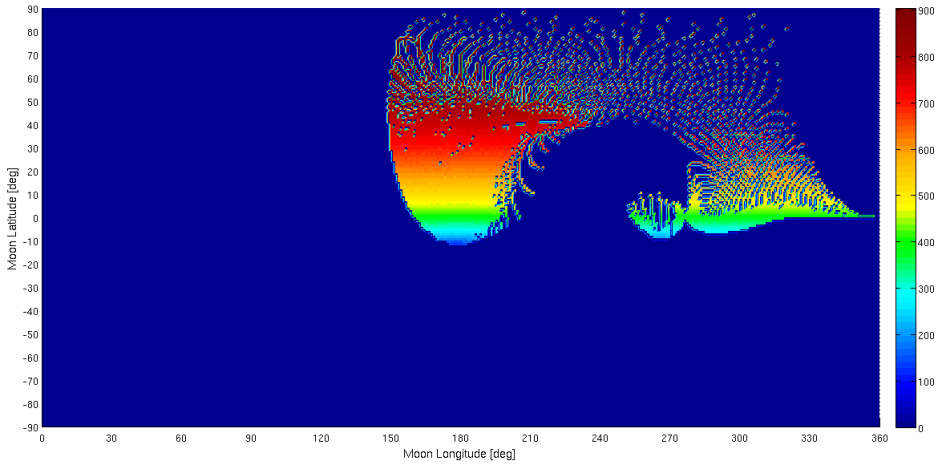

Figure 5.16: Average of ion trajectories initial velocity magnitude at the Moon surface as a function of Moon solar orbiting long/lat

$\mathbf{R}_{obs}$ = -1837.1 $\hat{\mathbf{x}}$ [km], $|\mathbf{V}_{obs}|$ = 400 [km/s], $\mathbf{V}_{sw}$ = -400 $\hat{\mathbf{x}}$ [km/s] and $\mathbf{B}$ = 4.95 $\hat{\mathbf{x}}$+4.95 $\hat{\mathbf{y}}$ [nT]

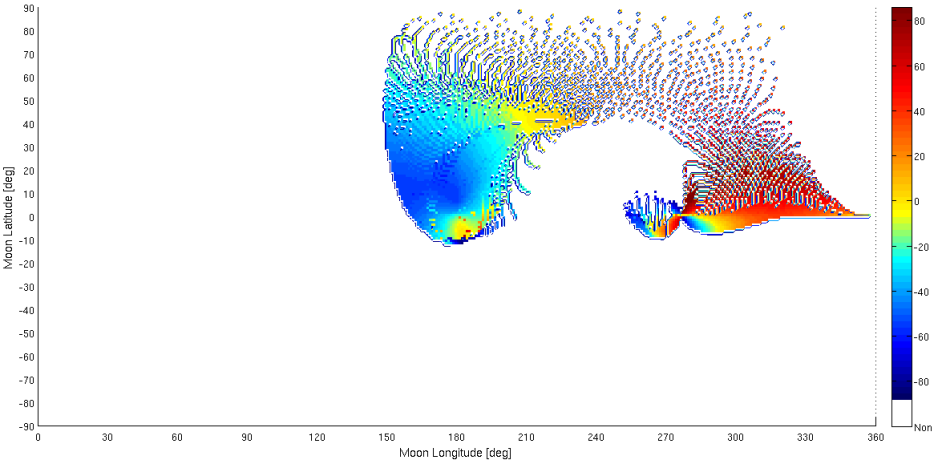

Figure 5.17: Average of ion trajectories initial velocity elevation angle at the Moon surface as a function of Moon solar orbiting long/lat

$\mathbf{R}_{obs}$ = -1837.1 $\hat{\mathbf{x}}$ [km], $|\mathbf{V}_{obs}|$ = 400 [km/s], $\mathbf{V}_{sw}$ = -400 $\hat{\mathbf{x}}$ [km/s] and $\mathbf{B}$ = 4.95 $\hat{\mathbf{x}}$+4.95 $\hat{\mathbf{y}}$ [nT]

observer position is changed, different results will be obtained for different observer positions. The simulation for some of the observer positions was run and the results can be found in Appendix 3.

Chapter 6

Conclusions

The motion of the charged particles in uniform and non-uniform electromagnetic fields was discussed and the ion velocities and trajectories in the stationary electromagnetic fields were studied analytically and numerically.
The Lorentz force is used to study the ion motion in an electric and magnetic field. It was assumed that the charged particles are collisionless and their motion is determined by the fields only. In a uniform magnetic field, the particle motion is a circular orbit around its guiding center along the magnetic field lines, gyrates with the gyro radius of r_L and the existence of electric field accelerates the charged particle along the magnetic field lines and makes drift in the particle motion perpendicular to the both electric and magnetic field lines.
Particles velocity and trajectory can be obtained by solving the equation of motion for any electric and magnetic field conditions. Different numerical methods exist to solve the equation of motion but in this report the Leap-Frog method was chosen to compute particle velocity because of simplicity, time reversibility and energy conservation.
The equation of motion can be applied to study ion trajectories in any electric and magnetic field conditions. It should be noted that the ions initial velocity to solve the equation of motion numerically has crucial role in the charged particle motion. In a uniform IMF and constant solar wind, ions with different initial velocities will have different trajectories and kinetic energies.
Our model was applied to study ion trajectories near the moon. Because of the absence of any strong magnetic field and no evidence of bow shock for the moon, solar wind plasma has direct interaction with the moon surface, looses its energy and makes a plasma cavity at the moon wake-side. Solar wind interaction with different objects can be simulated by the hybrid model and electric field and magnetic field variation can be computed near that object. The electromagnetic field results from the hybrid simulation near the moon were used as non-uniform fields in our ion trajectory model to study the ion motion near the moon. This model can be applied to study ion trajectories near any astrophysical body.
Our ion trajectory model was written in C++ and different solar wind velocity and IMF conditions can be applied to it to calculate the ion velocities and trajectories for any number of time steps. The outputs of the simulation are stored in two different file formats. Ion trajectories are saved in VTK file and the ion velocities and kinetic energies for any time step are stored in a simple text file. The VTK file can be visualized in different visualization software such as VisIt and the text file results can be plotted in Matlab or any other software that can read and plot the data.

Appendices

.1 Coordinate Systems

The coordinate system which is used in this report is the Moon solar orbiting frame. In this system the Moon center is located at the center of the coordinate and the x-axis is always pointing to the Sun. The z-axis is pointing the zenith and the y-axis is perpendicular to x and z axes. This coordinate system is used as the reference frame in this report.

Celestial Sphere

In a celestial sphere, the reference plane is the equatorial plane, perpendicular to the rotation axis. The intersection of this plane with the body surface is equator and all planes parallel with the equatorial plane are called parallels of latitude. Meridians are the planes perpendicular to the parallel planes. (see chapter 2 in [11])
Sub-solar point is the point which is made by intersection between the equatorial plane and the x-axis when it points to the Sun. The point opposite the sub-solar point is called 'solar point'.
Longitude (λ) is the angle between the meridian and the zero meridian passing through subsolar point. For the Earth's Moon and in this report, longitude is defined in the range [0°, +360°]. Zero degree is at sub-solar point and is measured counterclockwise around the z-axis.
Latitude (θ) is the angle between the parallel of latitude planes and the equatorial plane. It is in the range [-90°, +90°] and the parallel latitude planes below the equatorial plane have the negative latitudes and the ones above have the positive latitude angles.

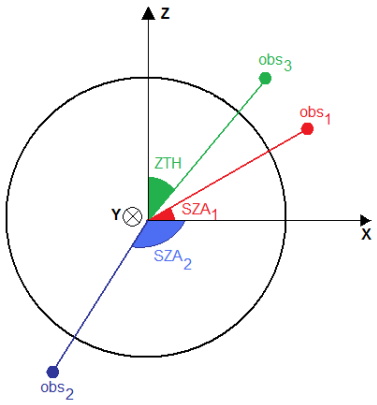

Figure 1: SZA and Zenith angles shown by three observers.

Solar Zenith Angle (SZA) is the angle between the Sun and the observer vector, which means the angle between the x-axis and the observer vector. Its range is [0, +180°].
Elevation angle is the angle between the direction of a vector and the parallel plane at the start point of that vector. Its range is [-90°, +90°].
Figure 1 shows three observers in the XZ plane. The x axis is pointing to the Sun and the y axis is going inside the paper. Observer 1 and 2 have the solar zenith angle of SZA_1 and SZA_2 and observer 3 makes the zenith angle of ZTH.

Spherical Coordinate System

Imagine point A in Figure 2 located on a sphere of radius r. This point has distance r to the origin of the coordinate system. The point lies on XY plane containing origin of the coordinate system. This cross section makes an angle ϕ from the XZ plane known as azimuth or longitude angle. The angle point A makes with Z axis is shown by θ, known as zenith angle. Therefore point A has the geometry of (r,ϕ,θ) in spherical coordinate system.

Conversion from the spherical coordinate to the Cartesian (Rectangular) coordinate system and vice versa is as follows:

$$r = \sqrt{x^2 + y^2 + z^2} \quad , \quad \phi = tan^{-1}\,(\frac{y}{x}) \quad , \quad \theta = cos^{-1}\,(\frac{z}{r})$$

$$x = r\ cos\phi\ sin\theta \quad , \quad y = r\ sin\phi\ sin\theta \quad , \quad z = r\ cos\theta$$

$$where:\ 0 \leqslant \theta < +180 \quad , \quad 0 \leqslant \phi < +360$$

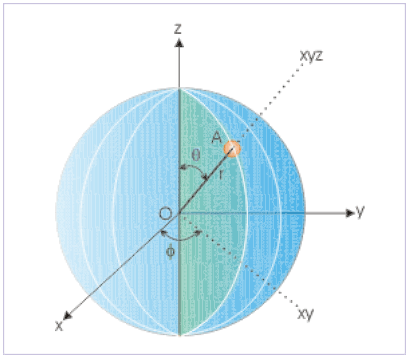

Figure 2: Spherical coordinate system.
By courtesy of `http://cnx.org/content/m13600`

Cylindrical Coordinate System

Consider point A on a cylinder of radius r (see Figure 3). The point lies on XY plane. The cross section makes an angle ϕ from the XZ plane known as azimuth angle. The third coordinate is denoted by z, the distance between the point and the XY plane along the z axis. Therefore point A has the geometry of (r,ϕ,z) in cylindrical coordinate system.

Conversion from the cylindrical coordinate to the Cartesian (Rectangular) coordinate system and vice versa is as follows:

$$r = \sqrt{x^2 + y^2} \quad , \quad \phi = tan^{-1}\,(\frac{y}{z})$$

$$x = r\ cos\phi \quad , \quad y = r\ sin\phi \quad , \quad z = z$$

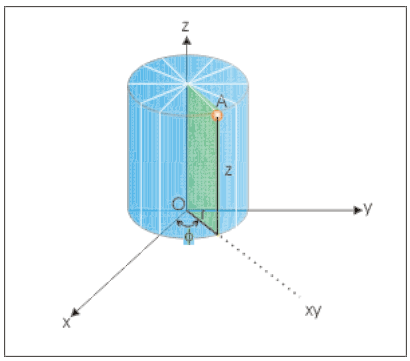

Figure 3: Cylindrical coordinate system.
By courtesy of `http://cnx.org/content/m13600`

Simulation Box

The simulation box defines the boundaries of our system. The Moon with the radius of 1737.1 [km] is located at the origin of the solar orbiting frame and also at the center of the simulation box. The box is limited to -5000 $\leq x \leq$ +5000 [km], -4000 $\leq y \leq$ +4000 [km] and -4000 $\leq z \leq$ +4000 [km], when x, y and z are the coordinates of a point in the simulation box in the Cartesian coordinate system.
The simulation box which is used in the hybrid model to simulate the solar wind interaction with the Moon has another definition. The length of this box is two times larger than what we defined in our simulation code (-10000 $\leq x_{hybrid} \leq$ +10000 [km]). Please note that these definitions are chosen arbitrarily to limit calculations in simulation models.

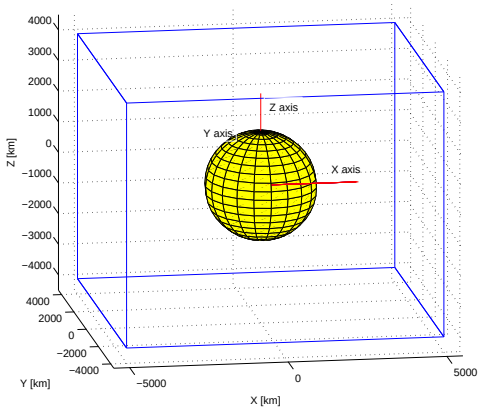

Figure 4: Simulation box definition in our simulation code.

.2 Ion Trajectories

The solar wind with the velocity of $\mathbf{V}_{sw} = -400\ \widehat{\mathbf{x}}$ [km/s] and the uniform interplanetary magnetic field $\mathbf{B} = +4.95\ \widehat{\mathbf{x}} + 4.95\ \widehat{\mathbf{y}}$ [nT] is assumed.
The observer is located at the lunar wake at position $\mathbf{R}_{obs} = -1837.1\ \widehat{\mathbf{x}}$ [km], considered to study ion trajectories coming to the observer position with the velocity magnitude the same as the solar wind (400 [km/s]). These ions would have different velocity directions at observer position and might come from different places. It was shown in entire chapters that these ions might come from the Moon surface or from the solar wind.
Several ions were launched in our simulation model backward in time from the observer position with different velocity and the ion trajectories were followed to see if they come from the Moon surface or not. Here we only want to show some ion trajectories which are coming from different places such as solar wind, Moon dayside and Moon nightside.

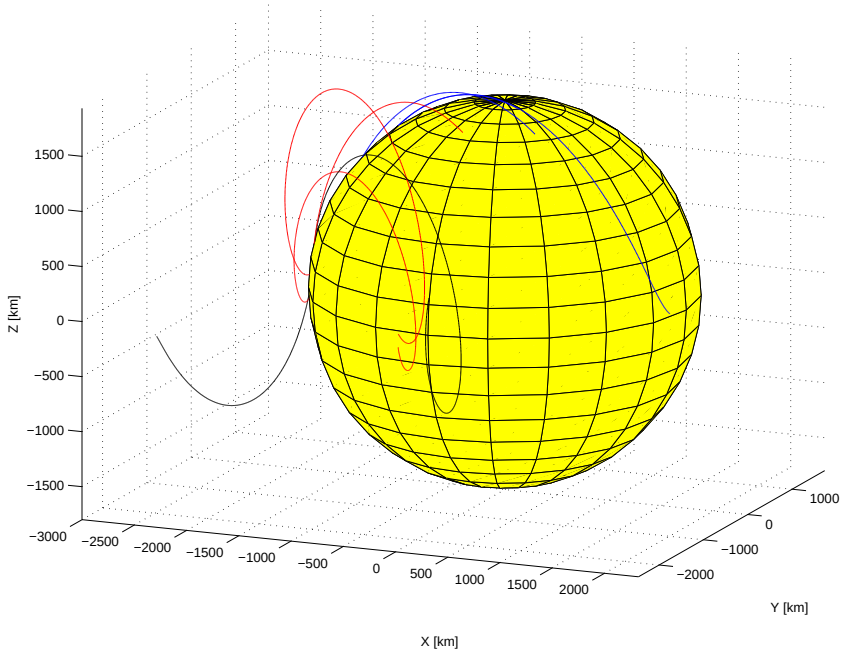

Figure 5: Ion trajectories coming to the observer position at $\mathbf{R}_{obs} = -1837.1\ \widehat{\mathbf{x}}$ [km] and velocity magnitude of 400 [km/s].

Figures 5 to 7 show some of those ions from different views. Observer position is hidden at the night side of the Moon in Figure 5 and the incoming ions from the Moon dayside are shown by blue trajectory and those which are coming from the night side are shown by red. The black color trajectories indicate those ion trajectories which are not coming from the Moon surface. Figures 6 and 7 show the Moon at the XY and the XZ planes.

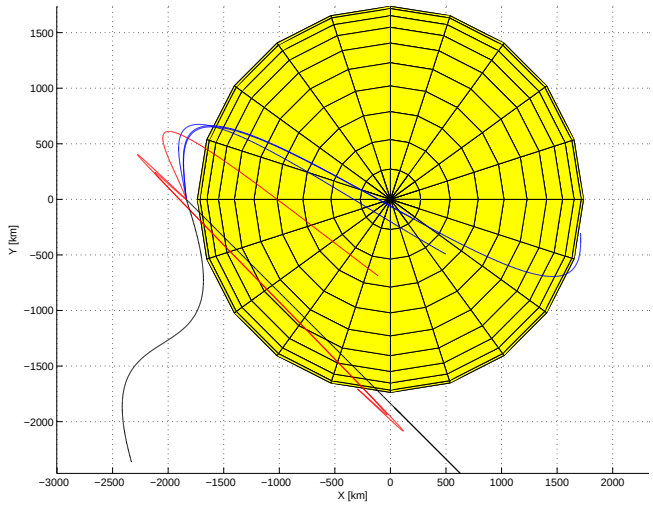

Figure 6: Ion trajectories at the XY plane coming to the observer position at $\mathbf{R}_{obs} = -1837.1\ \widehat{\mathbf{x}}$ [km] and velocity magnitude of 400 [km/s].

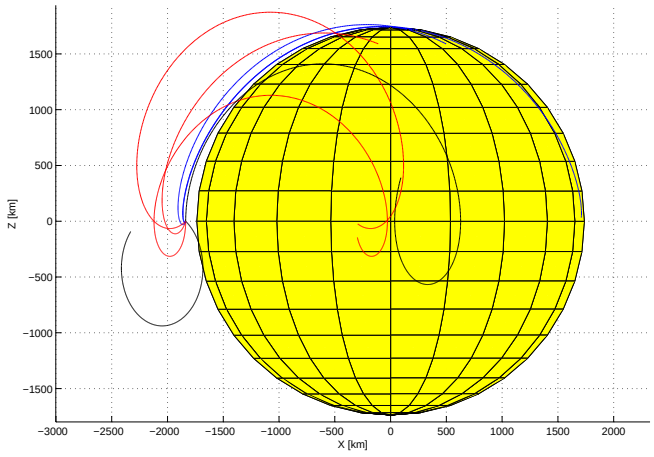

Figure 7: Ion trajectories at the XZ plane coming to the observer position at $\mathbf{R}_{obs} = -1837.1\ \widehat{\mathbf{x}}$ [km] and velocity magnitude of 400 [km/s].

.3 Samples of Ion Trajectories Near the Moon

A Chandrayaan polar orbit with altitude of 100 [km] (R_{orb} = 1837.1 [km]) from the Moon surface is assumed. Ion trajectories, final velocity angle, initial velocity and position at the Moon wakeside in the taken orbit and for solar wind velocity $\mathbf{V}_{sw}$ = -400 $\widehat{\mathbf{x}}$ [km/s] and $\mathbf{B}_{sw}$ = +4.95 $\widehat{\mathbf{x}}$ + 4.95 $\widehat{\mathbf{y}}$ [nT] are investigated here. In this order, seven observer positions on the satellite orbit and at the lunar wake are chosen and simulation code is run for all of these positions. The orbit and the observer positions are shown in Figure 8.

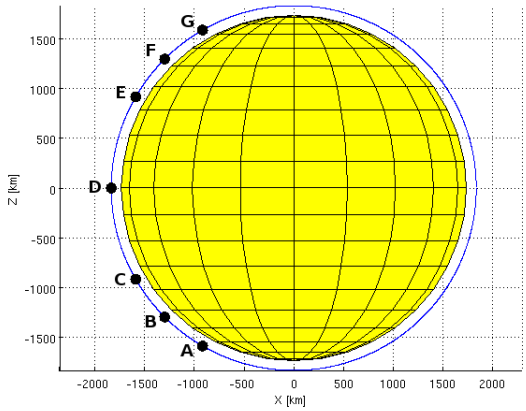

Figure 8: A polar orbit at 100 [km] altitude from the Moon surface. Seven observer positions are denoted by black dotes at the lunar wake.

The observer positions from A to G have the zenith angles of 150°, 135°, 120°, 90°, 60°, 45° and 30° respectively in the orbit. Point D is the observer position we discussed in chapter 5.

C1: The solar zenith angle of the trajectory's initial point on the Moon surface as a function of final velocity direction at the observer position.

Figures 11(A) to (G) compare the SZA of the ion trajectories initial point on the Moon surface as a function of final velocity direction at the observer positions shown in Figure 8.
The SZAs smaller than 90° indicate incoming ion trajectories from the Moon dayside and shown by blue contrast in the figures. On the contrary, the SZAs larger than 90° are shown by red contrast, illustrate ion trajectories coming from the nightside of the Moon. The Moon terminator is separated and shown by yellow color in the colorbar.
Figures 11(A) to (G) show that moving along the polar orbit from the Moon south pole to the equatorial plane, first the incoming ion trajectories from the dayside of the Moon surface are decreased and then increased near the equatorial plane. By passing the equatorial plane and going close to the north pole, the incoming ion trajectories from the dayside are again decreased.

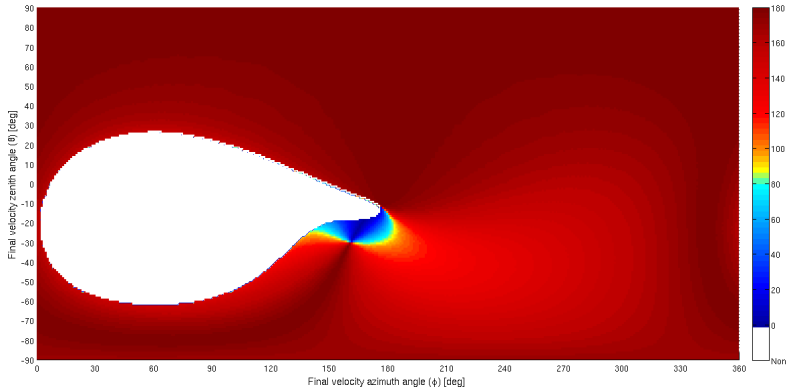

Figure 11(A): $\mathbf{R}_{obs_A} = R_{orb}\ cos(240)\ \widehat{\mathbf{x}} + R_{orb}\ sin(240)\ \widehat{\mathbf{z}}$ [km]

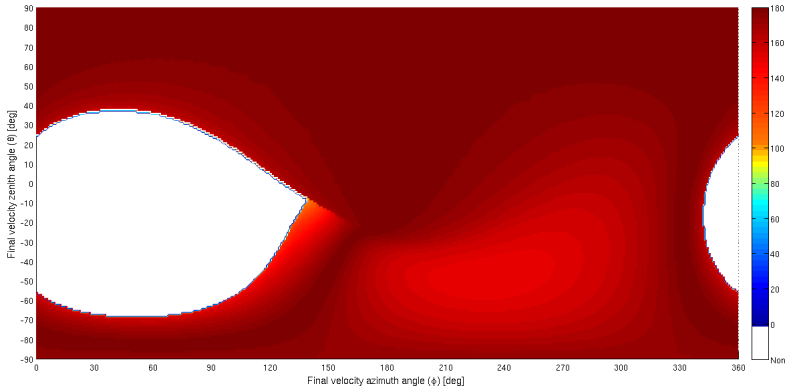

Figure 11(B): $\mathbf{R}_{obs_B} = R_{orb}\ cos(225)\ \widehat{\mathbf{x}} + R_{orb}\ sin(225)\ \widehat{\mathbf{z}}$ [km]

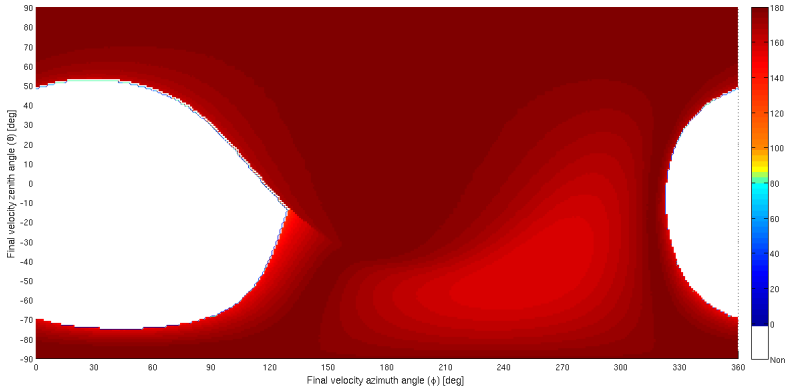

Figure 11(C): $\mathbf{R}_{obs_C} = R_{orb}\ cos(210)\ \widehat{\mathbf{x}} + R_{orb}\ sin(210)\ \widehat{\mathbf{z}}$ [km]

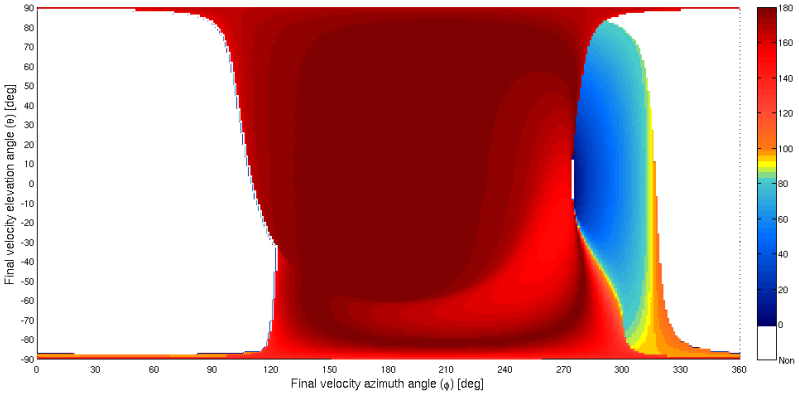

Figure 11(D): $\mathbf{R}_{obs_D} = R_{orb}\ cos(180)\ \widehat{\mathbf{x}} + R_{orb}\ sin(180)\ \widehat{\mathbf{z}}$ [km]

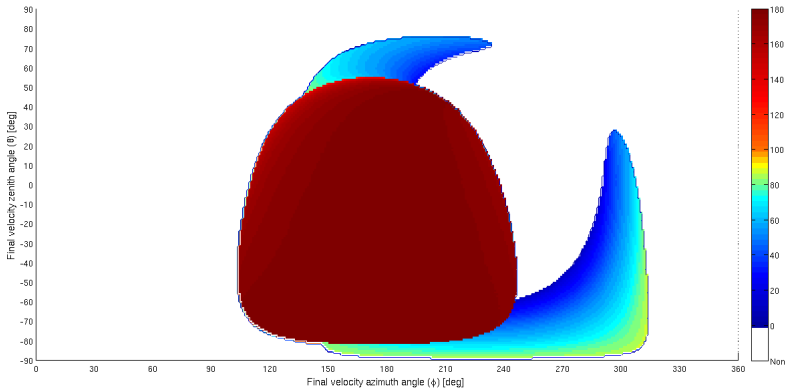

Figure 11(E): $\mathbf{R}_{obs_E} = R_{orb}\ cos(150)\ \widehat{\mathbf{x}} + R_{orb}\ sin(150)\ \widehat{\mathbf{z}}$ [km]

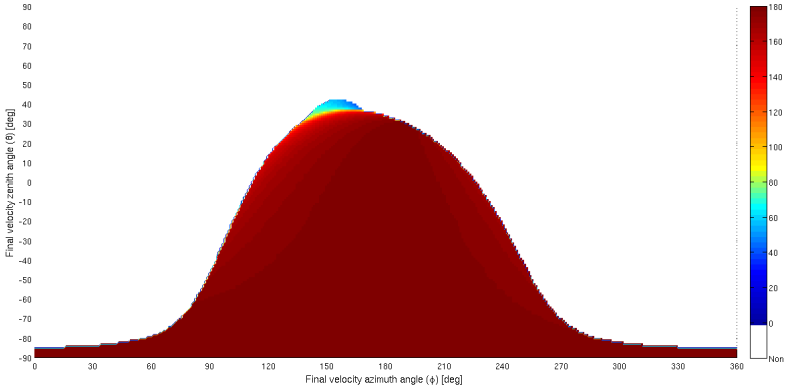

Figure 11(F): $\mathbf{R}_{obs_F} = R_{orb}\ cos(145)\ \widehat{\mathbf{x}} + R_{orb}\ sin(145)\ \widehat{\mathbf{z}}$ [km]

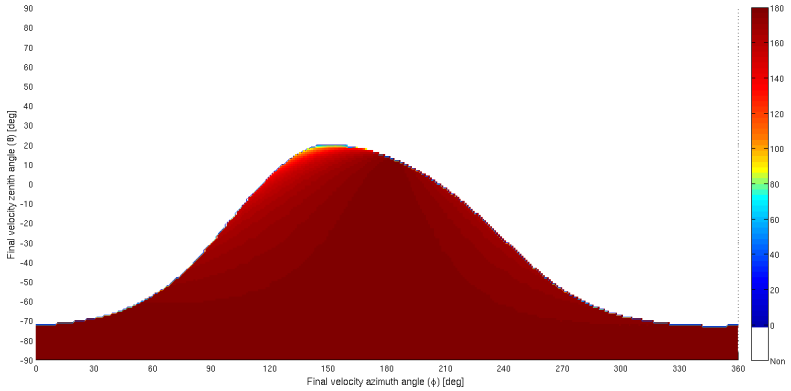

Figure 11(G): $\mathbf{R}_{obs_G} = R_{orb}\ cos(120)\ \widehat{\mathbf{x}} + R_{orb}\ sin(120)\ \widehat{\mathbf{z}}$ [km]

In general, the number of incoming trajectories from the Moon surface which is shown by colors in the figures is reduced by moving the observer from south to north in the polar orbit which is due to the ion trajectories. Also, the majority of incoming ion trajectories from the nightside have the final velocity azimuth angles almost between 120° and 240° and elevation angles almost between -80° and +50°. The incoming ion trajectories from the Moon surface can have different velocity angles at different observer positions.

C2: Ions initial velocity magnitude at the Moon surface shown by color map as a function of the trajectories velocity direction at the observer position indicated by azimuth and zenith angles.

Figures 12(A) to (G) illustrate the ion initial velocity magnitude at the Moon surface as a function of final velocity direction. Clearly can be seen that different ion initial velocity magnitude can be observed to reach observer positions. The ion initial velocity range varies between $0.1\mathbf{V}_{sw}$ and $2.2\mathbf{V}_{sw}$ in magnitude. Moving along the orbit from south to the equatorial plane, the ion initial velocity magnitude which leave the Moon surface and reach the observer position is increased and again dropped down from equatorial plane to the north.

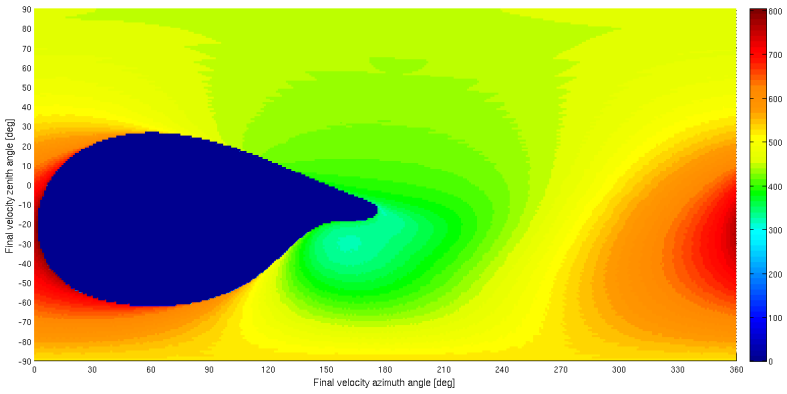

Figure 12(A): $\mathbf{R}_{obs_A} = R_{orb}\, cos(240)\, \widehat{\mathbf{x}} + R_{orb}\, sin(240)\, \widehat{\mathbf{z}}$ [km]

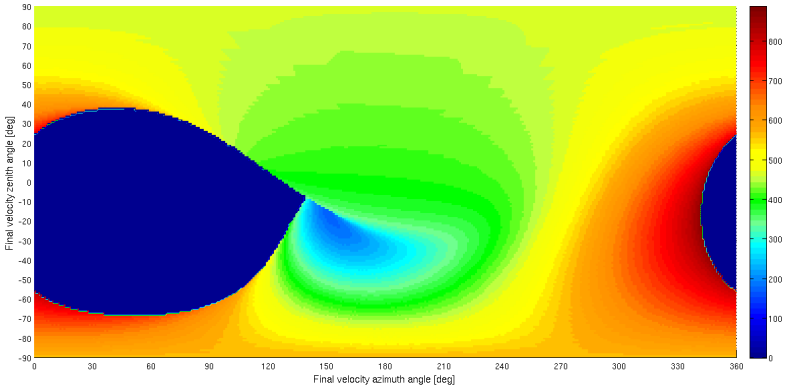

Figure 12(B): $\mathbf{R}_{obs_B} = R_{orb}\, cos(225)\, \widehat{\mathbf{x}} + R_{orb}\, sin(225)\, \widehat{\mathbf{z}}$ [km]

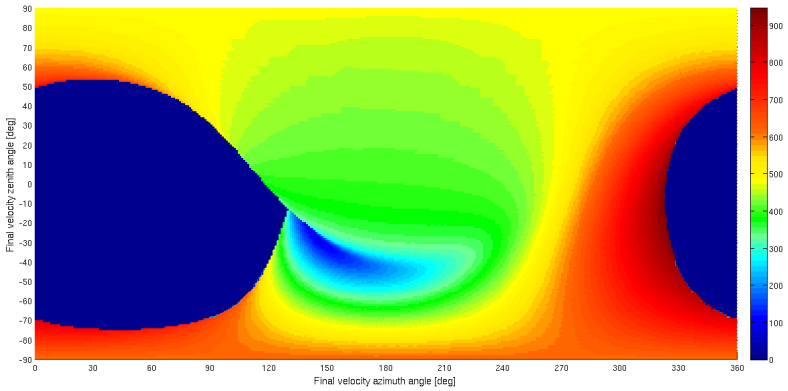

Figure 12(C): $\mathbf{R}_{obs_C} = R_{orb}\ cos(210)\ \widehat{\mathbf{x}} + R_{orb}\ sin(210)\ \widehat{\mathbf{z}}$ [km]

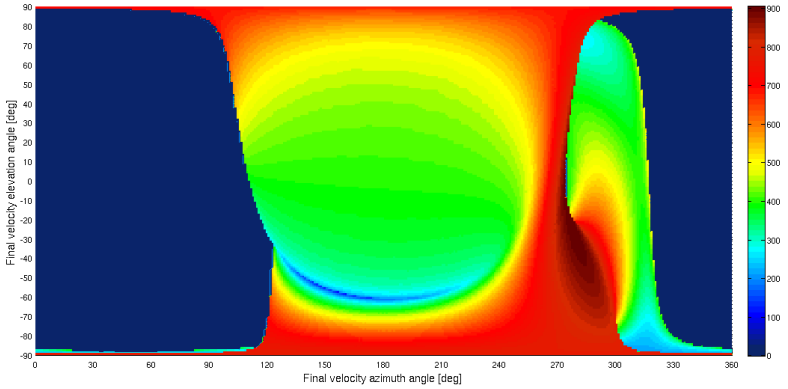

Figure 12(D): $\mathbf{R}_{obs_D} = R_{orb}\ cos(180)\ \widehat{\mathbf{x}} + R_{orb}\ sin(180)\ \widehat{\mathbf{z}}$ [km]

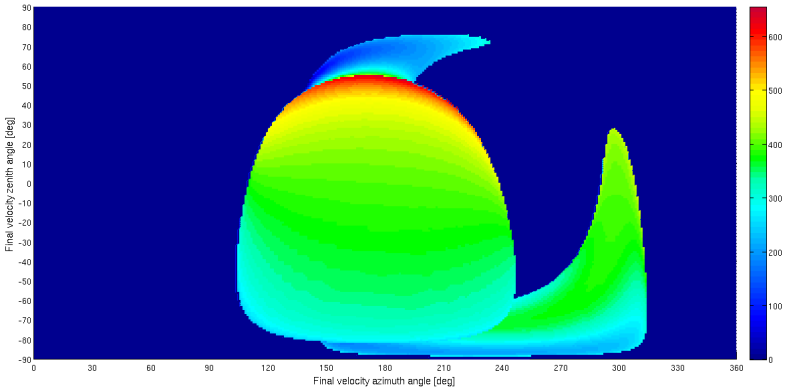

Figure 12(E): $\mathbf{R}_{obs_E} = R_{orb}\ cos(150)\ \widehat{\mathbf{x}} + R_{orb}\ sin(150)\ \widehat{\mathbf{z}}$ [km]

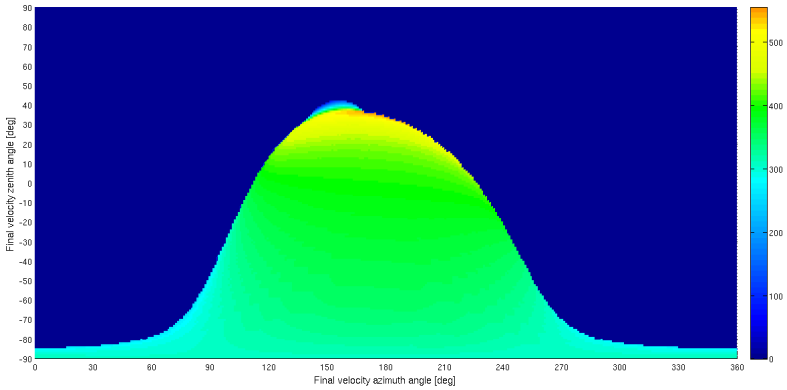

Figure 12(F): $\mathbf{R}_{obs_F} = R_{orb}\ cos(145)\ \widehat{\mathbf{x}} + R_{orb}\ sin(145)\ \widehat{\mathbf{z}}$ [km]

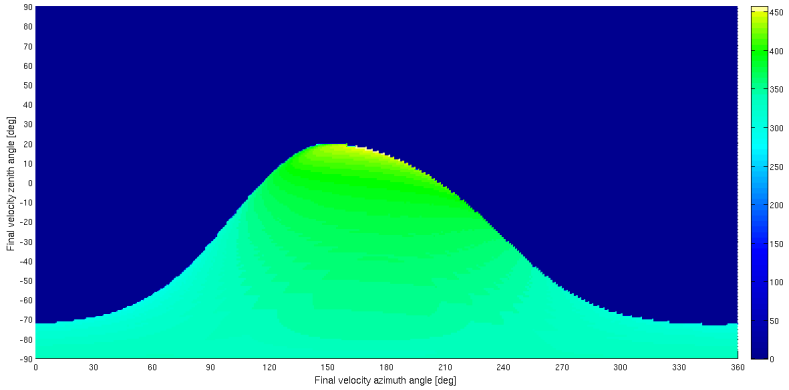

Figure 12(G): $\mathbf{R}_{obs_G} = R_{orb}\ cos(120)\ \widehat{\mathbf{x}} + R_{orb}\ sin(120)\ \widehat{\mathbf{z}}$ [km]

Ion initial velocity has its highest magnitude at the equatorial plane and in total, the incoming ion trajectories from the Moon surface which are observed at the northern parts of the orbit have lower initial velocity magnitude compare to the other places. In these figures we can not say anything clearly about the initial velocity, therefore we need to interpret the ion initial velocity at the Moon surface (see C4 and C5).

C3: Number of ions trajectory starting points at the Moon surface, moving to the Moon wakeside at uniform electromagnetic field and reaching the observer position.

Figures 13(A) to (G) show the number of ion trajectories leaving the Moon surface and reaching the observer at different observer positions as a function of Moon longitude and latitude. In these figures we can see clearly that when the observer is close to its orbital perigee at the south, the majority of ion trajectories come from the Moon nightside but it is possible that an ion trajectory reaches observer from the dayside, coming from the low latitudes close to the Moon south pole. When the observer moves to the equatorial plane, for azimuth angles almost between 150 and 120, no ion trajectory is observed from the Moon dayside. It proves our discussion about SZA.

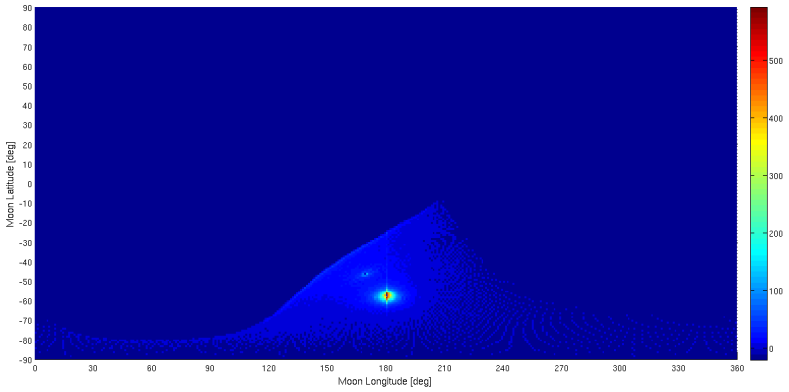

Figure 13(A): $\mathbf{R}_{obs_A} = R_{orb}\ cos(240)\ \widehat{\mathbf{x}} + R_{orb}\ sin(240)\ \widehat{\mathbf{z}}$ [km]

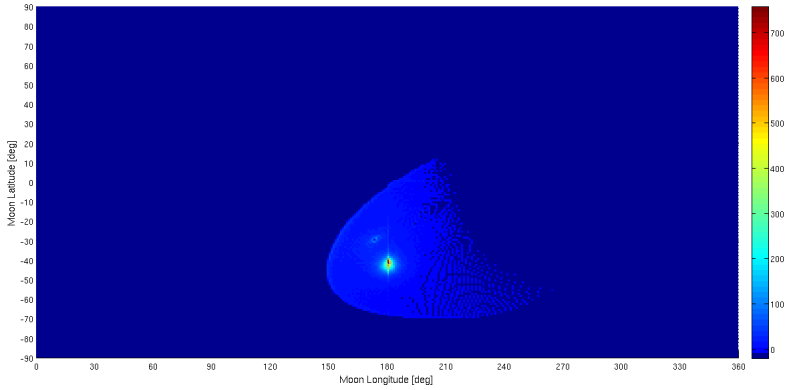

Figure 13(B): $\mathbf{R}_{obs_B} = R_{orb}\ cos(225)\ \widehat{\mathbf{x}} + R_{orb}\ sin(225)\ \widehat{\mathbf{z}}$ [km]

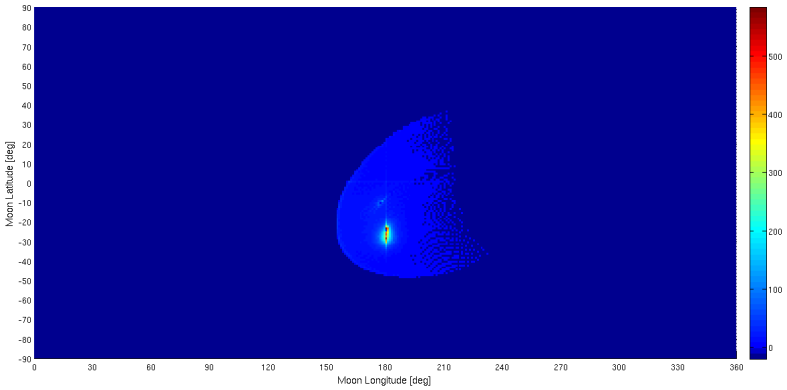

Figure 13(C): $\mathbf{R}_{obs_C} = R_{orb}\ cos(210)\ \widehat{\mathbf{x}} + R_{orb}\ sin(210)\ \widehat{\mathbf{z}}$ [km]

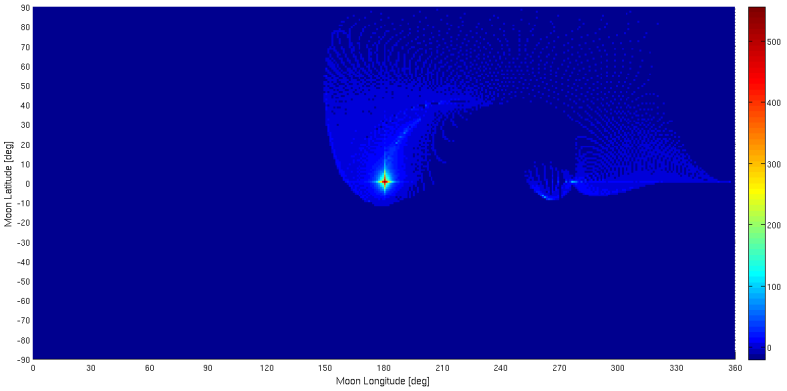

Figure 13(D): $\mathbf{R}_{obs_D} = R_{orb}\ cos(180)\ \widehat{\mathbf{x}} + R_{orb}\ sin(180)\ \widehat{\mathbf{z}}$ [km]

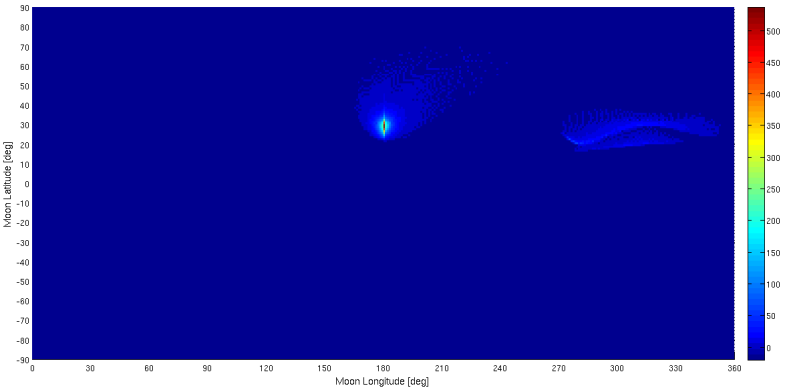

Figure 13(E): $\mathbf{R}_{obs_E} = R_{orb}\ cos(150)\ \widehat{\mathbf{x}} + R_{orb}\ sin(150)\ \widehat{\mathbf{z}}$ [km]

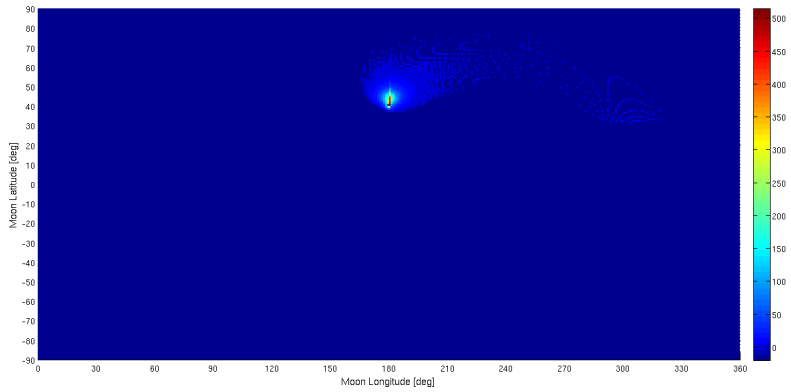

Figure 13(F): $\mathbf{R}_{obs_F} = R_{orb}\ cos(145)\ \widehat{\mathbf{x}} + R_{orb}\ sin(145)\ \widehat{\mathbf{z}}$ [km]

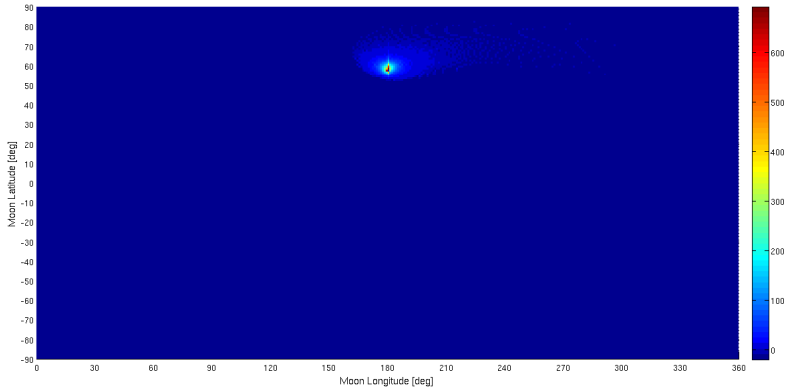

Figure 13(G): $\mathbf{R}_{obs_G} = R_{orb}\ cos(120)\ \widehat{\mathbf{x}} + R_{orb}\ sin(120)\ \widehat{\mathbf{z}}$ [km]

The maximal number of incoming ion trajectories from the Moon dayside and reaching the observer is when the observer is located at the equatorial plane or close to it. In this case, as we can see in Figure 13(D), some ion trajectories leave the Moon surface very close to the subsolar point. When the observer goes away from the equatorial plane and moves close to its orbital apogee, this chance is decreased and then disappeared.
The maximum number of ion trajectories coming from the same lunar longitude and latitude belongs to the sub-satellite point and the points around it.

C4: Average of ion trajectories initial velocity magnitude at the Moon surface as a function of Moon geographical coordinates.

Figures 14(A) to (G) show the ion trajectories initial average velocity magnitude at the Moon surface. The horizontal and vertical axes of figures denote the Moon longitude and latitude respectively. The general conclusion about initial average velocity is that all ion trajectories which leave the Moon surface at the same latitude as the sub-satellite point or somewhere close to it have the same velocity as the solar wind. The ions which leave the lunar surface from lower latitudes have smaller initial velocity than the solar wind but for those which leave the higher latitudes have larger initial velocity than the solar wind velocity magnitude. This can be extended for all ion trajectories coming from the Moon surface and there is no difference between the dayside and the nightside.

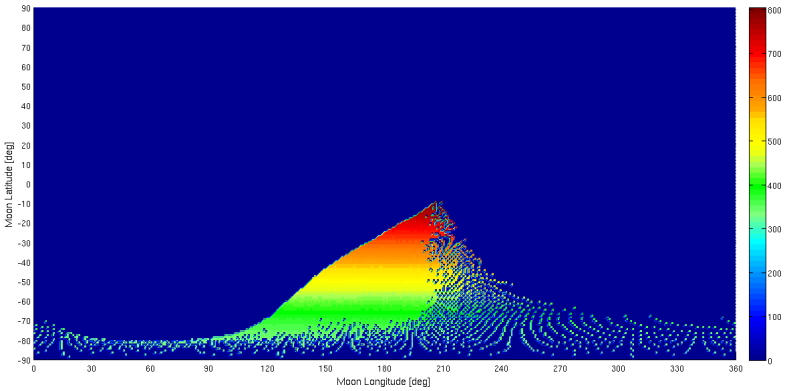

Figure 14(A): $\mathbf{R}_{obs_A} = R_{orb}\ cos(240)\ \widehat{\mathbf{x}} + R_{orb}\ sin(240)\ \widehat{\mathbf{z}}$ [km]

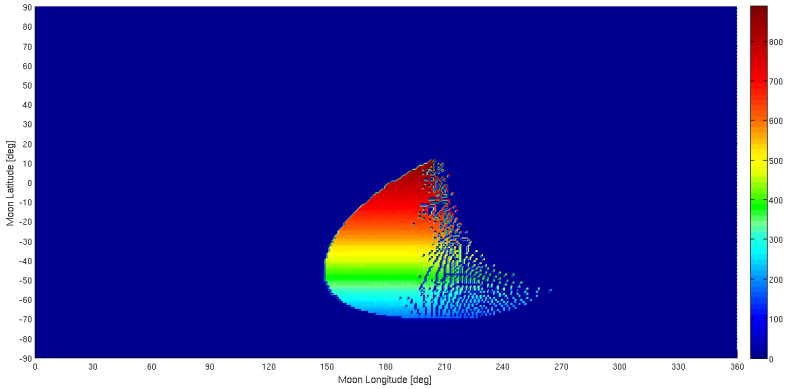

Figure 14(B): $\mathbf{R}_{obs_B} = R_{orb}\ cos(225)\ \widehat{\mathbf{x}} + R_{orb}\ sin(225)\ \widehat{\mathbf{z}}$ [km]

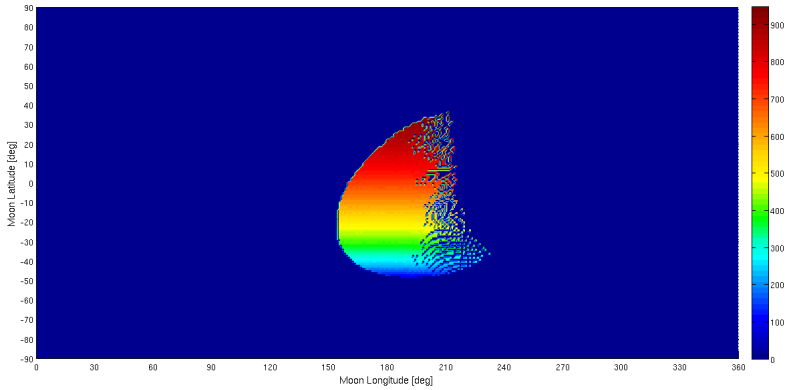

Figure 14(C): $\mathbf{R}_{obs_C} = R_{orb}\ cos(210)\ \widehat{\mathbf{x}} + R_{orb}\ sin(210)\ \widehat{\mathbf{z}}$ [km]

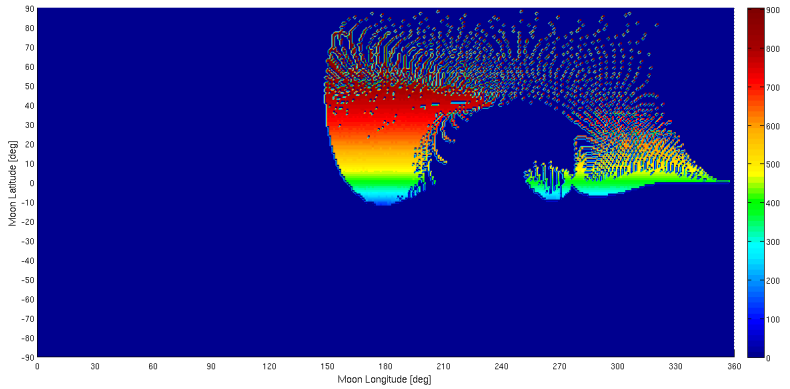

Figure 14(D): $\mathbf{R}_{obs_D} = R_{orb}\ cos(180)\ \widehat{\mathbf{x}} + R_{orb}\ sin(180)\ \widehat{\mathbf{z}}$ [km]

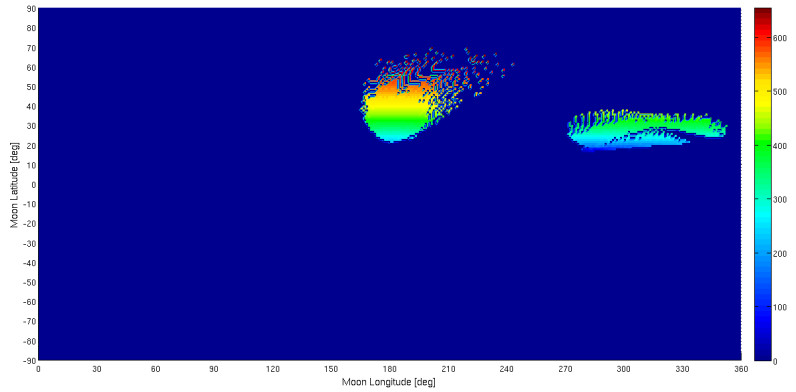

Figure 14(E): $\mathbf{R}_{obs_E} = R_{orb}\ cos(150)\ \widehat{\mathbf{x}} + R_{orb}\ sin(150)\ \widehat{\mathbf{z}}$ [km]

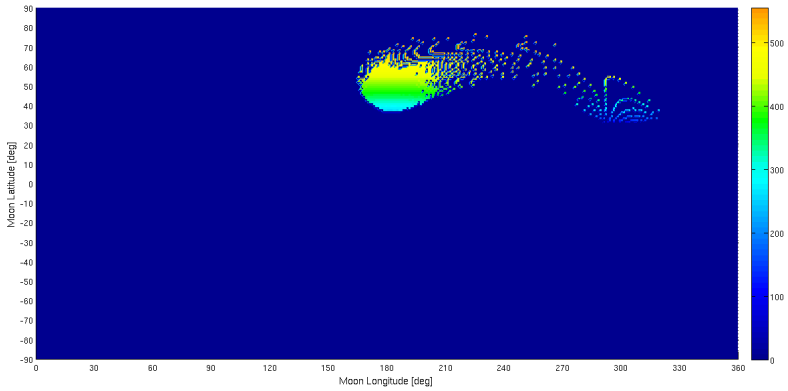

Figure 14(F): $\mathbf{R}_{obs_F} = R_{orb}\ cos(145)\ \widehat{\mathbf{x}} + R_{orb}\ sin(145)\ \widehat{\mathbf{z}}$ [km]

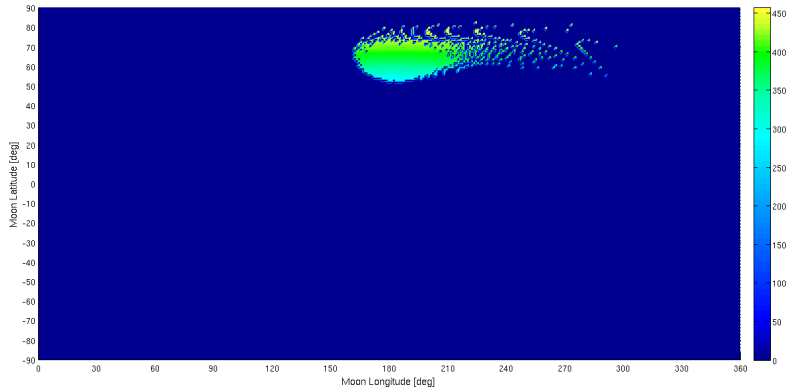

Figure 14(G): $\mathbf{R}_{obs_G} = R_{orb}\ cos(120)\ \widehat{\mathbf{x}} + R_{orb}\ sin(120)\ \widehat{\mathbf{z}}$ [km]

C5: Average of ion trajectories initial velocity angle at the Moon surface as a function of Moon geographical coordinates.

Figures 15(A) to (G) show the ion trajectories initial average velocity angle at the Moon surface. The horizontal and vertical axes of figures denote the Moon longitude and latitude respectively. We can see that when the observer is below the equatorial plane, the incoming ion trajectories from the Moon surface have the negative elevation angle. When it goes close to the equatorial plane and above it, the elevation angle is increased. It can also be seen that the majority of incoming ions from the Moon dayside to the observer while the observer is below the equatorial plane pass the Moon south pole and reach the observer. This is shown by the negative elevation angles.

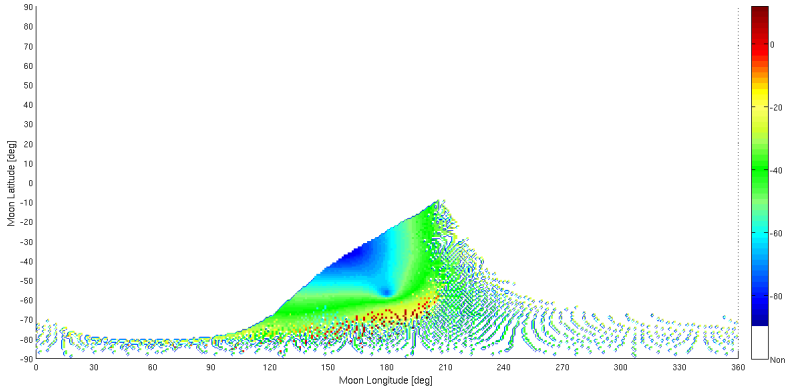

Figure 15(A): $\mathbf{R}_{obs_A} = R_{orb}\ cos(240)\ \widehat{\mathbf{x}} + R_{orb}\ sin(240)\ \widehat{\mathbf{z}}$ [km]

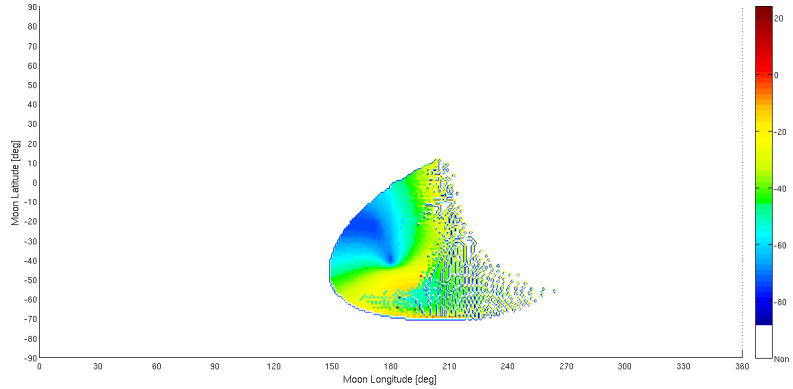

Figure 15(B): $\mathbf{R}_{obs_B} = R_{orb}\ cos(225)\ \widehat{\mathbf{x}} + R_{orb}\ sin(225)\ \widehat{\mathbf{z}}$ [km]

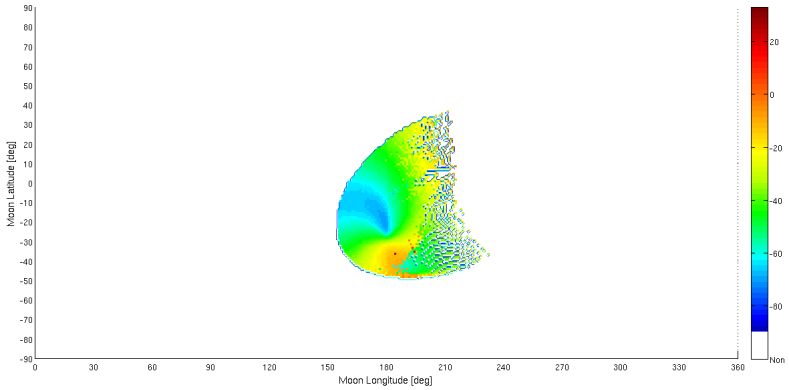

Figure 15(C): $\mathbf{R}_{obs_C} = R_{orb}\ cos(210)\ \widehat{\mathbf{x}} + R_{orb}\ sin(210)\ \widehat{\mathbf{z}}$ [km]

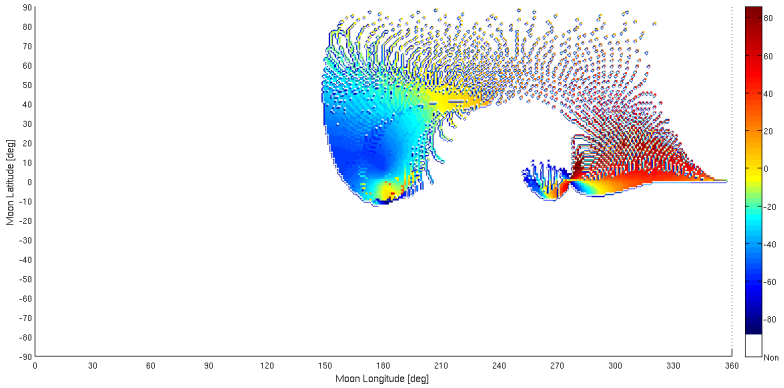

Figure 15(D): $\mathbf{R}_{obs_D} = R_{orb}\ cos(180)\ \widehat{\mathbf{x}} + R_{orb}\ sin(180)\ \widehat{\mathbf{z}}$ [km]

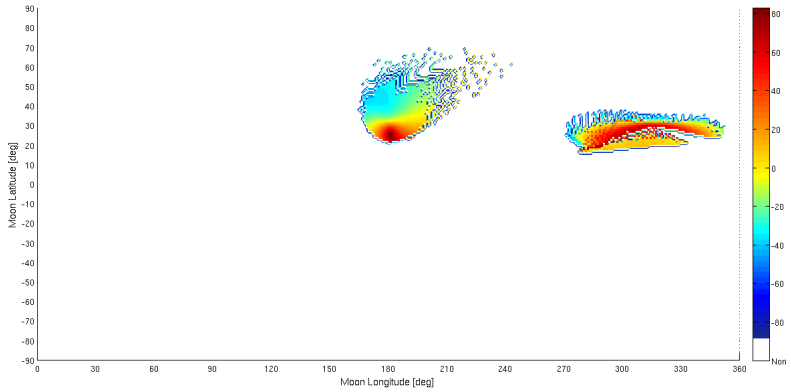

Figure 15(E): $\mathbf{R}_{obs_E} = R_{orb}\ cos(150)\ \widehat{\mathbf{x}} + R_{orb}\ sin(150)\ \widehat{\mathbf{z}}$ [km]

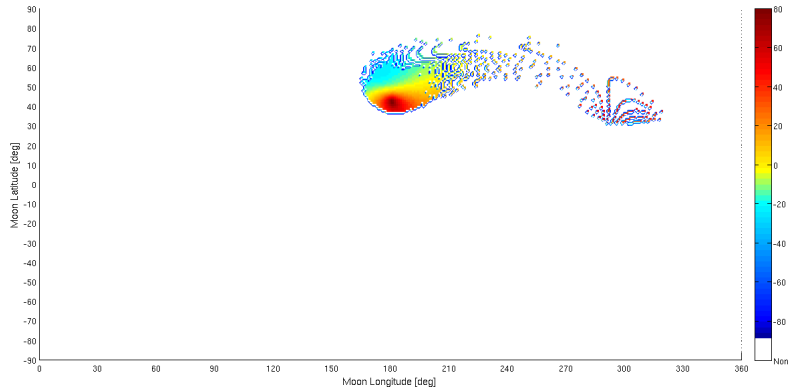

Figure 15(F): $\mathbf{R}_{obs_F} = R_{orb}\ cos(145)\ \widehat{\mathbf{x}} + R_{orb}\ sin(145)\ \widehat{\mathbf{z}}$ [km]

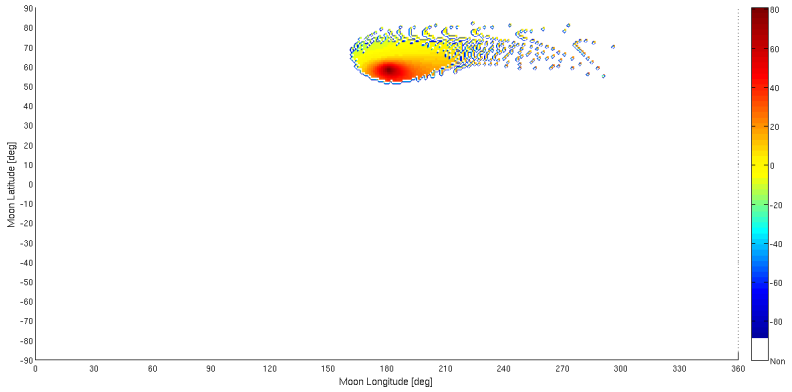

Figure 15(G): $\mathbf{R}_{obs_G} = R_{orb}\ cos(120)\ \widehat{\mathbf{x}} + R_{orb}\ sin(120)\ \widehat{\mathbf{z}}$ [km]

.4 Source Code Listings

The main C++ classes and functions which have been used in the simulation code are listed here:

Table 1: Error Class

Class name	`Error`
Function type	**Function name**
`void`	`Err(int iErrorNumber)` This function gets the error number and prints the related message to that number.
`void`	`ReadTxt(char* strFilename)` An error message can be saved in a text file format. This functions reads the file and prints its contents.

Table 2: Numeric Class

Class name	`Numeric`
Function type	**Function name**
`double`	`getGyroFreq(double Mass, vector <double> BField)` This function gives the magnetic field and particles mass and returns the calculated gyro frequency.
`vector<double>`	`calcNewVelocity (vector<double> Velocity, vector<double> BField, vector<double> EField, double Mass, double TimeStep)` This function calculates V_{n+1} from Lorentz force by using Leap-Frog method.
`void`	`RK4(double data[], double b[], double e[], int nElements, double t, double tau, void*)` This function calculates V_{n+1} from Lorentz force by using Runge-Kutta method.
`void`	`RKFehlBerg(double data[], double b[], double e[], int nElements, double t, double tau, void*)` This function calculates V_{n+1} from Lorentz force by using RK Fehlberg method.

The source code of some functions are listed here:

```
/*********************************************
*
* Class Name:           Numeric
* Function Name:        getGyroFreq
*
*
* Parameters:          This function gets the charged particle mass and magnetic field.
*
* Return values:       Returns the charged particle gyro frequency in the given magnetic field.
*********************************************/

double Numeric::getGyroFreq(double Mass, vector<double> B_Field)
{

     return  Q_CHARGE*getVectMagnitude(B_Field)/Mass;

}
```

```
/*********************************************
*
* Class Name:          Numeric
* Function Name:       calcNewVelocity
*
* Parameters:     This function gets the old velocity, magnetic field, electric field and particle mass and time step.
* Return values:  Returns the new velocity based on LEAP-FROG method.
*********************************************/

vector<double> Numeric::calcNewVelocity (vector<double> Velocity, vector<double> B_Field,
          vector<double> E_Field, double Mass, double TimeStep)
{
     vector<double> v1 = mul(( 1 - 0.5 * pow(getGyroFreq(Mass, B_Field), 2) * pow(TimeStep, 2)) , Velocity);
     vector<double> v2 = mul( Q_CHARGE*TimeStep/Mass , add( E_Field , curl(Velocity, B_Field)) );
     vector<double> v3 = mul( 0.5 * pow( Q_CHARGE * TimeStep / Mass , 2) , curl( E_Field , B_Field ));
     vector<double> v4 = mul( 0.5 * pow( Q_CHARGE * TimeStep / Mass , 2) * dot(Velocity, B_Field) , B_Field);
     return add( add(v1, v2) , add(v3, v4));
}
/*********************************************************************************************/
```

Table 3: QuickFlash Class

Class name	QFlash
Function type	**Function name**
vector< vector<double>>	readData(std::string filename, std::string dslist[], vector< vector<double> > pointslist) see the code description below the table.

```
/*********************************************
*
* Class Name:  QFlash
* Function Name:  readData
*
* Parameters:
*       file_name (STRING): HDF5 filename and full path
*       ds_list[] (STRING LIST): a list of dataset names in HDF5 file which should be read by this function.
*       for example, our HDF5 file contains Magnetic_Filed, Electric_Field, Electron_Density and Temperature but
*            we want to read Magnetic_Field and Electric_Field data only. The name of these two should be given by
*            this parameter.
*       points_list: (VECTOR LIST): a list of the points we want to read data.
*       Any point in simulation box might have its own value for any dataset.
*
* Return values:
*       It returns a list of double type vectors.
*       the list contains the value of selected datasets by ds_list for chosen points by points_list
*
*********************************************/

vector< vector<double> > QFlash::readData(std::string file_name, std::string ds_list[], vector< vector<double> > points_list)
{
     unsigned int num_points  = 0;
     unsigned int block_index = 0;
     unsigned int cell_index  = 0;
     vector< vector<double> > data;
     vector<double> myvector (0,0);
     vector<double>::iterator it;

     try
     {
          // Open the file
          QuickFlash::File::DataFile dfile(file_name);

          // Get AMR mesh info
          const QuickFlash::File::MeshInfo & meshinfo = dfile.get_mesh_info();
          const unsigned int dims = meshinfo.get_dims();

          for(int ds_index=0; ds_index<6; ds_index++)
```

```
            {
                 // Open the dataset
                 const QuickFlash::File::Dataset & dset = dfile.get_dataset(ds_list[ds_index]);
                 num_points = points_list.size();
                 for(int point_index=0; point_index< num_points; point_index++)
                 {
                      const vector<double> & coord = points_list[point_index];

                      if (coord.size() != dims)
                      {
                           cerr << endl << "ERROR ** Coordinate size does not match simulation "
                                << "dimensions [Class: QFlash, Func: readData] " << endl << endl;
                           //return -1;
                      }

                      // If the coordinate is within the simulation volume, get the data
                      if (meshinfo.in_bounds(coord))
                      {
                           // Use meshinfo to get the block and cell indexes for this coordinate
                           block_index = 0;
                           cell_index = 0;
                           meshinfo.get_cell_index(coord, block_index, cell_index);

                           // Retrieve the data for the block from the dataset
                           QuickFlash::Block::BlockData<double> block_data;
                           dset.get_block_data(block_index, block_data);

                           // Print out the data (the << operator for vectors is in
                           // quickflash_utils_text.hpp)
                           it = myvector.end();
                           myvector.insert ( it , block_data[cell_index] );
                           data.push_back( myvector );
                           it = myvector.begin();
                           myvector.erase(it);
                      }

                      else
                           cout << coord << " : out of bounds " << endl;
                 }
            }

            dfile.reset();

       } // End try

       catch (exception& ex)
       {
            Error objErr;
            objErr.Err(1002); // File not found
            cout << "ERROR ** " << ex.what() << "\n";
       }

       return data;
  }//End of readData function
```

/***/

A simple VTK file format which is used in our simulation code is shown here:

```
# vtk DataFile Version 1.0
Line representation of vtk
ASCII
DATASET POLYDATA
POINTS [number of points] float
...
...
[point geometries here]
...
...
LINES [number of conected line] [3  number of points]
[number of points conected by one line, starts from 0] [point numer 1] [point number 2] .... [point number n]
...
...
```

The code below shows a part of the 'DP' ion trajectory in VTK file format (see chapter 5.2).

```
# vtk DataFile Version 1.0
Line representation of vtk
ASCII

DATASET POLYDATA
POINTS 2000 float
8.99e+06      1.76e+06      -0.104026
8.98e+06      1.76e+06       0.376665
8.97e+06      1.76e+06       1.08726
8.96e+06      1.76e+06       2.03232
8.95e+06      1.76e+06       3.21636
8.94e+06      1.75999e+06    4.64384
8.93e+06      1.75999e+06    6.31921
8.92e+06      1.75999e+06    8.24683
8.91e+06      1.75999e+06    10.4311
8.9e+06       1.75998e+06    12.8762
8.89e+06      1.75998e+06    15.5865
8.88e+06      1.75997e+06    18.5661
8.87e+06      1.75997e+06    21.5629
8.86e+06      1.75996e+06    24.5812
.
.
    [1983 lines are hidden here]
.
.
-1.13873e+07   1.14881e+06    47616.3
-1.13978e+07   1.14799e+06    47709.4
-1.14083e+07   1.14717e+06    47806.8


LINES 1999 5997
2    0    1
2    1    2
2    2    3
2    3    4
2    4    5
2    5    6
2    6    7
.
.
   [1989 lines are hidden here]
.
.
2   1996   1997
2   1997   1998
2   1998   1999
```

Bibliography

[1] M. G. Kivelson, C. T. Russell, *Introduction To Space Physics*, Cambridge university press, 1995.

[2] May-Britt Kallenrode, *Space Physics*, Springer, 3rd edition, 2004.

[3] T. J. M. Boyd, J. J. Sanderson, *The Physics Of Plasma*, Cambridge University Press, 2003.

[4] Paul M. Bellan, *Fundamentals Of Plasma Physics*, Cambridge University Press, 2004.

[5] J. A. Bittencourt, *Fundamentals Of Plasma Physics*, Bittencourt, 3rd edition, 2003.

[6] Y. Kamide and A. Chian, *Handbook Of The Solar Terrestrial Environment*, Springer, Heidelberg, 2007.

[7] Thomas E. Cravens, *Physics Of Solar System Plasma*, 1997.

[8] Alejandro L. Garcia, *Numerical Methods For Physics*, Prentice Hall, 2nd edition, 2000.

[9] J. Stoer, R. Bulirsch, *An Introduction To Numerical Analysis*, Springer, 3rd edition, 2002.

[10] J. C. Butcher, *Numerical Methods For Ordinary Differential Equations*, Wiley Press, 2003.

[11] H. Karttunen, P. Krgöer, H. Oja, M. Poutanen, K.J. Donner, *Fundamental Astronomy*, Springer, 5th edition, 2007.

[12] S.I. Hayek, *Advanced Mathematical Methods In Science And Engineering*, CRC, 2000.

[13] Ernst Hairer, Christian Lubich, Michel Roche, *The Numerical Solution Of Differential Algebraic Systems by Runge-Kutta Methods*, Springer-Verlag, 1989.

[14] Ernst Hairer, Syvert Nørsett, Gerhard Wanner, *Solving Ordinary Differential Equations 1, 2*, Springer, 2008.

[15] J. Büchner, C. T. Dum, M. Scholer and group of editors, *Space Plasma Simulation*, Springer, Heidelberg 2003.

[16] George B. Arfken, Hans J. Weber, *Mathematical Methods For Physics*, Harcourt Academic Press, 5th edition, 2001.

[17] Jaan Kiusalaas, *Numerical Methods in Engineering with MATLAB*, Cambridge University Press, 2005.

[18] James R.Wertz and Wiley J.Larson, *Space Mission Analysis And Design*, Microcosm Press, 3rd edition, 2003.

[19] Daniel Hastings, Henry Garrett, *Spacecraft Environment Interactions*, Cambridge Atmospheric and Space Science Series, 1996.

[20] S. A. Ledvina, Y. J. Ma, E. Kallio, *Modeling and Simulating Flowing Plasma and Related Phenomena*, Springer Science and Business Media B.V. 2008 - Space Science Rev (2008) 139: 143-189, March 2008.

[21] J. S. Halekas, S. D. Bale, D. L. Mitchell, R. P. Lin, *Electrons And Magnetic Fields In The Lunar Plasma Wake*, Journal of geophysical research, Vol 110, A07222, 2005.

[22] J. W. Freeman, *Energetic Ion Bursts On The nightside Of The Moon*, Journal of geophysical research, Vol 77, No 1, January 1972.

[23] Brian Lee Beers, *Numerical Calculation Of The Lunar Wake In A Magnetohydrodynamic Model*, The physics of fluid journal, Vol 15, No 8, August 1972.

[24] D. Winske, L. Yin, *Hybrid Codes: Past, Present and Future*, Proceedings of ISSS-06 (2001): 1-4 , 2001.

[25] K. W. Ogilvie, N. F. Ness, *Dependence Of The Lunar Wake On Solar Wind Plasma Characteristics*, Journal of geophysical research, Space Physics, Vol 74, No 16, Aug 1969.

[26] Y. C. Whang, *Interaction Of The Magnetized Solar Wind With The Moon*, The physics of fluid, Vol 11, No 5, May 1968.

[27] F. C. Michel, *Magnetic Field Structure Behind The Moon*, Journal of geophysical research, Space Physics, Vol 73, No 5, Mar 1968.

[28] N. Borisov, U. Mall, *Plasma Distribution And Electric Fields Behind The Moon*, Physics Letters A 265 (2000) 369-376, Feb 2000.

[29] Paul C. Birch and Sandra C. Chapman, *Detailed Structure And Dynamics In Particle-in-Cell Simulations Of The Lunar Wake*, ArXiv:astro-ph/0107280v1 16 Jul 2001, Feb 2008.

[30] Stas Barabash et. al, *SARA on Chandrayaan-1*, Geophysical Research Abstracts, Vol. 9, 04452, 2007, SRef-ID: 1607-7962/gra/EGU2007-A-04452.

[31] Stas Barabash et. al, *Investigation of the solar wind Moon interaction onboard Chandrayaan-1 mission with the SARA experiment*, Current Science, Vol.96, No.4, 25 Feb 2009.

[32] Stas Barabash and Rick McGregor, *Chandrayaan-1 and IRF's instrument SARA*, 24 Oct 2008, available at `http://documents.irf.se/get_document.php?group=Administration&docid=984`.

[33] VTK User's Guide, *VTK File Format*, Version 4.2, Kitware `http://www.kitware.com`, 2007.

[34] Wikipedia, the free encyclopedia, `http://en.wikipedia.org`.